RNA-dependent DNA Damage Response



Zhichao Liu

Linacre College

University of Oxford

A thesis submitted for the degree of
Doctor of Philosophy

Trinity 2023

Abstract

DNA double-strand breaks (DSBs) are the most lethal form of DNA damage, and they require a delicate coordination between transcriptional activity and repression for effective repair. Long nascent transcripts produced near DSBs can be processed into small non-coding RNAs, called DDRNA or diRNA in DICER and DROSHA-dependent manner, which aid in recruiting DNA damage response (DDR) factors. Additionally, these transcripts can form DNA: RNA hybrids and R-loop structures when they bind to their template DNA. These structures accumulate near DSBs and enhance the DDR process, but their precise functions and the mechanisms governing transcription around DSBs remain elusive.

Furthermore, transcriptional repression near DSBs is essential for DDR, creating a complex interplay between transcriptional activation at DSBs and repression nearby, which is regulated by the chromatin landscape. How is chromatin landscape modulated remains poorly understood.

In Chapters 3 and 4 of my study, I demonstrate that the GATAD2B-NuRD complex associates with DSBs in a transcription and R-loop-dependent manner. This interaction leads to a chromatin boundary formation, promoting histone deacetylation and chromatin condensation around DSBs. The presence of this complex near damaged genomic regions is crucial for silencing of gene expression on the same DNA strand. In the absence of the GATAD2B-NuRD complex, chromatin relaxes excessively, and DNA end resection is extended, resulting in the failure of homologous recombination (HR) repair.

In Chapter 5 of my thesis, I investigate the role of DROSHA in regulating transcription around DSBs. I propose that DROSHA positively influences DSB-induced transcription by releasing paused RNA Pol II from DSB ends. Depletion of DROSHA leads to RNA Pol II

stalling near DSBs, with the interaction between CBP80 and DROSHA potentially playing a crucial role.

In summary, my findings highlight the GATAD2B-NuRD complex as a coordinator in the intricate interplay between transcription and the chromatin landscape. Additionally, I emphasize DROSHA's significance as a regulator of DSB-induced transcription within the RNA-dependent DNA damage response.

Acknowledgment

Completing this DPhil journey has been a profoundly enriching experience, and I would like to express my deep gratitude to the individuals and institutions who have supported and guided me along the way.

First and foremost, I am immensely thankful to my supervisor, Prof. Monika Gullerova, for providing me with the opportunity to join her lab. She not only demonstrated a high level of academic research but also taught me how to develop exciting new ideas. With her kind assistance, I have honed my data analysis and experimental skills, making my DPhil journey both exciting and exceptional.

I also wish to extend my gratitude to Prof. Wei-Guo Zhu from Shenzhen University, who generously hosted me for my research during the COVID-19 pandemic. Due to international travel restrictions, I found myself temporarily stranded in China during this challenging period. Prof. Zhu kindly provided me with all the necessary resources for my project and offered invaluable suggestions. Thanks to his support, the disruptions caused by the pandemic in my DPhil studies were minimized.

I must also express my thanks to all the members of the Gullerova and Zhu labs for their continuous support and valuable input. Special thanks go to Kamal Ajit for his bioinformatic analysis, Yupei Wu for his assistance during the lockdown period, and Dr. Adele Alagia and Dr. Qilin Long for their guidance in ionizing radiation experiments. Dr. Meliti Skouteri deserves recognition for her role in training me as an independent researcher at the start of my DPhil journey.

I consider myself extremely fortunate to have had close-knit groups of friends both at the Sir William Dunn School of Pathology and Linacre College. They brought immense happiness

and created unforgettable memories. In times of difficulty, their unwavering support was invaluable, and without them, my DPhil experience might have been much tougher. I am truly grateful for these wonderful friends.

My heartfelt thanks go to my family for their unwavering support and understanding throughout this journey. Their love, encouragement, and unwavering belief in me have been my pillars of strength.

Finally, I want to express my deep appreciation to my beloved, who stood by me throughout the final year of my DPhil study. Her delicious cooking and care played a vital role in helping me successfully complete my DPhil journey.

Contributions

I have included data generated by Kamal Ajit, Yupei Wu, and Svenja Hester in my thesis to . Specifically, S.H. performed Mass Spectrometry for S9.6 immunoprecipitation samples and analysis of data generated from this experiment (Figure 3-3). K.A. performed all ChIP-Seq and DRIP-seq analyses in this thesis. Y.W. helped me with a few chromatin RNA and mRNA RT-qPCR experiments during the lockdown of COVID-19 under my instruction. Both Y.W. and K.A. were listed as co-authors for the manuscript we submitted for peer review.

Abbreviations

Ago	**Argonaute**
DDR	DNA damage response
DSB	DNA double-strand break
DNA	Deoxyribonucleic acid
DGCR8	DiGeorge syndrome critical region 8
BER	Base excision repair
NER	Nucleotide excision repair
ROS	Reactive oxygen species
ChIP	Chromatin immunoprecipitation
IR	Ionizing radiation
UV	Ultraviolet
MRN complex	Mre11-Rad50-NBS1 complex
ATM	Ataxia-telangiectasia mutated
ATR	Ataxia telangiectasia and Rad3-related protein
DNA-PK	DNA-dependent protein kinase
MMR	Mismatch repair

OGG1	8-Oxoguanine DNA glycosylase1
HR	Homologous recombination
NHEJ	Non-homologous End Joining
SSA	Single strand annealing
MMEJ	Microhomology-mediated end joining
ssDNA	Single-stranded DNA
CtIP	CtBP-interacting protein
PARP1	Poly [ADP-ribose] polymerase 1
lncRNAs	Long non-coding RNAs
XPF	Xeroderma pigmentosum complementation group F
XPG	Xeroderma pigmentosum complementation group G
ERCC1	Excision repair cross-complementing group 1
EXO1	Exonuclease 1
LINP1	LncRNA In Non-Homologous End Joining Pathway 1
DDSR1	DNA damage-inducible lncRNA DNA damage-sensitive RNA1
BRCA1	Breast cancer type 1 susceptibility protein
DDRNA	DNA damage-response RNAs

53BP1	TP53-binding protein 1
Nt	Nucleotide
mRNA	Messenger RNA
MDC1	Mediator of DNA Damage Checkpoint 1
DiRNA	Double-strand break-induced RNAs
RNA Pol	RNA polymerase
rRNA	ribosomal RNA
CTD	C-terminal domain
dsRNA	Double-stranded RNA
DARTs	Damage-responsive transcripts
dilncRNAs	Damage-induced long non-coding RNAs
NuRD	Nucleosome Remodeling Deacetylase
SiRNA	Small interfering RNA
Qpcr	Quantitative Real-time polymerase chain reaction
MiRNA	MicroRNA
RNAi	RNA interference
RNA	Ribonucleic acid

Co-IP	co-immunoprecipitation
PLA	Proximity Ligation Assay
MNase	Micrococcal nuclease
RNase H	Ribonuclease H
HDAC1	Histone deacetylase 1
DAPI	4’, 6-diamidino-2-phenylindole
GO	Gene Ontology
STRING	Search Tool for the Retrieval of Interacting Genes/Proteins
IF	Immunofluorescence
BLESS	Breaks labeling, enrichment on streptavidin, and next-generation sequencing
DIvA	DSB inducible via AsiSI
Kb	Kilobase
GFP	Green Fluorescent Protein
BrdU	5-bromo-2'-deoxyuridine
DMSO	Dimethylsulfoxide
ETO	Etoposide

TPL3	Triptolide
CBP80	nuclear cap binding protein subunit 1

Table of Content

1.Background 16
1.1 Introduction 16
1.2 DNA damage response 16
1.2.1 Sources and Types of DNA Damage 16
1.2.2 DNA damage response network 19
1.2.3 DNA repair 20
1.3 DNA double-strand break repair 21
1.3.1 Homologous recombination 21
1.3.2 Non-homologous end joining 24
1.3.3 Alternative DSB repair pathways 26
1.4 Roles of RNA in DDR 28
1.4.1 Roles lncRNA in DDR 29
1.4.3 Transcription repression around DSBs 31
1.4.4 DSBs-induced *de novo* transcription 33
1.4.5 Transcription-coupled DSB repair 35
1.4.6 R-loops and DNA: RNA hybrids 36
1.5 Chromatin remodeling in DDR 41
1.5.1 Chromatin relaxation upon DNA damage 42
1.5.2 Local chromatin remodeling during the DSB repair 43
1.5.3 Repressive chromatin markers *in cis* at DSBs 44
1.5.4 NuRD complex 45
1.6 DROSHA 46
1.6.1 microRNA processing 47
1.6.2 DROSHA in transcription regulation and RNA processing 48
1.6.3 DROSHA in maintenance of genome integrity 50
2. Methods and Materials 52
2.1 Tissue Culture 52
2.1.1 List of cell lines 52
2.1.2 Culture Conditions 53
2.2 Experimental techniques 53

2.2.1 Subcellular fraction 53
2.2.2 S9.6 Immunoprecipitation 54
2.2.3 Silver staining 55
2.2.4 Western Blotting 55
2.2.5 Mass Spectrometry 56
2.2.6 Proximity Ligation Assay (PLA) 57
2.2.7 Laser Micro-irradiation 58
2.2.8 Chromatin Immunoprecipitation (ChIP) 59
2.2.9 ChIP-seq library preparation 59
2.2.10 Chromatin RNA extraction 60
2.2.11 Total RNA extraction 60
2.2.12 qRT-PCR 61
2.2.13 MNase Chromatin Accessibility Assay 61
2.2.14 PH2B-PAGFP Chromatin Relaxation Assay 62
2.2.15 Genomic DNA extraction 62
2.2.16 HR and NHEJ reporter Assay 63
2.2.17 Immunofluorescence 63
2.2.18 Comet Assay 63
2.3 Quantification and Statistical Analysis 64
2.3.1 Statistical analysis of real-time PCR results 64
2.3.2 Quantification and statistical analysis of Immunofluorescence and PLA Results 64
2.4 Bioinformatic analyses 65
2.4.1 ChIP-Seq data processing 65
2.4.2 BLESS Seq data processing 66
2.4.3 DRIP-Seq data processing 66
2.4.4 Metagene Profiles 66
2.4.5 BoxPlots 67
2.4.6 IGV profiles and Heatmaps 67
2.4.7 Analysis of Mass Spectrometry results 68
2.5 List of Antibodies 68
2.6 List of Reagents 71
2.7 List of Plasmids 72

2.8 List of Oligonucleotides 73
2.8.1 List of siRNA 73
3. Screening for novel R-loop binding factors related to the DNA Damage Response 77
3.1 Introduction 77
3.2 Verification of S9.6 Immunoprecipitation 78
3.3 Screening novel R-loops interactors relevant to DDR 79
3.4 Components of NuRD complex were identified as novel R-loops interactors relevant to DDR 84
3.5 Components of NuRD complex interact with R-loops *in vivo* 85
3.6 GATAD2B and MBD3 are recruited to DSBs in transcription and R-loop dependent manner 87
3.7 GATAD2B controls HDAC1 recruitment to DSBs 91
3.8 GATAD2B and HDAC1 occupancy at DSBs overlaps with that of R-loops 94
3.9 GATAD2B and HDAC1 occupancy at DSBs is prone to high transcription activity and HR-prone loci 97
3.10 Discussion 100
4. The role of R-loops and GATAD2B-NuRD complex in DNA Damage Response 105
4.1 Introduction 105
4.2 R-loops repress transcription *in cis* to DSBs 105
4.3 GATAD2B-NuRD complex represses transcription *in cis* to DSBs 108
4.4 R-loops and GATAD2B-NuRD complex reduce H4K12 acetylation level within their chromatin boundary 109
4.5 R-loops and GATAD2B-NuRD complex facilitate histone deacetylation around DSBs 111
4.6 R-loops and GATAD2B-NuRD complex limit chromatin accessibility upon DSBs 115
4.7 GATAD2B-NuRD complex prevents chromatin hyper-relaxation upon DSBs 117
4.8 R-loops and GATAD2B-NuRD complex prevent hyper DNA end resection upon DSBs 118
4.9 The GATAD2B-NuRD complex regulates HR repair efficiency 121
4.10 The GATAD2B-NuRD complex facilitates the kinetics of DSB repair 124
4.11 Hypothetical model of chromatin boundaries between open and condensed chromatin 125
4.12 Discussion 126
5. The role of DROSHA in RNA-dependent DDR 131
5.1 Introduction 131

5.2 DROSHA is localized to DSBs in a transcription-dependent manner 132
5.3 DROSHA interacts with RNA Pol II upon DNA damage 134
5.4 DROSHA KD leads to enrichment of active Pol II in proximity to DSB ends 136
5.5 DROSHA interacts with CBP80 upon DNA damage 139
5.6 CBP80 could be localized to DSBs in a DROSHA-dependent manner 141
5.7 CBP80 interacts with RNA Pol II CTD Y1P upon DNA damage 143
5.8 Discussion 144
6. Conclusions and perspectives 146
6.1 Conclusions 146
6.2 Future work 148
7. Bibliography 152

1.Background

1.1 Introduction

It is widely acknowledged that proteins play a crucial role in the cellular response to DNA damage. Recent research has shed light on the significance of RNA and RNA-binding proteins in the DNA damage response, particularly in the context of DNA double-strand breaks (DSBs)(1). Nonetheless, the precise mechanisms by which these molecules contribute to the DNA damage response remain inadequately understood. It has been reported that DSBs can induce *de novo* transcription and unusual RNA: DNA: RNA hybrids or R-loops formation could also be observed around DSBs(2-5). Investigating how those structures are formed and how DSB-induced *de novo* transcription is regulated is paramount in advancing our comprehension of DNA damage response mechanisms.

In this thesis, I focus on studying the novel functions of R-loops and their binding factors in DNA damage response, and how RNA binding protein DROSHA regulates DSB-induced *de novo* transcription. Here, I will introduce background knowledge that is relevant to this study.

1.2 DNA damage response

1.2.1 Sources and Types of DNA Damage

Human cells encounter a multitude of distinct DNA damage events daily, posing significant threats to genome stability. Notably, an estimated 70,000 DNA lesions

could potentially arise within human cells on a daily basis(6). If those DNA lesions are left unrepaired or repaired improperly, fatal consequences, including loss of genetic information, cell death, mutagenesis, and premature aging, could be triggered(7). DNA damage can stem from both internal and external factors(8, 9). A major endogenous source of DNA damage is DNA replication. Primarily, replication stress can lead to the stalling of replication forks, consequently inciting DNA and chromosome damage(10, 11). Secondly, errors like base substitutions, insertions, or deletions may manifest during replication, culminating in point mutations and frame-shift mutations(12, 13). Additionally, topoisomerase malfunction during replication can also give rise to DNA damage(14). An additional endogenous source of DNA damage is the generation of reactive oxygen species (ROS) through cellular metabolism. These ROS entities can produce oxidized DNA and inflict DNA strand breaks through aggressive interactions with DNA molecules. Furthermore, numerous exogenous sources contribute to the accumulation of DNA damage(15). Details of these sources of endogenous DNA damage and different types of DNA damage induced by these factors are listed in Table 1-1.

Table 1-1 Endogenous DNA damage

Source of endogenous DNA damage	Types of DNA lesions generated
Cytosine deamination	Base transition
Oxidative DNA damage	8-oxo-G, SSB, DSB

DNA methylation	N7-methylguanine, N3-methyladenine, O6-methylguanine
Depurination	Abasic sites

Environmental factors are also significant contributors to DNA damage. Ionizing radiation (IR), for instance, can instigate the formation of both single-strand breaks and double-strand breaks(8). Additionally, ultraviolet (UV) light from sunlight can induce approximately ~10^5 DNA lesions per cell each day(9). Furthermore, various chemical reagents can elicit a spectrum of DNA damage types. A comprehensive breakdown of the diverse sources of environmental DNA damage and the corresponding array of DNA lesions prompted by these factors is presented in Table 1-2.

Table 1-2 Exogenous DNA damage

Source of exogenous DNA damage	Types of DNA lesions generated
Ionizing Radiation (IR)	SSB, DSB, base lesions
Ultraviolet (UV) radiation	SSB, DSB, CPDs, (6- 4) PPs

Alkylating agents	adducted DNA bases, Abasic sites
Aromatic amine	Adducted DNA bases (C8-guanine lesion)
Polycyclic aromatic hydrocarbon (PAH)	Adducted DNA bases
Other chemical reagents (eg. Etoposide)	SSB, DSB, base lesions

1.2.2 DNA damage response network

To overcome those threats to DNA and genome integrity, cells have evolved complicated mechanisms termed DNA damage response (DDR) to detect the DNA damage, signal their presence, and coordinate several biological activities to ensure efficient DNA damage repair. The DDR constitutes an elaborate network of signal transduction, requiring the seamless coordination of various biological activities(7). As my DPhil study mainly focuses on response of DNA double-strand breaks (DSBs). Here, I will describe DDR specific for DSBs as an example to give a brief introduction of this complex network.

Once DSBs have been generated, DSB sensors including PARP1, MRN complex and Ku70-Ku80 complex will be recruited to the broken DNA loci and activate

downstream transducers(16-18), ATM, ATR and DNA-PKcs, all of which are members of the phosphoinositide 3-kinase family(19). Once activated, these kinases initiate a signaling cascade that subsequently activates numerous downstream effectors. These effectors collectively govern a wide array of biological processes, including cell cycle arrest, transcriptional regulation, chromatin remodeling, RNA processing, energy homeostasis, and notably, proficient DNA repair. It was also reported that defects in DDR could result in several severe diseases, including neurological degeneration, premature and cancers(7, 9, 20).

1.2.3 DNA repair

Efficient repair of damaged DNA stands as a pivotal aspect of the DNA damage response (DDR). Tailored mechanisms have evolved in cells to address diverse types of DNA lesions(21). Mismatch repair (MMR) mechanisms operate to rectify base mismatches arising during DNA replication(22), while base excision repair (BER) mechanisms address minor damage or base modifications(23). For more complex lesions, nucleotide excision repair (NER) mechanisms come into play(24). NER encompasses the recognition and removal of several types of damaged DNA caused by UV radiation, including cyclobutane pyrimidine dimers, 6-4 pyrimidine-pyrimidone photoproducts, and other bulky DNA adducts(25). Two modes of NER are at work: transcription-coupled repair (TC-NER), initiated when RNA polymerase stalls at damaged DNA sites, and global genomic NER (GG-NER), activated in other instances of damaged DNA(24, 25). In the case of DNA strand breaks, distinct mechanisms are employed based on the nature of the break: single-strand break repair (SSBR) or double-strand break repair (DSBR).

Numerous enzymes are integral to the DNA repair process. Exonuclease EXO1, for instance, participates in MMR to excise mismatched bases(26). Following this, DNA polymerase and DNA ligase are recruited to synthesize and ligate the replaced DNA, respectively. BER relies on DNA glycosylase OGG1, which recognizes and repairs the abundant base lesion 8-oxoguanine (8-oxoG)(27, 28). Additionally, DNA helicases play a role by unwinding DNA helices, and recombinases are essential for DSB repair(21, 29). Within the DNA repair process, the coordination and tight regulation of these diverse enzymes are imperative to ensure accurate and effective repair of damaged DNA. In the next section, I will introduce DSB repair to clarify how these enzymes are coordinated during repair process.

1.3 DNA double-strand break repair

DNA DSBs are the most dangerous kind of DNA lesions. If this damage is left unrepaired or repaired incorrectly, several catastrophic consequences, such as aging, cancers or even death of individuals can be triggered. DSBs are mainly repaired by two different pathways, homologous recombination (HR) and non-homologous end joining (NHEJ)(30). Here, I will provide an overview of these two pathways, as well as alternative pathways to repair DSBs.

1.3.1 Homologous recombination

Homologous recombination (HR) serves as a critical mechanism during both mitosis and meiosis, facilitating the exchange of genetic information between sister chromatids(31). Its significance extends to playing crucial roles in the repair of DNA

double-strand breaks (DSBs) and the maintenance of genome stability.

Within eukaryotic cells, HR mechanisms employed for DSB repair can be subdivided into three distinct sub-pathways: gene conversion, also known as double-strand break repair (DSBR), synthesis-dependent strand annealing (SDSA), and the less common break-induced replication (BIR)(31-33). The differentiation between DSBR and SDSA hinges on the potential formation of the double Holiday junction structure, while their initial steps are similar(32). In both pathways, the MRN complex is initially recruited to identify the broken DNA ends. Subsequently, Mre11 processes and cleaves the 5' strands of the broken DNA ends in a 3'-5' direction, resulting in the creation of short ~30 nt single-stranded DNA (ssDNA) overhangs(34). These overhangs are pivotal for initiating the long-range end resection process. Following this, CtIP is recruited to the DSBs in an ATM-dependent manner. This protein collaborates with Dna2 to further resect the DNA end, generating an elongated ssDNA overhang that extends approximately 2kb from the broken DNA end(35-37). These exposed ssDNA segments are then coated by replication protein A (RPA), which serves to stabilize the ssDNA. Subsequently, Rad51 is recruited to the DSBs and displaces RPA, instigating the process of strand invasion.

Following the initiation of the Rad51-dependent strand invasion process, a search for homologous sequences on sister chromatids ensues, leading to D-loop formation. Within the synthesis-dependent strand annealing (SDSA) pathway, the invaded 3' single-stranded DNA (ssDNA) segment is elongated by DNA polymerases(32, 38). Subsequently, the newly synthesized DNA pairs with the ssDNA overhang on the other damaged DNA end. This step is followed by the initiation of DNA synthesis on complementary strands, culminating in the ligation of the broken DNA ends.

Conversely, within the double-strand break repair (DSBR) pathway, the second 3' ssDNA overhang will anneal with the complementary strand on sister chromatids post-strand invasion. This event serves to stabilize the D-loop structure, ultimately leading to the formation of a double Holliday junction. This structural configuration facilitates the exchange of genetic information between sister chromatids, fostering gene crossover(39).

In certain instances, DNA double-strand breaks (DSBs) can arise at telomeres or replication forks, resulting in the formation of single-ended DSBs. These single-ended DSBs can activate a less common homologous recombination (HR) mechanism known as break-induced replication (BIR)(40, 41). Similar to the synthesis-dependent strand annealing (SDSA) pathway, the 3' single-stranded DNA (ssDNA) overhangs that emanate from these broken ends invade strands harboring homologous sequences(42, 43). This event leads to the formation of D-loop structures, with the invading strands serving as templates to initiate DNA synthesis at the 3' invaded DNA ends. As the leading strands are extended, the synthesis of lagging strands on the complementary strands is also triggered, leading to the comprehensive repair of DSBs(33, 41). Intriguingly, this pathway also serves as an alternative mechanism for telomere lengthening, referred to as alternative lengthening of telomeres (ALT). ALT operates in a telomerase-independent manner, allowing for the maintenance of telomere length through a distinctive utilization of the BIR pathway(44, 45).

Overall, HR requires homologous sequences as repair templates, ensuring DSB repairs' accuracy. It mainly occurs at S/G2 phase of the cell cycle, when the sister chromatid could be used as repairing templates(46, 47). The model of different HR repair pathways is shown in Figure 1-1.

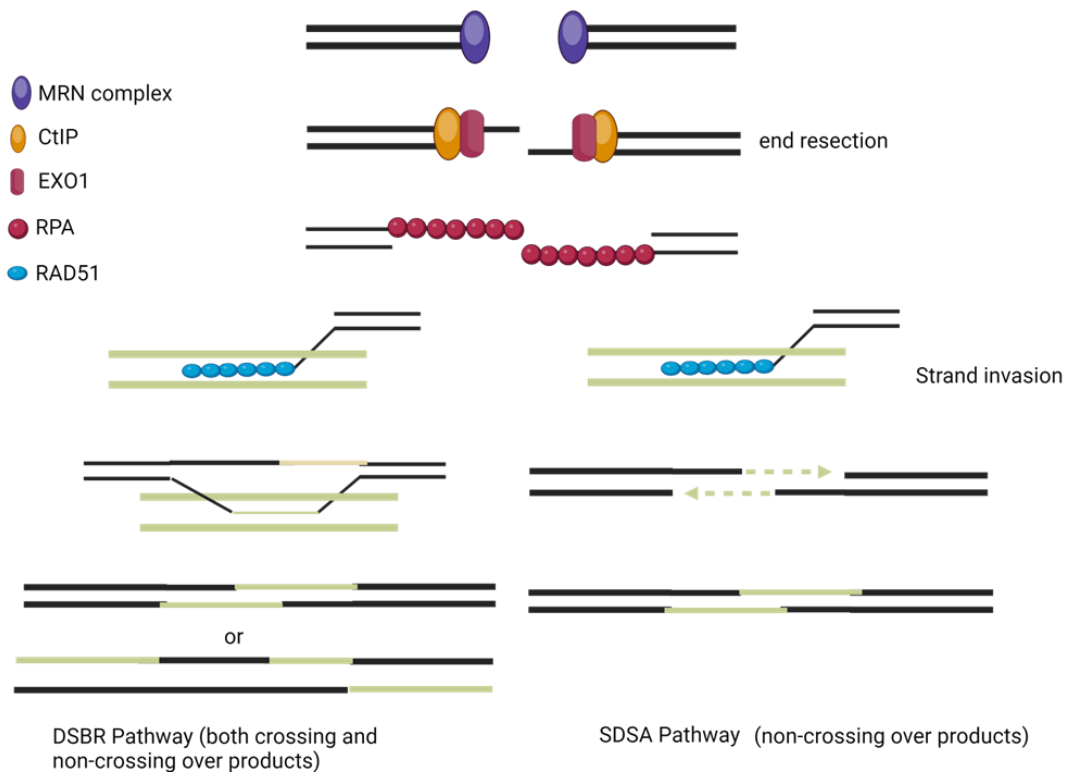


Figure 1-1 Homologous Recombination (HR) pathway. Diagrams showing how DSBs are recognized and repaired by two different sub-HR pathways DSBR and SDSA. These two pathways share initial several steps. While during the strand invasion process. Double holiday junction structures could be formed if DSBs are repaired by DSBR pathway, while single holiday junction structures were observed in those DNA damage repaired by SSA pathway. Consequently, crossingover products could be detected in DSBR pathway.

1.3.2 Non-homologous end joining

Another major pathway for DNA double-strand break (DSB) repair is non-homologous end joining (NHEJ)(48). In this pathway, the Ku70/Ku80 protein complex recognizes DSBs and binds to the broken DNA ends, effectively preventing extensive end resection(49). This interaction results in the formation of a Ku: DNA complex, which serves as a platform for the recruitment of additional factors crucial to this repair process, including nucleases and DNA polymerase(50). DNA-PKcs, a kinase, is subsequently recruited to the DSBs and interacts with Ku, leading to its autophosphorylation and activating Artemis(19). Once activated by DNA-PKcs, Artemis, initially possessing 5' exonuclease activity, forms a complex with the kinase.

This complex gains a spectrum of endonuclease activities, encompassing 5' endonuclease, 3' endonuclease, and DNA hairpin opening capabilities. Consequently, this versatile complex processes a wide array of diverse DNA ends, preparing them for subsequent stages of NHEJ. Furthermore, within the NHEJ pathway, DNA ends can also undergo processing by DNA polymerases Polμ and Polλ(51, 52). These polymerases interact with Ku70/Ku80 through their BRCT domain. Upon recruitment to DSBs, these polymerases can fill in gaps in non-complementary strands, employing either a template-dependent or template-independent manner. This step renders the broken DNA ends suitable for ligation. Upon proper processing of both broken DNA ends, the XRCC4-ligase IV (LIG4) complex assembles at the DSB site and catalyzes the ligation process, culminating in the completion of the DNA repair through NHEJ(53).

In summary, unlike HR, NHEJ does not rely on homologous sequences as repair templates. Instead, it rapidly rejoins the broken DNA ends, a process that can be completed in approximately three hours. As a result, NHEJ can operate throughout the cell cycle, making it the primary DSB repair method during the G1 phase(46, 47). However, due to the involvement of Artemis and DNA polymerases, insertions or deletions of bases can occur during the processing of broken ends, rendering this pathway error-prone and less accurate. An overview of the NHEJ process is depicted in Figure 1-2.

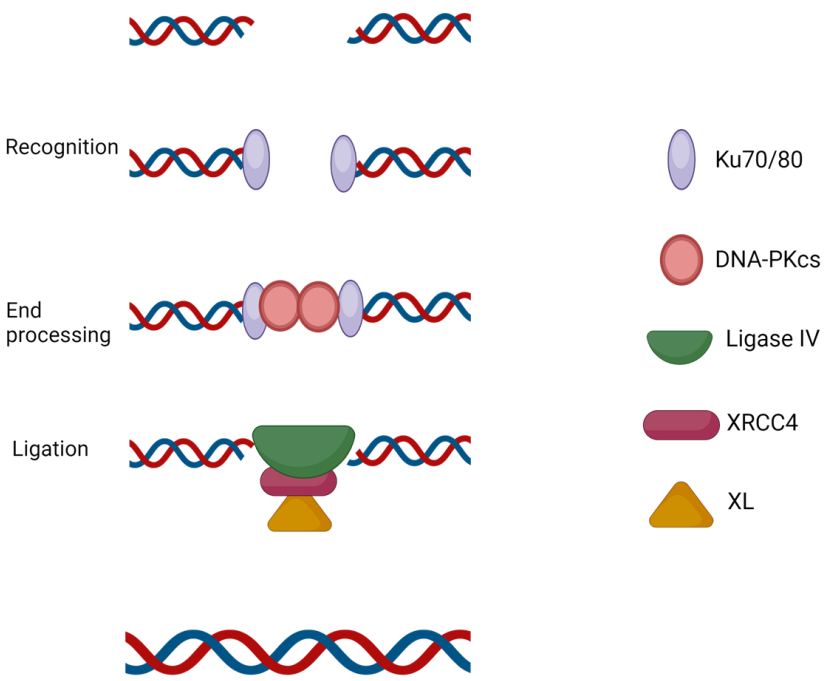


Figure 1-2 Non-homologous End joining (NHEJ) pathway. Diagrams showing how DSBs are recognized and repaired by NHEJ pathway. Different from HR pathways, two broken DNA ends could be processed and directly ligated together without the required of homologous template. In this pathway, DSBs are recognized by Ku70/Ku80 complex, and signaling of this pathway is enlarged by DNA-PKcs. While DNA ligase IV coordinate with XRCC4 and XLF to ligate two broken DNA ends.

1.3.3 Alternative DSB repair pathways

In addition to homologous recombination (HR) and non-homologous end joining (NHEJ), two alternative pathways exist for the repair of DNA double-strand breaks (DSBs): micro-homology mediated end joining (MMEJ) also known as alternative end-joining (Alt-NHEJ) and single-strand annealing (SSA)(54). MMEJ relies on microhomologies, short stretches of 4 to 20 nucleotides located on both DNA ends(55, 56). This pathway comprises at least five essential steps: DNA end resection, annealing of microhomology, removal of heterologous flaps, DNA synthesis to fill gaps, and ligation of broken ends(57). The initiation of MMEJ occurs when the MRN

complex detects broken DNA ends. Once activated, MMEJ shares the initial end resection step with HR(58). Notably, the efficiency of MMEJ is significantly reduced in mammalian cells deficient in the MRN complex, Mre11, or CtIP, underscoring the significance of end resection in this pathway(59). After the formation of 3' ssDNA overhangs, microhomologies become exposed, leading to their annealing. The precise molecular mechanisms governing microhomology annealing remain unclear, but PARP1 appears to play a vital role. In vitro assays have demonstrated that nuclear extracts from PARP1 knockout cells fail to anneal broken DNA ends, while annealing of microhomologies can be observed with nuclear extracts from wild-type cells(60). If the annealed microhomologies are internal to the ssDNA overhang, unpaired heterologous 3' flaps are removed in an XPF/ERCC1-dependent manner to enable efficient DNA end extension. Subsequently, DNA polymerase θ is recruited to the DSBs for gap filling, followed by the ligation of DNA ends by DNA ligase III/I upon completion of this fill-in synthesis(59, 61).

Similar to MMEJ, SSA requires end resection for initiation and encompasses the same five essential steps. The primary distinction between these pathways lies in the requirement for longer ssDNA overhangs and homology in SSA(62). Following CtIP/EXO1-dependent generation of 3' ssDNA overhangs, longer homologies (>20 nt) are annealed in a Rad52-dependent manner in SSA(63). This is followed by the removal of unpaired non-homologous overhangs by ERCC1/XPF. Fill-in synthesis and ligation of DNA ends complete the repair pathway, although the specific DNA polymerases and ligases involved in these steps remain unclear.

In summary, MMEJ and SSA are two alternative pathways for DSB repair. It is believed that excessive DNA end resection can facilitate both pathways, although

MMEJ does not require long ssDNA overhangs for activation(64, 65). Repair through these pathways often results in significant loss of genetic information, particularly at repetitive sequences, rendering them error prone. An overview of these two pathways is illustrated in Figure 1-3.

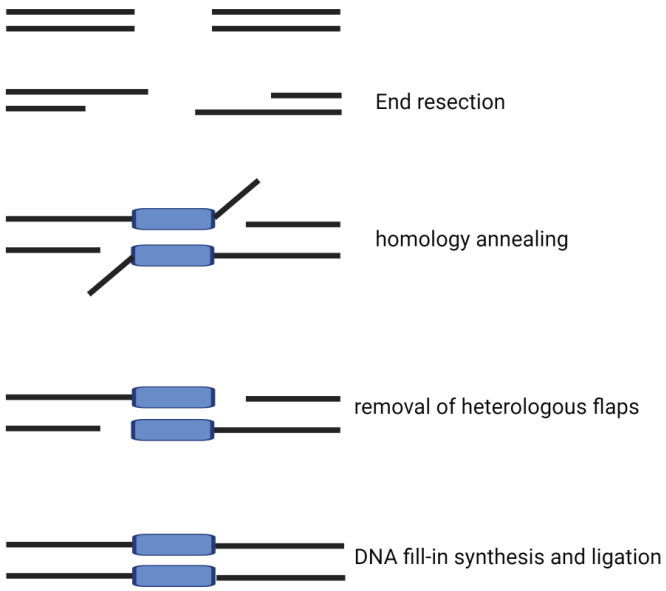


Figure 1-3 Micro-homology mediated End joining (MMEJ) and Single-strand annealing (SSA) pathway. Diagrams showing how DSBs are recognized and repaired by two alternative DSB repair pathways MMEJ and SSA. These two pathways share identical five steps including end resection, homology annealing between two resected ssDNA, removal of heterologous flaps, DNA fill-in synthesis and ligation. However, MMEJ just requires 4-6 nt microhomology annealing, while SSA requires longer homology to anneal.

1.4 Roles of RNA in DDR

Previously, the predominant focus in the DNA damage response (DDR) was on proteins. However, recent studies have illuminated the crucial roles of RNA within these intricate networks. RNA molecules have emerged as pivotal contributors to

DDR(1, 66, 67), not only exerting regulatory influence over the expression of DDR-related proteins but also actively participating in the DDR network itself. This section aims to provide an introductory insight into how RNA molecules contribute to DDR.

1.4.1 Roles lncRNA in DDR

Long non-coding RNAs (lncRNAs), transcripts exceeding 200 nucleotides in length primarily synthesized by RNA Pol II, are gaining recognition. With an estimated count of over 30,000 distinct lncRNAs from human cells, surpassing protein-coding genes in number, the functions of most lncRNAs remain enigmatic. However, a subset of lncRNAs has been implicated in regulating diverse biological activities, including chromatin remodeling, gene expression modulation, and cell cycle regulation. Remarkably, lncRNAs have also been found to influence DDR, either through direct interactions or indirect modulation.

One exemplary lncRNA is LINP1, which is under the regulation of p53(68). This non-coding RNA forms direct interactions with key NHEJ factors, the Ku70/Ku80 complex, and DNA-PKcs, acting as a scaffold to stabilize these proteins on chromatin. Consequently, LINP1 ensures efficient NHEJ repair. Intriguingly, when LINP1 is knocked down, NHEJ efficiency is significantly diminished, underscoring its pivotal role in DDR. Additionally, certain p53-independent lncRNAs have also been implicated in DDR. For instance, DDSR1, a lncRNA whose transcription is triggered by ATM, serves as an illustrative example. Upon induction of DNA double-strand breaks (DSBs), DDSR1 expression increases approximately 2.5-fold(69). This RNA has been found to facilitate the recruitment of BRCA1 to DSB sites. Notably,

knockdown of DDSR1 leads to a 50% reduction in homologous recombination (HR) efficiency.

1.4.2 DDRNA and DiRNA

Interestingly, it has been reported that small non-coding RNAs can be generated at sites of DNA double-strand breaks (DSBs), termed DNA damage-response RNAs (DDRNAs)(70), which also play direct roles in DDR. In a notable study, it was revealed that knockdown of Dicer and DROSHA, two essential RNA processing enzymes, significantly reduces the formation of foci containing 53BP1, pATM, and MDC1, key DDR factors(70, 71). Notably, knockdown of other factors involved in miRNA biogenesis, including three GW182-like proteins, does not impact the formation of DDR foci for these factors. This suggests that DROSHA and Dicer participate in DDR through a miRNA-independent mechanism. Intriguingly, treatment with RNaseA leads to a reduction in the number of DDR foci, but this effect is rescued by transfection of 20-35 nt RNA fragments purified from cells with induced DSBs(70). This suggests that DNA damage induced small RNAs are crucial for the recruitment of DDR factors. Furthermore, transfection of locus-specific synthesized small RNAs can also rescue the impaired recruitment of DDR factors caused by RNaseA treatment, supporting the notion that DSB-induced small RNAs originate from the DSB ends.

Another class of small RNAs, termed double-strand break-induced RNAs (diRNAs)(72), has also been identified. These diRNAs, ranging from 21 to 24 nucleotides in length, were initially discovered in *Arabidopsis thaliana* and later

observed in mammalian cells(73). In plants, it was found that the precursors of diRNAs are produced in a manner dependent on RNA Pol IV and ATR, and these longer transcripts are subsequently processed into shorter segments by Dicer-like proteins. Intriguingly, RNA-dependent RNA polymerase has been identified as a crucial factor for the biogenesis of diRNAs, suggesting that a longer double-stranded RNA structure might be required for Dicer-like processing. DiRNAs have also been implicated in DDR(72). Upon incorporation into AGO2, an RNA-binding protein, diRNAs can recruit Rad51 to DSB sites, promoting homologous recombination repair(74). Moreover, these small RNAs have been shown to facilitate the recruitment of chromatin remodeling factors and DNA methylation when they bind to AGO2 in response to DNA damage(75).

1.4.3 Transcription repression around DSBs

Transcription regulation plays a crucial role in DNA damage response (DDR). DSBs have been reported to induce RNA polymerase arrest and transcriptional repression in cis to the site of damage. In this section, I will introduce the mechanisms through which transcription is repressed in response to DSBs.

Upon laser micro irradiation, the assembly of the RNA polymerase I (Pol I) initiation complex is disrupted in an ATM/NBS1/MDC1-dependent manner(76). Additionally, the elongating RNA Pol I is removed, suggesting that these DDR factors contribute to the repression of ribosomal RNA (rRNA) transcription. Site-specific DSBs generated at the 28s rDNA loci also result in the downregulation of rRNA transcription, further implicating ATM in the repression of Pol I transcription in the vicinity of DSBs(77).

ATM also exerts an inhibitory effect on RNA Pol II-mediated transcription near DSBs(78). This is achieved through the triggering of H2A ubiquitination at active transcription sites upon DSB induction, leading to RNA Pol II dephosphorylation while maintaining overall levels of the polymerase in the proximity of DSBs. This transcriptional silencing program can also target several transcription factors and chromatin remodelers. For instance, ATM phosphorylates the transcription elongation factor ENL1, resulting in transcriptional repression(79). Furthermore, ATM targets BRD7, a component of the PBAF complex, upon DNA damage, leading to phosphorylated BRD7's interaction with the MRN complex(80, 81). This interaction promotes H2A-K119 ubiquitination and thereby regulates transcription in the vicinity of DSBs.

DNA-PKcs, another kinase involved in DDR, also negatively regulates transcription near DSBs(82). Following DNA damage, DNA-PKcs recruits the E3 ubiquitin ligase WWP2 in a transcription-dependent manner to ubiquitinate the largest subunit of RNA Pol II, RPB1(83). This ubiquitination marks RPB1 for degradation via the proteasome pathway. Notably, DNA-PKcs-mediated eviction of RNA Pol II predominantly occurs within gene bodies, and this transcriptional regulation further promotes the non-homologous end joining (NHEJ) repair pathway.

In addition to PI3K kinases, PARP1, a critical factor in DDR, also functions as a master transcriptional regulator upon DNA damage(84). PARP1 recruits various chromatin remodeling factors and transcription factors to damaged DNA sites. The Polycomb repressive complex (PRC) is one such target of PARP1, establishing a transient repressive chromatin structure around DSBs to suppress transcription(85). Other chromatin remodeling factors, such as ZMYND8, CHD4, KDM5A, EHMT2,

and EZH2, are also part of the PARP1-dependent transcription repression program(86-89). Moreover, the negative elongation factor NELF-E is a substrate of PARP1, and its localization to DSBs is essential for PARP1-mediated transcriptional repression(90).

1.4.4 DSBs-induced *de novo* transcription

Recent studies have intriguingly suggested that broken DNA ends can function as functional promoters, activating de novo transcription in response to DNA double-strand breaks (DSBs) to generate long non-coding transcripts that play important roles in ensuring efficient DNA repair(91). Specifically, the MRN complex orchestrates the assembly of the preinitiation complex (PIC) at DSB ends, facilitating the recruitment of active RNA Pol II to initiate bidirectional transcription(92-94). This process leads to the synthesis of damage-induced long non-coding RNAs (dilncRNAs), which serve as precursors for DNA damage-response RNAs (DDRNAs) and participate in recruiting various DDR factors(3). Furthermore, dilncRNAs can directly contribute to DDR by promoting end resection, a critical step in HR repair.

Another study has highlighted the significance of c-Abl-mediated phosphorylation of the RNA Pol II C-terminal domain (CTD) at Tyrosine 1 in DSB-induced de novo transcription(2). Upon DNA damage, Y1P RNA Pol II transcribes away from DSB ends, and the resulting long transcripts hybridize with their template DNA, forming DNA: RNA hybrids. This hybridization initiates antisense transcription, leading to the formation of double-stranded RNAs (dsRNAs) or damage-responsive transcripts (DARTs) (Figure 1-4). The presence of dsRNA structures upon DNA damage was

confirmed through immunofluorescence using the J2 antibody(95), which specifically detects dsRNA. Notably, overexpressing RNase H1 to eliminate DNA: RNA hybrids significantly reduce dsRNA levels, underscoring the importance of DNA: RNA hybrids-dependent antisense transcription in dsRNA formation. These long non-coding RNAs also regulate the recruitment of DDR factors 53BP1 and MDC1, contributing to effective DDR(2).

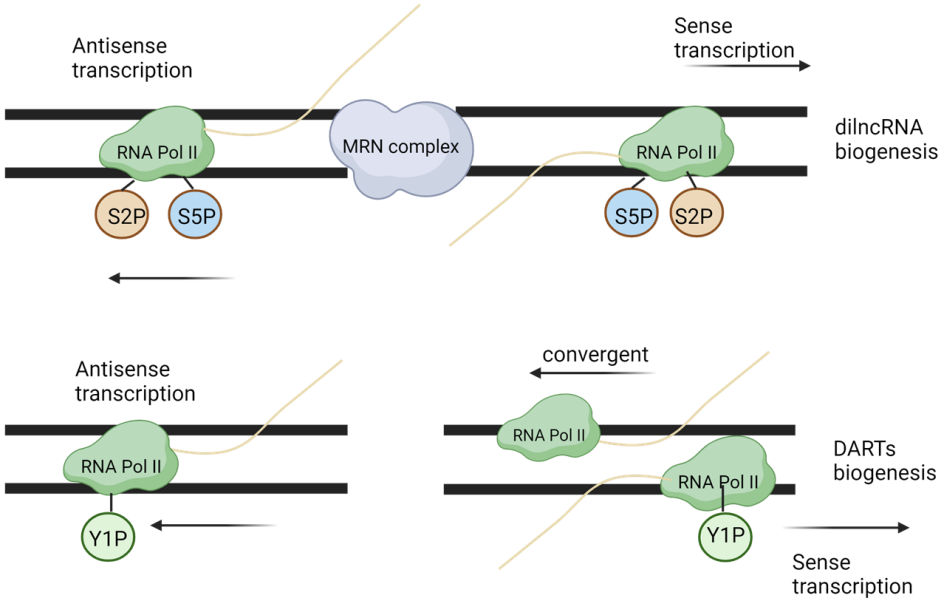


Figure 1-4 Models of DSB-induced *de novo* transcription. DSBs could act as functional promoters to facilitate transcription of long non-coding RNA around DSBs. In the first model. RNA pol II could be recruited to DSBs by MRN complex to facilitate transcription of dilncRNA. N this pathway, CTD Ser2 and Ser 5 of RNA Pol II was found to be phosphorylated by CDK9, which is crucial for lncRNA transcription. In the second model, Tyr1 residue of RNA Pol II CTD was found to be phosphorylated by c-Abl upon DNA damage, which enables bidirectional transcription of RNA polymerase around DSBs.

Interestingly, DSBs can also activate RNA Pol III-dependent transcription near the sites of damage(96). Upon DNA damage, the MRN complex facilitates the localization of RNA Pol III to DSBs, and in collaboration with CtIP, RNA Pol III

drives RNA synthesis. The transcripts produced by RNA Pol III at DSB ends hybridize with resected single-stranded DNA overhangs to protect against nuclease attack and thereby enhancing HR efficiency.

1.4.5 Transcription-coupled DSB repair

Indeed, transcription status has been shown to have a significant impact on the choice of DNA double-strand break (DSB) repair pathways(97). The connection between transcription and DSB repair was initially observed in yeast, where it was noted that DNA damage occurring within actively transcribed genes was repaired more efficiently than in transcriptionally inactive regions(98).

In human cells, transcription has been found to play a crucial role in directing DSB repair toward the homologous recombination (HR) pathway. When genome-wide DSBs were induced using the endonuclease AsiSI, the HR factor RAD51 was preferentially recruited to transcriptionally active regions, including promoter regions(99). This transcription-dependent recruitment of RAD51 was further confirmed by inducing DSBs at transcriptionally active and inactive loci using KillerRed, a light-excitable chromophore that releases reactive oxygen species (ROS)(100). Additionally, transcription was shown to enhance HR efficiency by approximately 70% as measured by a DR-GFP reporter cassette, providing further evidence for the regulatory role of transcription in DSB repair pathway choice(101).

Cell cycle progression is well-established to govern the choice of DSB repair pathways, with HR being inhibited in the G0/G1 phase due to the absence of sister chromatids for template-based repair. However, a compelling study has revealed that

transcription can override this cell cycle-dependent inhibition and promote HR repair even in the G0/G1 phase(102). Notably, HR-associated factors such as RAD51C, RPA1, and RAD52 were observed to localize to DSB sites generated at highly transcribed loci, and this recruitment was shown to be dependent on the Cockayne syndrome B (CSB) protein. Intriguingly, impairing the formation of DNA: RNA hybrids, which result from the interaction between RNA transcripts and DNA, by overexpressing RNase H led to reduced recruitment of these HR factors(102). This strongly suggests that DNA: RNA hybrids play a crucial role in driving RNA-templated HR repair, particularly during the G0/G1 phase of the cell cycle.

1.4.6 R-loops and DNA: RNA hybrids

R-loops are three stranded structures consisting of a DNA: RNA hybrids and a displaced ssDNA. The formation of R-loops is driven by various DNA structural features, including high GC content, DNA negative supercoiling, and DNA nicks(103). Previously, these structures were thought to be transcription byproducts, posing threats to genome stability. Specifically, the displaced single-stranded DNA (ssDNA) in these three-stranded structures is more susceptible to attacks by nucleases, which could result in DNA nicks and ssDNA breaks(104, 105). Additionally, the unpaired ssDNA within R-loops serves as a suitable substrate for various DNA-modifying enzymes, such as AID. AID can deaminate cytosines on the ssDNA, leading to C to T conversions. Subsequent DNA replication cycles may then incorporate these mutations, potentially causing genetic alterations. Furthermore, DNA: RNA hybrids within R-loops can act as barriers during DNA replication. This collision between the replication and transcription machinery can lead to replication stress and an increased

risk of DNA damage, especially DSBs.

However, several studies have unveiled the beneficial functions of R-loops(5, 103, 106). Specifically, R-loops are involved in class switch recombination, a process critical for antibody class diversification. Additionally, these three-stranded structures have been shown to play important roles in transcription regulation. First, R-loops have the capacity to recruit condensed chromatin modifiers, such as G9a and PRC2, which deposit repressive histone markers, such as H3K9me2 or H3K27me3(107). These modifications result in the termination or silencing of transcription, thereby exerting a regulatory influence over gene expression. Conversely, R-loops can also contribute to positive transcription regulation by promoting chromatin relaxation. Chromatin remodeling complexes like TIP60-p400 and the H3K4 methyltransferase MLL interact with R-loops located at promoter regions(108). These interactions lead to the opening of chromatin around these promoters, facilitating active transcription. Furthermore, R-loops can serve as recruitment platforms for transcription factors. For instance, transcription factor NF-κB can be recruited to transcription start sites via interactions with R-loops(109). Additionally, in promoters containing CpG islands, these three-stranded structures are recognized by GADD45, and this protein subsequently recruits DNA demethylase TET, leading to the demethylation of promoter DNA and ensuring efficient transcription(110, 111).

Recently, an increasing number of studies have revealed that R-loops play a crucial role in maintaining genome stability(5). These intriguing structures have also been found to form around DNA double-strand breaks (DSBs) and positively regulate DNA damage response (DDR) and DSB repair processes. Notably, a study led by Takaaki and colleagues shed light on the interplay between Rad52 and R-loop formation,

which can influence the choice between homologous recombination (HR) and non-homologous end joining (NHEJ) repair pathways(97). The researchers observed that both the overexpression of RNase H and the deletion of Rad52 led to compromised recruitment of replication protein A (RPA) and Rad51, while γH2AX kinetics remained unchanged compared to the control group. This suggests a dynamic interplay between transcriptional state and Rad52 in modulating repair pathway selection. Further investigations revealed that R-loop removal could hinder Rad52's localization to DNA DSBs, indicating an interconnected relationship between R-loop formation and Rad52 function. Subsequent studies confirmed that Rad52 promotes the recruitment of XPG, an endonuclease that processes R-loops and initiates the HR pathway(97). Another study proposed that the resolution of R-loops at transcriptionally active loci could also regulate the choice of DSB repair pathways. This study unveiled that Senataxin (SETX) is specifically recruited to sites of DNA DSBs in euchromatin and facilitates the removal of R-loops surrounding the DSBs. Intriguingly, the knockout of SETX increased the presence of 53BP1 foci, although it did not impact repair efficiency or translocation events(112).

R-loops also play a role in facilitating the recruitment of various DNA damage response (DDR) factors. Particularly during the S/G2 phase of the cell cycle, dilncRNA has been observed to hybridize with the resected 3' single-stranded overhang, leading to the formation of DNA: RNA hybrids. These hybrid structures subsequently contribute to the recruitment of BRCA1, a key factor involved in homologous recombination (HR) repair(113). In addition, when these hybrids are removed by overexpression of RNase H, there is a significant reduction in the enrichment of HR factors at DNA double-strand breaks (DSBs), underscoring the essential role of these three-stranded structures in localizing HR factors to DSB sites.

Furthermore, the recruitment of RAD51, another critical player in HR repair, to broken DNA ends also appears to occur in a manner dependent on R-loops and the Cockayne syndrome group B (CSB) protein(100, 114).

R-loops also have a role in regulating the end resection process, which is a crucial step in DNA double-strand break (DSB) repair. Initially, R-loops were thought to hinder end resection. This notion was supported by evidence that overexpressing RNase H1, an enzyme that degrades the RNA strand of DNA: RNA hybrids, results in the extension of the single-stranded DNA overhang at site-specific DSBs(115). Additionally, knockdown of factors involved in removing R-loops was found to reduce end resection efficiency(116-118). However, it has been proposed that DNA: RNA hybrids can activate a non-canonical end resection pathway, thereby positively regulating the length of single-stranded DNA (ssDNA) produced during end resection. Data from single molecule analysis of resection tracks (SMART) revealed that the depletion of EXOSC10, a factor implicated in R-loop processing, significantly increases the length of resected ssDNA overhang(119). Knockdown of EXOSC10 also leads to the accumulation of R-loops, suggesting that DNA: RNA hybrids can indeed promote end resection. Furthermore, depletion of other factors involved in processing DNA: RNA hybrids, such as XPF, XPG, and SETX, has been shown to trigger extensive end resection(97, 112). These findings collectively emphasize the significance of DNA: RNA hybrids in facilitating the extension of end resection during DNA repair processes.

Interestingly, RNA molecules within DNA: RNA hybrids can serve as templates for repair, giving rise to RNA-templated DNA double-strand break (DSB) repair(120). This groundbreaking concept was initially demonstrated by Storici and colleagues in

Saccharomyces cerevisiae, where they identified that RNA-containing or RNA-only nucleotides could be utilized as repair templates for DSBs(121). This novel repair mechanism involves Rad52, which facilitates the annealing of single-stranded DNA (ssDNA) with RNA(102). In vitro experiments have indicated that Rad52 promotes the annealing of RNA with DNA, resulting in the formation of DNA: RNA hybrids that bridge the two broken ends of the DSB and facilitate the subsequent ligation of the DNA segments(122). This RNA-templated DSB repair process has also been observed in human cells. Factors associated with classical non-homologous end joining (NHEJ) repair, such as 53BP1 and PNKP, have been shown to bind to nascent or pre-mRNA near DSBs through RNA-ChIP experiments(123). These interactions are significantly impaired by RNase H treatment, confirming the importance of RNA in this repair process. Recent studies have also revealed that DNA polymerase-ζ possesses reverse transcriptase activity and can be recruited to DSBs in a RAD52-dependent manner(124, 125). This polymerase then acts as a reverse transcriptase to synthesize DNA in an RNA-templated manner, contributing to the completion of DSB repair. This RNA-templated repair pathway is particularly valuable in the G0/G1 phase of the cell cycle when classical homologous recombination (HR) is inhibited, thereby ensuring repair accuracy under such circumstances. DSBs-induced DNA: RNA hybrids and R-loops structures are illustrated in Figure 1-5.

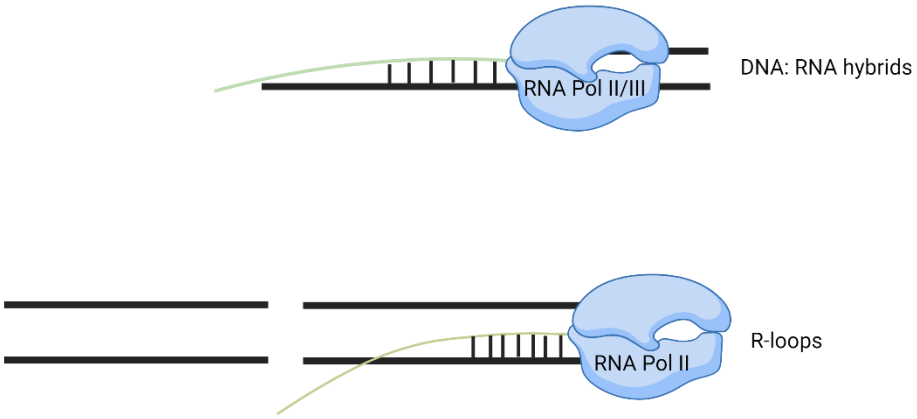


Figure 1-5 DSBs-induced DNA: RNA hybrids and R-loops structures. Upon induction of DSBs, RNA Pol II- or RNA Pol III-mediated de novo nascent RNAs could hybridize with 3' ssDNA overhangs generated from resected broken DNA ends, forming two-strand DNA: RNA hybrids. Additionally, DSB-induced de novo transcripts, as well as RNA synthesized from existing transcription, can also anneal with their respective templates from dsDNA to create three-strand R-loop structures around DSBs.

1.5 Chromatin remodeling in DDR

In eukaryotic cells, DNA molecules are wrapped around histones to form nucleosomes, which could be further processed and folded into higher condensed structures. These condensed chromatin structures were proven to impede the access of DNA damage response (DDR) factors to damaged DNA, which limits the DNA repair process. Consequently, chromatin remodeling is one of the crucial steps in DDR to ensure efficient and accurate DNA repair, and this process was reported to participate in several stages of DDR(7, 9). In this section, I will provide an introduction about how chromatin remodeling is involved in the DDR process.

1.5.1 Chromatin relaxation upon DNA damage

It has been revealed that the nuclease sensitivity of chromatin transiently increases upon DNA damage, indicating an increase in chromatin accessibility(126). Subsequently, a model describing the dynamic change of chromatin structure upon DNA damage, termed the "access-repair-restore" (ARR) model, was proposed(127). According to this model, chromatin decompaction is triggered upon DNA lesions to provide access for DNA damage response (DDR) factors to repair the broken DNA. This is followed by the reorganization of chromatin to restore the original structures of the local chromatin.

Several core double-strand break (DSB) sensors and mediators have been reported to play important roles in the formation of open chromatin structures at the initial stage of DDR(128). Specifically, PARP1 can directly PARylate histones, weakening their interaction with DNA and facilitating nucleosome disassembly, leading to an open chromatin structure(129). Additionally, PARP1 can recruit several chromatin remodelers to modify chromatin structures upon DNA damage. CHD2, which localizes to DSBs in a PARP1-dependent manner, deposits the histone variant H3.3 into chromatin, resulting in the relaxation of local chromatin structure(130). CHD4, a component of the NuRD complex, is also recruited to DSBs by PARP1(86). These chromatin remodelers are known to remove heterochromatin factors such as HP1 from chromatin, triggering an open chromatin structure. Another DSB sensor, ATM, has been reported to positively regulate chromatin relaxation at the early stage of DNA damage. This kinase phosphorylates the transcriptional repressor KAP1, leading to chromatin relaxation at DSBs(126). Additionally, SNF2H, the catalytic subunit of ISWI chromatin-remodeling complexes, can be phosphorylated upon DNA damage,

further relaxing heterochromatin to facilitate DSB repair(131). Moreover, histone modifications, particularly acetylation, can also decompact chromatin by inhibiting their interaction with DNA(132).

1.5.2 Local chromatin remodeling during the DSB repair

Histone modifications and changes in chromatin structure have been found to contribute to the regulation of the DSB repair process and the choice of repair pathway, leading to distinct chromatin patterns during HR and NHEJ repair. Here, I will introduce how chromatic dynamics were regulated during HR and NHEJ repair.

In recent findings, phosphorylation of H4Y51 by the tyrosine kinase receptor TIE2 was identified, promoting recruitment of ABL-1 and participation in the NHEJ pathway(133). Additionally, a shift from monoubiquitylation to acetylation on H2BK120 was observed during NHEJ. This transition is mediated by the deubiquitinase and SAGA complex, which possesses acetylase activities(134). In vitro studies confirmed acetylation of this histone residue by SAGA, and knockdown of components of this complex impaired NHEJ efficiency, emphasizing the significance of this modification transition in DSB repair. Moreover, H3K36 methylation emerged as another key regulator of NHEJ, with increased levels of H3K36me2 and H3K36me3 observed near NHEJ-prone DSBs(135). The deposition of histone variants was also found to impact this repair pathway. Specifically, H2A.Z is positioned around DSBs, facilitating chromatin relaxation and Ku70 localization to promote DSB repair(136).

Similarly, the HR repair pathway is tightly controlled by chromatin remodeling.

Chromatin characteristics preferentially enriched at NHEJ-prone loci, including H2A.Z, H3.3, and H2BK120ub, are downregulated at HR-prone regions(135). Chromatin structures and histone modifications also facilitate crucial HR steps, such as end resection and RAD51 assembly(137). Nucleosomes were observed to inhibit end resection in vitro, highlighting the importance of nucleosome eviction for efficient generation of single-stranded DNA (ssDNA)(138). Several chromatin remodelers are localized to DSBs to regulate end resection by controlling nucleosome density. In yeast, the chromatin remodeler INO80 facilitates ssDNA extension at DSBs, promoting proteasome-dependent histone degradation to reduce nucleosome density(137). SMARCAD1, an ATP-dependent chromatin remodeler that repositions, exchanges, and assembles nucleosomes, is also localized to DSBs and enhances end resection and HR repair through its ATPase activity(139). Furthermore, histone modifications play a role in end resection. H3K36me3 recruits LEDGF to DSBs, facilitating CtIP localization and efficient end resection(140). H3K9me2 aids in the recruitment of BRCA1/BARD1, activating the HR pathway and promoting end resection(141). The methylation status of H4K20 similarly influences pathway choice by affecting loading of 53BP1 or BRCA1, indirectly regulating end resection.

1.5.3 Repressive chromatin markers *in cis* at DSBs

As introduced in Section 1.4, double-strand breaks (DSBs) are thought to induce transcriptional repression in the vicinity of the break site. Despite the local chromatin decondensation that occurs upon DNA damage, transcriptional repression is often associated with the presence of repressive chromatin markers. Consequently, several chromatin remodeling factors, including HP1, components of the NuRD complex,

G9a, KAP1, Suv39h1, and Polycomb proteins(85, 142, 143), as well as histone markers related to heterochromatin structure (such as H3K9me2, H3K9me3, H3K27me3)(144), have been identified around DSBs. Upon their recruitment to DSB sites, these histone markers and chromatin modifiers collaborate to enforce transcriptional repression in cis at the DSB.

Interestingly, key DNA damage response (DDR) factors have been found to regulate the localization of these reported repressive chromatin markers at DSB sites. The recruitment of repressive Polycomb, MTA1, and CHD4 was shown to be mediated by PARP1(85), as treatment with a PARP inhibitor hindered the recruitment of these chromatin remodelers to DSBs. Moreover, PARP1 itself was observed to induce transcriptional repression upon DNA damage, suggesting its potential involvement in the same pathways as these chromatin modifiers. Additionally, DNA damage-induced ubiquitylation, which is dependent on the ATM kinase, was identified as a crucial histone modification for locally silencing transcription around DSBs(78).

1.5.4 NuRD complex

The NuRD complex is primarily regarded as a repressive complex that combines ATP-dependent chromatin remodeling and histone deacetylase activities. Comprising multiple subunits, this complex includes histone deacetylases HDAC1/2, ATP-dependent remodeling enzymes CHD3/4, histone chaperones RbAp46/48, CpG-binding proteins MBD2/3, the GATAD2A (p66α) and/or GATAD2B (p66β) subunits, as well as specific DNA-binding proteins MTA1/2/3(145).

Given its chromatin remodeling functions, the NuRD complex plays a role in

regulating several critical biological processes, such as embryonic development, cellular differentiation, and transcriptional repression(145). Furthermore, certain components of this complex have been found to participate in the response to DSBs. As previously mentioned, CHD4 and MTA1 can be recruited to DSBs in a PARP1-dependent manner(85, 86), contributing to the transcriptional repression in cis to the DSB. Additionally, CHD3 and CHD4 have been reported to facilitate chromatin relaxation and enhance homologous recombination (HR) repair efficiency. Another component of the NuRD complex, HDAC1, has been shown to promote efficient non-homologous end joining (NHEJ) repair(146). This role of HDAC1 in NHEJ repair was validated through assays utilizing GFP-based NHEJ and HR reporter cassettes. Furthermore, treatment with HDAC1 inhibitors led to a significant increase in H3K56ac and H4K16 levels around DSBs, suggesting that H3K56 and H4K16 are potential targets of HDAC1 in the context of DNA damage.

1.6 DROSHA

Recent studies have emphasized the significance of components within the RNA interference (RNAi) pathways in the DNA damage response (DDR). As mentioned earlier, the biogenesis of DDRNA relies on Dicer and DROSHA(70), both of which are key factors in RNAi pathway. Additionally, Dicer has been found to influence the Nucleotide Excision Repair (NER) pathway. Following UV treatment, Dicer has been observed to facilitate the recruitment of MMSET to sites of DNA damage. This recruitment triggers the demethylation of H4K20, subsequently promoting the enlistment of XPA, a core factor in TC-NER. Moreover, other RNAi factors, such as the Ago proteins, also contribute significantly to DDR. These proteins form

associations with DiRNA and assist in the recruitment of various DDR factors, including Rad51 and MMSET(74). This collaborative effort ensures ample homologous recombination repair and precise chromatin remodeling at damaged DNA sites.

DROSHA is an RNase III enzyme that plays a pivotal role in recognizing and cleaving hairpin-structured embedded transcripts. It consists of various domains, including a P-rich domain and an R/S-rich domain at its N-terminal, followed by a platform and a PAZ domain in its middle part. Additionally, it features two RNase III domains and a dsRNA binding domain at its C-terminal(147, 148). DROSHA can interact with its binding partner DGCR8 to form the microprocessor complex, which participates in the microRNA processing pathway and RNA interference (RNAi). Recent studies have also uncovered non-canonical functions of DROSHA. Here, I will introduce roles of DROSHA in miRNA biogenesis, gene expression regulation, RNA processing, and genome stability maintenance.

1.6.1 microRNA processing

MicroRNAs (miRNAs) are small non-coding RNAs that are around 21-24 nucleotides in length(67). They regulate gene expression by pairing with mRNA through complementary sequences, leading to either transcriptional or translational regulation. The biogenesis of miRNAs initiates with RNA polymerase II transcription(149). In this process, long primary transcripts called primary miRNAs (pri-miRNAs) are generated. These pri-miRNAs contain hairpin structures that are recognized by DROSHA and its binding partner DGCR8(150). These hairpins are cleaved by

microprocessor complex into 70 nucleotide precursor miRNAs (pre-miRNAs), which are then exported to the cytoplasm in an EXO5-dependent manner(151). Further processing by Dicer generates short miRNA duplexes, with one mature strand incorporated into the RNA-induced silencing complex (RISC) containing Argonaute (Ago) proteins and TRBP. This complex guides the silencing of target mRNA to regulate gene expression.

During pri-miRNA processing, DROSHA and DGCR8 specifically recognize double-stranded RNA (dsRNA) structures within hairpins. Remarkably, both proteins act as rulers, cleaving substrates at specific sites. DROSHA cleaves hairpins around 11 base pairs away from the basal junction of dsRNA and single-stranded RNA (ssRNA), as well as around 22 base pairs from the apical junction between the terminal loops and dsRNA(152, 153). Additional motifs located on basal ssRNA and terminal loops can significantly enhance DROSHA cleavage. CNNC motifs located about 17-18 nucleotides downstream of the 3p mature miRNA in a subset of pri-miRNAs recruit splicing factor SRSF3 and helicase DDX17, facilitating DROSHA processing efficiency(154, 155). Similarly, UG motifs at basal and UGU/GUG/UGUG motifs at apical terminal loops were found to positively regulate pri-miRNA cleavage by DROSHA, although these motifs are only present in a small percentage of miRNAs.(156)

1.6.2 DROSHA in transcription regulation and RNA processing

Apart from its canonical role in miRNA processing, DROSHA is involved in transcriptional regulation in both positive and negative manners. Chromatin

immunoprecipitation (ChIP) coupled with quantitative PCR/sequencing data have revealed that DROSHA localizes to promoter regions. It has been observed that promoter bound DROSHA can activate transcription independently of miRNA processing. Knockdown (KD) of DROSHA does not lead to miRNA downregulation but significantly inhibits transcription of certain genes, including GAPDH, TAF7, and PTB.(157) Additionally, co-immunoprecipitation (Co-IP) results suggest an interaction between DROSHA and CBP80, a component of the cap-binding complex. KD of CBP80 also inhibits gene transcription, indicating that CBP80 functions in the same pathway as DROSHA to positively regulate transcription.

Interestingly, DROSHA has been found to facilitate premature termination of transcription at promoter regions(158). Using an HIV promoter model, DROSHA and DGCR8 were shown to repress the transcriptional activity of the promoter. KD of these two factors enhanced transcription of an HIV promoter-driven luciferase construct and increased RNA polymerase II (Pol II) enrichment at active transcription regions. DROSHA was found to recruit several proteins known to terminate transcription, including XRN2, SETX, and Rrp6, to promoters, suggesting that DROSHA collaborates with these factors to promote premature transcription termination(158). Additionally, DROSHA was demonstrated to facilitate the termination of lncRNA transcription(159). Importantly, it was observed that DROSHA, rather than canonical cleavage and polyadenylation (CPA), terminates the transcription of lncRNAs containing miR-122. Chromatin RNA sequencing (RNA-seq) data revealed that DROSHA and DGCR8 can terminate the majority of long ncRNAs containing miRNA sequences. Knockdown of Dicer did not affect this process, indicating that microprocessor complex-mediated RNA cleavage is essential for lncRNA transcription termination, which is miRNA-independent.

Furthermore, DROSHA also regulates alternative splicing(160). The exon 5 of the eukaryotic translation initiation factor 4H (eIF4H) gene transcript forms a hairpin structure that can be recognized by DROSHA and DGCR8. KD of DROSHA enhances the splicing of exon 5, which is independent of its RNA cleavage function. Additionally, DROSHA can modulate its own splicing. In this scenario, DROSHA recognizes the junction of exon 7 and intron 7, promoting exon skipping and facilitating the generation of alternative transcripts.

1.6.3 DROSHA in maintenance of genome integrity

Recent studies have highlighted DROSHA's significant contributions to maintaining genome stability and the DNA damage response (DDR) process(70, 161). One intriguing finding is that DROSHA regulates the activities of transposable elements. Knockdown (KD) of DROSHA leads to a notable increase in LINE-1 and Alu retrotransposon levels, suggesting its role in suppressing these potentially disruptive elements in the genome(162, 163). Moreover, DROSHA has been associated with nucleotide excision repair (NER), a crucial mechanism for repairing UV-induced DNA damage. Depletion of DROSHA renders cells more sensitive to UV-C and UV-B radiation, highlighting its involvement in facilitating NER(164). Strikingly, overexpression of DROSHA, even when lacking dsRNA binding activity (ΔC114) and miRNA processing ability, rescues the UV hyposensitivity phenotype. This implies that DROSHA's functions in the DDR are independent of its well-known miRNA-related activities.

Notably, recent studies have shed light on the critical role of DROSHA in the

response and repair of DSBs. It has been observed that DROSHA can localize to DSBs in a manner dependent on the MRN complex, which is an essential player in DSB recognition and repair(165). This localization of DROSHA to DSB sites has been linked to the efficient functioning of the NHEJ repair pathway. Furthermore, DROSHA knockdown not only impairs NHEJ but also disrupts HR efficiency. Specifically, silencing of DROSHA results in diminished recruitment of key repair factors, such as 53BP1, BRCA1, and RAD51, to DSB sites(71, 161). The depletion of DROSHA has also been associated with the formation of shorter single-stranded DNA (ssDNA) overhangs, a crucial step in the end resection process essential for HR. Additionally, DROSHA has been identified as a driver of R-loop formation around DSBs, although the precise molecular mechanism underlying this phenomenon remains poorly understood.

2. Methods and Materials

2.1 Tissue Culture

2.1.1 List of cell lines

Name of Cell lines	Organism	Tissue	Source
HEK293T	Homo sapiens, human	Embryonic kidney	ATCC, CRL-3216
HeLa	Homo sapiens, human	Human cervical adenocarcinoma	ATCC, CCL-2
U2-OS	Homo sapiens, human	Osteosarcoma; Bone	ATCC, HTB96
AsiSI-ER U2-OS	Homo sapiens, human	Osteosarcoma; Bone	A gift from Dr. Xingzhi Xu
DR-GFP U2-OS	Homo sapiens, human	Osteosarcoma; Bone	A gift from Dr. Xingzhi Xu
EJ5-GFP U2-OS	Homo sapiens, human	Osteosarcoma; Bone	A gift from Dr. Gaelle Legube
HCT116	Homo sapiens,	colorectal	ATCC, CCL-247

	human	carcinoma; Colon	
HCT 116 DROSHA -/-	Homo sapiens, human	colorectal carcinoma; Colon	A gift from Dr.V. Narry Kim

2.1.2 Culture Conditions

All human cell lines applied in this study (HEK293T, HeLa, U2OS, DR-U2OS, EJ5-U2OS, AsiSI-ER) were cultured in DMEM media (Thermo Fisher Scientific) supplemented with 10%-20% fetal bovine serum, L-glutamine, and penicillin/streptomycin. All human tissues were cultured under the conditions of 37℃ and 5% CO_2.

2.2 Experimental techniques

2.2.1 Subcellular fraction

The cells were washed twice with ice-cold PBS, scraped, and harvested. The collected cells were then transferred to 1.5 ml Eppendorf tubes. To lyse the collected cells, 5 volumes of cell lysis buffer (5 mM Tris-HCl pH 8.0, 85 mM KCl, 0.5% NP-40, 1x protease inhibitor cocktail (Roche), and 1x phosphatase inhibitor) were added, and the mixture was kept on ice for 10 minutes. Afterward, the lysed cells were centrifuged at 500x g for 5 minutes. The supernatant obtained from the centrifugation was collected as the cytoplasmic fraction, while the nuclei pellet was washed twice with cell lysis buffer without NP-40. Subsequently, the nuclei pellet was lysed in two volumes of

nuclei lysis buffer (10 mM Tris-HCl pH 7.5, 200 mM NaCl, 2.5 mM MgCl2, 0.2% sodium deoxycholate [NaDOC], 0.1% SDS, 0.05% sodium lauroyl sarcosinate [Na sarkosyl], and 0.5% Triton X-100, 1x protease inhibitor cocktail (Roche), and 1x phosphatase inhibitor). The lysed nuclei were then diluted 1:4 in dilution buffer (10 mM Tris-HCl pH 7.5, 200 mM NaCl, 2.5 mM MgCl2, 0.5% Triton X-100, 1x protease inhibitor cocktail (Roche), and 1x phosphatase inhibitor).

2.2.2 S9.6 Immunoprecipitation

The protocol for this assay was previously described(166). In brief, nuclei from ionizing radiation-treated or non-treated HEK293T cells were extracted using cell lysis buffer (5 mM PIPES pH 8.0, 0.5% NP-40, and 85 mM KCl, 1x protease inhibitor cocktail (Roche), and 1x phosphatase inhibitor) on ice for 10 minutes. The isolated nuclei were then resuspended in nuclear lysis buffer (10 mM Tris-HCl pH 7.5, 200 mM NaCl, 2.5 mM MgCl2, 0.2% sodium deoxycholate [NaDOC], 0.1% SDS, 0.05% sodium lauroyl sarcosinate [Na sarkosyl], and 0.5% Triton X-100, 1x protease inhibitor cocktail (Roche), and 1x phosphatase inhibitor) and subjected to 10 minutes of sonication using the Diagenode Bioruptor. The extracts were then precleared by adding Protein G dynabeads, followed by overnight immunoprecipitation with S9.6 antibodies in a cold room. Protein G dynabeads were added to bind with the antibody, and the samples were washed four times with dilution buffer and twice with dilution buffer without Triton X-100. The beads were then either eluted in 2x Laemmli buffer (0.1 M Tris-HCl, 4% (w/v) SDS, 20% glycerol, 10% (v/v) β-Mercaptoethanol, 0.005% bromophenol blue) and incubated at 70 °C for 20 minutes or further prepared for MS.

2.2.3 Silver staining

Nuclear extracts or IP samples were incubated in 2x Laemmli buffer (0.1 M Tris-HCl, 4% (w/v) SDS, 20% glycerol, 10% (v/v) β-Mercaptoethanol, 0.005% bromophenol blue) at 95 ℃ for 10 minutes. The samples were then loaded into 4-15% Mini-Protean TGX gels (Bio-Rad) and electrophoresed in 1x running buffer at 120V for 1 hour. Subsequently, the gels were washed twice with water and fixed in a solution of 30% ethanol:10% acetic acid (6:3:1 water:ethanol: acetic acid) for 15 minutes each. Afterward, the gels were washed twice with 10% ethanol and water, respectively, before being incubated with the silver stain working solution for 30 minutes. Finally, the gels were incubated with the developing solution until protein bands appeared.

2.2.4 Western Blotting

Whole-cell extracts, nuclear extracts, or IP samples were incubated in 2x Laemmli buffer (0.1 M Tris-HCl, 4% (w/v) SDS, 20% glycerol, 10% (v/v) β-Mercaptoethanol, 0.005% bromophenol blue) at 95 ℃ for 10 minutes. The protein samples were then separated by their molecular weight through gel electrophoresis, and the proteins on the gels were transferred onto nitrocellulose membranes using a Bio-Rad machine at 25V, 2.5 A for 10 minutes. Ponceau S staining of the membranes was performed to check the transfer efficiency. Subsequently, the membranes were blocked in 5% milk in PBS with 0.2% Tween-20 (PBST) at room temperature for 1 hour before incubating with primary antibodies overnight in a cold room. Afterward, the membranes were washed three times in PBST for 5 minutes each and then incubated with secondary antibodies at room temperature for 1 hour. Following that, the membranes were

washed three times in PBST before adding the ECL substrate. The signals were visualized on Amersham™ Hyperfilm™ ECL (Cytiva)

2.2.5 Mass Spectrometry

Beads were subjected to a series of washes, including two washes in cold dilution buffer and two washes in cold PBS. The elution of proteins from the beads was carried out using 0.2M Glycine (pH 2) for 7 minutes at 4°C, followed by neutralization with 1M Tris (pH 8). This elution step was repeated twice to ensure efficient protein recovery. For in-solution protein samples, denaturation was performed using 4M urea in ammonium bicarbonate buffer (100 mM) at room temperature for 10 minutes. Subsequently, cysteine residues were reduced using TCEP (10 mM) for 30 minutes at room temperature, followed by alkylation with 2-Chloroacetamide (50 mM) for 30 minutes at room temperature in the dark. Pre-digestion was carried out with LysC enzyme (1 g/100 g of sample) for 2 hours at 37°C. This was followed by overnight digestion with trypsin enzyme (1 g/40 g of sample) at 37°C. The urea concentration was reduced to 2M in ammonium bicarbonate buffer (100 mM), and calcium chloride was added at a final concentration of 2 mM before the trypsin digestion. On the next day, trypsin digestion was stopped by the addition of formic acid (5%). The digested peptides were centrifuged at 13,200rpm at 4°C for 30 minutes to remove any undigested material. The supernatant containing the peptides was loaded onto a handmade C18 stage tip, which had been pre-activated with 100% acetonitrile, and centrifuged at 4,000 rpm at room temperature. The peptides were washed twice with TFA 0.1% and then eluted using 50% acetonitrile / 0.1% TFA. The eluted peptides were dried using a speed vacuum. Prior to liquid

chromatography coupled with tandem mass spectrometry analysis (LC-MS/MS), the peptides were resuspended in 2% acetonitrile / 0.1% formic acid.

Peptides were then trapped on an Acclaim™ PepMap™ 100 C18 HPLC Columns (PepMapC18; 300µm x 5mm, 5µm particle size, Thermo Fischer) using solvent A (0.1% Formic Acid in water) at a pressure of 60 bar and separated on an Ultimate 3000 UHPLC system (Thermo Fischer Scientific) coupled to a QExactive mass spectrometer (Thermo Fischer Scientific). The peptides were separated on an Easy Spray PepMap RSLC column (75µm i.d. x 2µm x 50mm, 100 Å, Thermo Fisher) and then electrospray directly into an QExactive mass spectrometer (Thermo Fischer Scientific) through an EASY-Spray nano-electrospray ion source (Thermo Fischer Scientific)using a linear gradient (length: 60 minutes, 5% to 35% solvent B (0.1% formic acid in acetonitrile and 5% dimethyl sulfoxide), flow rate: 250 nL/min). The raw data was acquired on the mass spectrometer in a data-dependent mode (DDA). Full scan MS spectra were acquired in the Orbitrap (scan range 380-1800 m/z, resolution 70000, AGC target 3e6, maximum injection time 100 ms). After the MS scans, the 15 most intense peaks were selected for HCD fragmentation at 28% of normalized collision energy. HCD spectra were also acquired in the Orbitrap (resolution 17500, AGC target 1e5, maximum injection time 128 ms) with first fixed mass at 100 m/z.

2.2.6 Proximity Ligation Assay (PLA)

These experiments were performed following the manufacturer's instructions. Specifically, cells were fixed with a 4% paraformaldehyde solution at room

temperature for 10 minutes, followed by washing with PBS and a 10-minute lysis step using 0.2% Triton-X 100. Subsequently, the cells were blocked in PLA blocking buffer at 37℃ for 1 hour, and then primary antibodies were diluted and incubated with the samples overnight in a cold room. The primary antibodies were captured by PLA probes, which were then ligated using a ligase, followed by amplification using a polymerase.

For S9.6-related PLA, cells were pre-extracted with CSK buffers (10 mM PIPES, 100 mM NaCl, 300 mM Sucrose, 3 mM MgCl2, 1 mM EGTA, 0.7% Triton X-100, 1x protease inhibitor cocktail) in a cold room for 15 minutes before fixation with 4% PFA, as described in a previous report. After fixation, each sample required a 1-hour incubation at room temperature with the RNase treatment solution (0.1% BSA, 3 mM MgCl2, 1:200 (v/v) RNAse T1, 1:200 (v/v) ShortCut RNAse III in PBS).

2.2.7 Laser Micro-irradiation

Cells were transfected with GFP- or mCherry-tagged plasmids related to the study 72 hours prior to the experiments. Subsequently, the cells were seeded on glass-bottomed dishes (NEST) and pre-treated with 10 μM BrDU 24 hours before irradiation. DNA damage was induced by applying a UV laser (16 Hz pulse, 40% laser output) generated from the Micropoint System (Andor). Live-cell images were captured using a Nikon A1 confocal imaging system at intervals of 5 or 10 seconds. The images were then analyzed using ImageJ, and the intensities of the damaged, non-damaged, and background areas were measured to calculate the relative intensities of the stripped areas.

2.2.8 Chromatin Immunoprecipitation (ChIP)

AsiSI-ER U2OS cells were treated with 400 nM 4-Hydroxytamoxifen (4-OHT) 4 hours prior to fixation with a 1% formaldehyde solution for 10 minutes. The fixed cells were then quenched with 125 mM glycine at room temperature for 10 minutes and scraped at a cold room. Subsequently, the tissues were lysed in the aforementioned cell lysis buffer and nuclei lysis buffer (50 mM Tris-HCl pH 8.0, 1% SDS, and 10 mM EDTA) on ice and sonicated for 15 minutes. The samples were then cleared and diluted using dilution buffer (16.7 mM Tris-HCl pH 8.0, 0.01% SDS, 1% Triton-X 100, 167 mM NaCl, 1 mM EDTA) at a 1:4 ratio. Antibodies and beads were added for immunoprecipitation, and the beads were washed once with washing buffers A (20 mM Tris-HCl, 2 mM EDTA, 0.1% SDS, 1% Triton X-100, 150 mM NaCl), B (20 mM Tris-HCl, 2 mM EDTA, 0.1% SDS, 1% Triton X-100, 500 mM NaCl), C (10 mM Tris-HCl, 1 mM EDTA, 1% NP-40, 1% sodium deoxycholate, 0.25 M LiCl) and twice in washing buffer D (10 mM Tris-HCl, 1 mM EDTA) before elution in ChIP elution buffer (1% SDS and 100 mM NaHCO3) at room temperature for 30 minutes. The eluted samples were then de-crosslinked at 65℃ overnight, and the immunoprecipitated DNAs were extracted using the Phenol-Chloroform extraction method for subsequent qPCR and sequencing experiments. For primers, refer to Table S1.

2.2.9 ChIP-seq library preparation

ChIP-seq libraries were prepared using the KAPA HTP Library Preparation Kit complemented with NEXTflex DNA Barcodes from Bioo Scientific. 10 ng of DNA

was used as starting material for input and ip samples. Libraries were amplified using 13 cycles on the thermocycler. Post-amplification libraries were size selected at 250-450bp in length using Agencourt AMPure XP beads from Beckman Coulter. Libraries were validated using the Agilent High Sensitivity DNA Kit.

2.2.10 Chromatin RNA extraction

Chromatin RNA extraction was performed using a published protocol(167). Briefly, AsiSI-ER U2OS cells were harvested, and nuclei were isolated by lysing the cells in HLB+N buffer (10 mM Tris-HCl pH 7.5, 10 mM NaCl, 2.5 mM MgCl2, and 0.5% (vol/vol) NP-40) followed by centrifugation. The samples were then resuspended in NUN1 buffer (20 mM Tris-HCl pH 8.0, 75 mM NaCl, 0.5 mM EDTA, and 50% (vol/vol) glycerol), and chromatin was extracted by adding NUN2 buffer (20 mM HEPES-KOH pH 7.6, 300 mM NaCl, 0.2 mM EDTA, 7.5 mM MgCl2, 1% (vol/vol) NP-40, and 1 M urea) followed by centrifugation. The chromatin pellets were then dissolved in TRIzol, and the chromatin-bound RNA was isolated by adding chloroform.

2.2.11 Total RNA extraction

Cell pellets were resuspended and lysed using TRIzol LS Reagent (Invitrogen) to release RNA into the solution. The samples were then incubated at room temperature for 15 minutes after the cell pellets were completely dissolved in the TRIzol solution. Total RNA present in the TRIzol reagent was extracted using Phenol-Chloroform methods following the manufacturer's instructions. The concentrations of the RNA

samples were measured using a NanoDrop™ Lite Spectrophotometer (Thermo Fisher Scientific).

2.2.12 qRT-PCR

1 µg purified mRNA or chromatin-bound RNA was set as the template of reverse transcription and mixed with oligo dT or site-specific primers respectively. SuperScript™ Reverse Transcriptase (Thermo Fisher Scientific) was then added to initiate the reverse transcription. Real-time PCR was performed on a Rotor-Gene RG3000 machine (Corbett Research) with SensiMix™ SYBR No-Rox Mastermix (Bioline Reagents) and sequence-specific primer pairs.

2.2.13 MNase Chromatin Accessibility Assay

Cells were collected in clean Eppendorf tubes and lysed in buffer A (50 mM Tris-HCl pH 8.0, 0.1% Triton-X 100, 150 mM NaCl, 1 mM EDTA) to extract chromatin. The chromatin pellets were then resuspended in digestion buffer (15 mM Tris-HCl pH 7.5, 60 mM KCl, 15 mM NaCl, 0.25 M Sucrose, 1 mM CaCl2, 0.5 mM DTT) containing 100 units of MNase (NEB) and incubated at 37℃ for 5 minutes. The digested chromatin was then treated with Protease K and RNase A to remove proteins and RNA. The DNA was subsequently purified using Phenol-Chloroform extraction methods and separated by 1.2% agarose gel electrophoresis.

2.2.14 PH2B-PAGFP Chromatin Relaxation Assay

Wild-type U2OS cells were transfected with PH2B-PAGFP plasmids(86), which encode photoactive H2B, 96 hours prior to laser micro irradiation. Then, 48 hours prior to laser micro irradiation, siRNA against GATAD2B was transfected. One hour before laser micro irradiation, all cells were treated with 0.3 µg/ml Hoechst 33342 for 1 hour at 37°C. Just before imaging, the growth medium was replaced with phenol red-free Leibovitz's L-15 medium (Life Technologies) supplemented with 20% FBS, 2 mM glutamine, 100 µg/ml penicillin, and 100 U/ml streptomycin. The chromatin relaxation was recorded and imaged using an Olympus live cell imaging microscope. The thickness of laser stripes was then calculated as the relative chromatin relaxation, normalized to the thickness of stripes just after laser micro irradiation.

2.2.15 Genomic DNA extraction

HeLa cells were transfected with plasmids encoding IPpoI-ER. After 48 hours of transfection, the cells were treated with 2 µM 4-OHT for 3 hours. Following the treatment, the culture media was replaced with 4-OHT-free DMEM media, and the cells were further cultured for 6 hours. Subsequently, the cells were trypsinized and lysed using nuclear lysis buffer (0.5% SDS, 150 mM NaCl, and 50 mM Tris-HCl pH 8.0) containing protease K and RNase A. The lysis was performed at 50 °C overnight to allow for genomic DNA extraction. The genomic DNA was then extracted using the Phenol-Chloroform method, and qPCR was performed to analyze specific regions of interest.

2.2.16 HR and NHEJ reporter Assay

DR-U2OS or EJ5-U2OS reporter cell lines were transfected with siRNA using Lipofectamine RNAi Max (Life Technologies) 48 hours prior to I-SceI lentivirus transduction. After being infected with lentivirus containing I-SceI, the reporter cell lines were cultured at 37°C for 48 hours before being trypsinized and resuspended in PBS. The samples were then analyzed using a BD Accuri C6 flow cytometer, and the percentage of GFP-positive cells was determined.

2.2.17 Immunofluorescence

Cells were seeded on glass-bottomed dishes or coverslips 24 hours prior to ionic irradiation, as described earlier. Following CSK pre-extraction and fixation, coverslips were blocked with 3% BSA at 37°C for 1 hour. Subsequently, the samples were incubated with primary antibodies overnight at a cold room, followed by incubation with secondary antibodies at 37°C for 1 hour. Afterward, the cells were mounted on slides using Fluoroshield Mounting Medium with DAPI (Abcam). Images were acquired using an Olympus Fluoview FV1200 confocal microscope.

2.2.18 Comet Assay

The assay was conducted following the instructions provided by the manufacturer (bio-techne). In brief, 5 × 10^3 cells in 5 µl PBS were mixed with 50 µl of molten LMAgarose at 37°C and spread onto CometSlides. The CometSlides were then transferred to 4°C. Following that, the slides were lysed in lysis buffer (containing 2.5

M NaCl, 100 mM Na2EDTA, and 10 mM Tris, with a final pH of 10.0) supplemented with 10% DMSO and 1% Triton-X 100 at 4°C for at least 2 hours. Next, the samples were immersed in electrophoresis buffer (containing 300 mM NaOH, 1 mM EDTA) to allow DNA unwinding for 30 minutes. Electrophoresis was carried out at 21V and 200 mA under cold conditions. Following electrophoresis, the slides were washed four times and stained with Propidium Iodide for 30 minutes before being imaged using a fluorescence microscope.

2.3 Quantification and Statistical Analysis

2.3.1 Statistical analysis of real-time PCR results

The real-time PCR (qPCR) results were analyzed using the raw take-off (Ct) values, which were determined as the median of two or three technical replicates. The delta-delta Ct method was applied to calculate the percentage of input or the relative fold change. Statistical analysis was conducted using the GraphPad Prism8 software.

Unless specified otherwise, two-tailed Student's t-tests were employed to determine significant differences. A significance level of $P < 0.05$ was considered indicative of a significant difference.

2.3.2 Quantification and statistical analysis of Immunofluorescence and PLA Results

For IF and PLA, at least fifty cells were analyzed. Foci numbers were quantified by

cell profiler software. For laser, fluorescence intensity was measured by the software ImageJ. Unless indicated, two-tailed Student's t-tests were applied for statistical analysis, while * refers to $p < 0.05$, ** refers to $p < 0.01$, *** refers to $p < 0.001$ and **** refers to $p < 0.0001$.

2.4 Bioinformatic analyses

2.4.1 ChIP-Seq data processing

GATAD2B +4OHT, GATAD2B -4OHT, HDAC1 +4OHT, and HDAC1 -4OHT samples were sequenced using Illumina NextSeq 500 (single end 151 bp reads). The read quality of the fastq files was checked using FastQC (https://www.bioinformatics.babraham.ac.uk/projects/fastqc/) before and after adapter trimming. The trimmed reads were then mapped to the hg19 genome following the standard ChIP seq-pipeline. The classic ChIP-seq pipeline consists of BWA (http://bio-bwa.sourceforge.net/) for alignment and samtools (http://www.htslib.org/) for duplicate removal (rmdup), sorting (sort), and indexing (index). deepTools (https://deeptools.readthedocs.io/en/develop/)(168) bamCompare was used to calculate log2 fold change at each nucleotide position between +4OHT and -4OHT for GATAD2B and HDAC1 samples. Read count normalization was applied as part of bamCompare to normalize for sequencing depth between samples. H4K12Ac +4OHT and H4K12Ac -4OHT Chip-seq samples from (135) (E-MTAB-5817) were processed using the same approach for downstream analysis plots.

RNA Pol II S5p ChIP from a previous study(112) (E-MTAB-6318) was processed using the classical ChIP pipeline as well. Read count coverage was calculated for each

of the 80 inducible DSB sites (+-5kb) using bedtools multicov (https://bedtools.readthedocs.io/en/latest/)(Quinlan and Hall, 2010). The top 20 sites with the highest coverage were annotated as high transcriptional activity and the bottom 20 as low transcriptional activity.

2.4.2 BLESS Seq data processing

BLESS Seq (E-MTAB-5817) was processed using the same protocol as detailed in a previous publication(135). Read count coverage was calculated for all annotated DSBs (+-500bp) using bedtools multicov. The sites were then ordered based on read count coverage for representing the cleavage efficiency of DSB sites.

2.4.3 DRIP-Seq data processing

DRIP Seq samples +/- 4OHT from a previous research work(112) (E-MTAB-6318) were processed using the classical ChIP pipeline. Log2 Fold Change was calculated using bamCompare at each nucleotide position with read count normalization. bamCompare outputs were exported as bigwig files for further downstream analysis.

2.4.4 Metagene Profiles

computeMatrix operation of deepTools was used to calculate the average profile of log2Fold Change (+4OHT/-4OHT) from the bigwig files generated using bamCompare. The bin size was set to 500 and region length was set to +-10kb with

reference to DSB. The average profile matrices created for GATAD2B, HDAC1, and DRIP-Seq were then combined and plotted using the Matplotlib package of Python.

2.4.5 BoxPlots

Read count coverage around DSBs (+/- 2.5 kb) was calculated using bedtools multicov and then normalized to CPM using the total read count of the respective sample. The plots were made with the matplotlib package of Python. The Wilcoxon two-sample test was used to determine statistical significance with a p-value cut-off set at 0.01. Statistical tests were run using the scipy python package.

2.4.6 IGV profiles and Heatmaps

Coverage files containing CPM normalized read count per nucleotide position were generated for each sample using deep tools bamCoverage. The coverage files were exported in bigwig format and loaded into the IGV browser (https://software.broadinstitute.org/software/igv/) for visualizing the normalized read density around break sites.

The coverage files were also used to make the heatmaps comparing cleavage efficiency and read density of HDAC1 and GATAD2B around DSB in 4OHT-treated samples. plotHeatmap function of deepTools was used to make the heatmaps with regions set as all annotated DSBs arranged in ascending order of cleavage efficiency.

2.4.7 Analysis of Mass Spectrometry results

The acquired QExactive Raw MS data were processed by MaxQuant (version 1.5.0.35i) for peak detection and quantification. MS spectra were searched against the database was processed by the freely available MaxQuant software package. This software package is capable of identifying and quantifying most types of mass spectrometry data. Data were searched against the Uniprot homo sapiens [UPR_Homo sapiens_9606_UP000005640] alongside a list of common contaminants provided by the software. The search parameters for the Andromeda search engine (within MaxQuant) were full tryptic specificity, allowing two missed cleavage sites, the fixed modification was set to carbamidomethyl, (C) and the variable modification to acetylation (protein N-terminus), oxidation (M). Match between runs was applied. All other settings were set to default leading to a Protein discovery rate (FDR) of 0.01. The 'Intensity' columns for all samples were subjected to a log2 transformation and, subsequently, normalization of each column was achieved by subtracting the median intensity from each protein intensity.

2.5 List of Antibodies

Antibodies	Manufacturer	Identifier
Rabbit-Anti-GATAD2B	Abcam	Ab76925
Rabbit-Anti-MBD3	Abcam	Ab157464

Mouse Anti-HDAC1	Santa Cruz	Sc-81598
Anti-phospho-Histone H2A.X (Ser139), clone JBW301	Merck Millipore	05-636
Anti-Phospho-Histone H2A.X (Ser139) (20E3) Rabbit mAb	Cell Signaling Technology	9718S
Anti-DNA-RNA Hybrid Antibody, clone S9.6, mouse monoclonal	Merck	MABE1095
Anti-DNA–RNA hybrid antibody, clone S9.6, rabbit monoclonal	Absolute Antibody	Ab01137-23.0
Histone H3ac (pan-acetyl) antibody, Rabbit polyclonal	Active Motif	39140
Histone H4ac (pan-acetyl) antibody, Rabbit polyclonal	Active Motif	39043
Anti-Histone H3	Abcam	Ab1791
Anti-Histone H4 Polyclonal antibody	Proteintech	16047-1-AP
Anti-beta Tubulin antibody	Abcam	Ab6046
Anti-RNA polymerase II CTD	Abcam	Ab26721

repeat YSPTSPS antibody		
Anti-RNA polymerase II CTD repeat YSPTSPS (phospho S2) antibody	Abcam	Ab5095
Anti- XRN2 Antibody (H-3)	Santa Cruz	sc-365258
Anti-BrdU antibody, Mouse monoclonal	Sigma	B-8434
Anti-Rad51 Antibody	Abcam	Ab63801
Anti-V5 tag antibody [SV5-P-K]	Abcam	Ab206566
Donkey Anti-Rabbit IgG (H+L) Highly Cross-Adsorbed Secondary Antibody, Alexa Fluor™ 488	Thermo Fisher	A-21206
Donkey anti-Mouse IgG (H+L) Highly Cross-Adsorbed Secondary Antibody, Alexa Fluor™ 555	Thermo Fisher	A-31570
Rabbit anti-Phospho RPA32 (S4/S8) Antibody	Bethyl Laboratories	A300-245A
Anti-RNA Helicase A (DHX9)	Abcam	ab26271

Anti-DROSHA Antibody	Abcam	ab12286
Anti-RNA Pol II Antibody (8WG16)	Abcam	ab817
Anti-RNA Pol II S2P Antibody	Abcam	ab5095
Anti-RNA Pol II Y1P Antibody	Active Motif	61383

2.6 List of Reagents

Names	Manufacturer	Identifier
Triptolide	Cayman Chemical	CAY11973
DRB	Cayman	10010302
Olaparib	Cayman	CAY-10621
4-OHT	Cayman	CAY-14854
5-Bromo-2'-deoxyuridine (5-BrDU)	Sigma	B-5002
RNaseH	New England Biolabs	M0297S
Lipofectamine 3000	Thermo Fisher	L3000008

Lipofectamine RNAiMAX	Thermo Fisher	13778075
Hoechst 33342	Thermo Fisher	R37605
Dynabeads Protein A	Thermo Fisher	10002D
Micrococcal Nuclease	New England Biolabs	M0247S
Dynabeads Protein G	Thermo Fisher	10004D
Duolink In Situ Red Starter Kit Mouse/Rabbit	Sigma	DUO92101-1KT
CometAssay Electrophoresis Starter Kit	Bio-Techne	4250-050-ESK

2.7 List of Plasmids

Names	Source	Identifier
ppyCAG_RNaseH1_WT	Addgene	#111905
pCMV-mCherry-RNaseH1	This Study	N/A
pCMV-GFP-MBD3	This Study	N/A

pCMV-GFP-GATAD2B	This Study	N/A
pH2B-PAGFP	Dr. Rebecca Smith	N/A
pBABe-HA-IPpOI-ER	Addgene	#32565

2.8 List of Oligonucleotides

2.8.1 List of siRNA

Names	Manufacturer	Identifier
SiGATAD2B siGENOME SMARTPOOL	Dharmacon	M-013892-01-0010
SiMBD3 siGENOME SMARTPOOL	Dharmacon	M-013616-01-0010
ON-TARGETplus Non-targeting Control	Dharmacon	D-001810-01-20

2.8.2 List of primers

Name	Sequences (5'-3')
DROSHA-F	GAGACCTAGCCTAGTTTTCCTG

DROSHA-R	AATGCACATTCACCAAAGTCAA
GAPDH-F	AACCTGCCAAATATGATGAC
GAPDH-R	AGGAAATGAGCTTGACAAAG
7SK-F	AGGACCGGTCTTCGGTCAA
7SK-R	TCATTTGGATGTGTCTGCAGTCT
RBMXL1-qF	CGCACCGGATAGCATGTTT
RBMXL1-qR	TACTGCGCAATCTGGATGCT
CCNB1-qF	AAGAGCAAGCAGTCAGACCA
CCNB1-qR	TGGTCTCCTGCAACAACCTG
28s-F	TTCCCTCCGAAGTTTCCCTC
28s-R	ACTAGGCACTCGCATTCCAC
RBMXL1-NF	TTGTTAAAGTTGGCTTGCTTGGG
RBMXL1-NR	TGGTGACAGTGGCTTCATGG
CCNB1-NF	AATGCCTGCAAATGCCTGGT
CCNB1-NR	AGCTGTGGTAGAGTGCTGATCTT

DS2 +0.3-F	CCAGCAGTAAAGGGGAGACAGA
DS2 +0.3-R	CTGTTCAATCGTCTGCCCTTC
DS2 +1.8-F	GAAGCCATCCTACTCTTCTCACCT
DS2 +1.8-R	GCTGGAGATGATGAAGCCCA
DS2 +3.6-F	GCCCAGCTAAGATCTTCCTTCA
DS2 +3.6-R	CTCCTTTGCCCTGAGAAGTGA
DS1 +0.3-F	AGGACTGGTTTGCAAGGATG
DS1 +0.3-R	ACCCCCATCTCAAATGACAA
DS1 +1.0-F	AGGAATTGACTGCGGTGTTC
DS1 +1.0-R	GGGGAGGAGGAAAGGTGTAG
DS1 +2.0-F	GCCATAACAGAGGGTGGAAA
DS1 +2.0-R	AACTTTAGGATGGGGCTGCT
DS1+3.0-F	TGTAGCCACAGTTTGCCTGT
DS1+3.0-R	CTCCTCTATTGTCACCTGGAAGAC
DS1+5.0-F	GGCCAACATCCCTGATGACTAC

DS1+5.0-R	CACCCTTGCCAGCATTTGTT
Dicer-F	GCACCTTTATGAAGACCCGC
Dicer-R	TACAGCCAGCGATGCAAAGA
actin-F	CACAGAGCCTCGCCTTTGC
actin-R	AATCCTTCTGACCCATGCCC

3. Screening for novel R-loop binding factors related to the DNA Damage Response

3.1 Introduction

R-loops were previously thought to be transcription byproducts, which might lead to blocked and collapsed replication forks, posing a threat to genome stability(103, 104). However, the formation of DNA damage-induced R-loops has also been widely observed as mentioned in Charpter 1. Additionally, these structures are prone to forming within highly transcribed genomic loci(112, 169). It has also been reported that R-loops play positive roles in DDR and facilitate the recruitment of several DDR factors, especially those in the HR pathway(97, 113). However, whether R-loops have other functions in this biological network remains unclear. It has also been shown that R-loops can regulate several biological processes under normal conditions, including transcription regulation and chromatin remodeling(105, 106, 170, 171), both of which are essential steps in DDR(4, 7, 172). Whether R-loops could contribute to regulation of transcription and chromatin remodeling upon DNA damage and how this regulation could facilitate the efficient DNA repair and maintenance of genome stability remains unclear.

To clarify the functions of R-loops in DNA damage response, it is important to screen for proteins that can interact with R-loops, particularly those that exhibit preferential binding upon DNA damage. The S9.6 antibody, known for its specific recognition of DNA: RNA hybrids with an affinity of 0.6 nM (166, 173, 174), can be utilised to detect R-loops *in vivo*. Employing this antibody, I have chosen to isolate the R-loops

interactome under normal conditions and IR treatment, followed by mass spectrometry-based proteomic analysis to identify proteins that exhibit a preferential binding with R-loops upon DNA damage. The results from this analysis contribute to better understanding of the roles of R-loops in DDR.

In addition to the functions of R-loops in DDR, I was keen to investigate the cellular localization of selected potential R-loops binding factors upon DNA damage, as well as their occupancy at DSBs.

3.2 Verification of S9.6 Immunoprecipitation

As mentioned above, the S9.6 antibody that specifically recognizes DNA: RNA hybrids, which was utilized to identify R-loops binding factors in HeLa cells. To verify if known DNA: RNA interacting factors could be captured by this antibody, I tested whether known R-loop interactors could be detected in my IP fractions. Indeed, silver staining of proteins immunoprecipitated with the S9.6 antibody revealed a distinct subset of proteins, which were different from nuclear-extracted input samples. Furthermore, almost no proteins were detectable in the immunoprecipitated samples derived from the negative control (Figure 3-1a), suggesting that the S9.6 antibody pulled down a specific set of proteins. Moreover, I employed immunoblotting analysis and successfully detected previously identified R-loop interactors such as DHX9, H3, and XRN2 in my IP samples (166)(Figure 3-1b). This result indicates that the DNA: RNA hybrid interactome could be effectively precipitated using the S9.6 antibody. Collectively, these results validate the utility of this method in capturing DNA: RNA hybrid interactors.

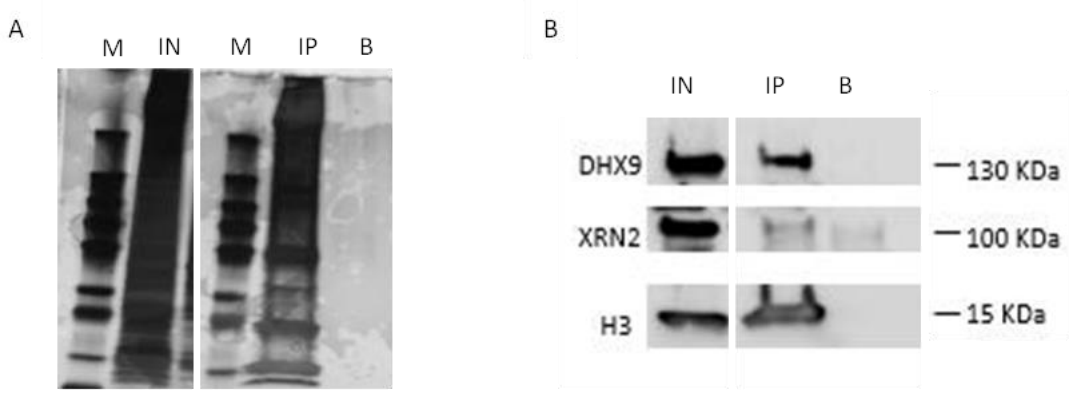


Figure 3-1 Verification of S9.6 Immunoprecipitation. (A) Imaging of silver staining showing that the S9.6 antibody immunoprecipitated a subset of proteins that were different from input and negative control. M, protein marker; IP, the S9.6 IP sample; B, beads only control. (B) Imaging of western blot indicating several known R-loops binding factors, such as DHX9, XRN2, and histone H3 could be detected from S9.6 IP samples but not from negative control samples.

3.3 Screening novel R-loops interactors relevant to DDR

To gain a better understanding of the functions of R-loops in DDR, I employed the S9.6 antibody for mass spectrometry-based proteomics. Specifically, HEK293T cells were subjected to 10 Gy irradiation (IR) and allowed to recover for 20 min. Then, nuclear extracts from control (-IR) and irradiated (+IR) HEK293 cells were incubated with S9.6 antibody to isolate the R-loop interactome in both conditions. I performed silver staining experiments and detected subsets of proteins, which were different from input samples. Additionally, known R-loops interacting factors including DHX9, H3, and XRN2 were also detected in IP samples from both -IR and +IR samples (Figure 3-2). This suggests that R-loops interactome from control and DNA damage conditions were successfully isolated. The IP samples were then applied for mass spectrometry-based proteomics.

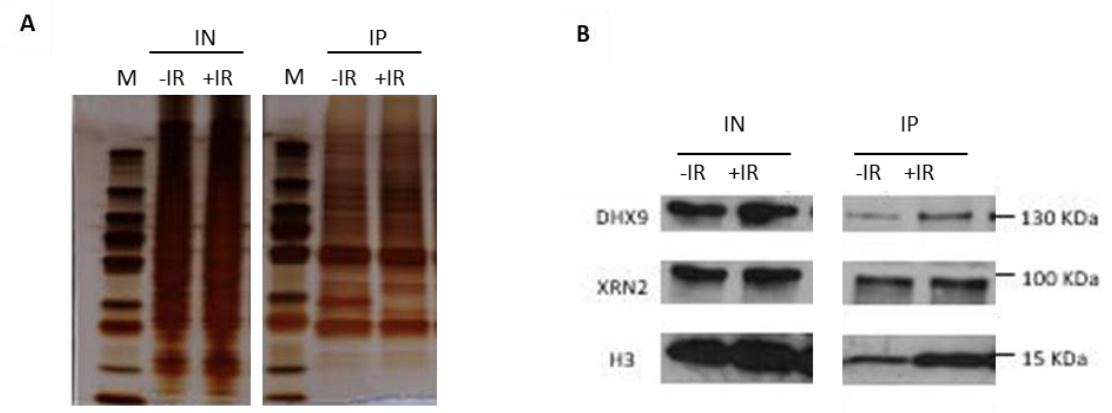


Figure 3-2 Quality control for S9.6 IP-Mass spectrometry samples. (A) Imaging of silver staining showing subsets of complex protein mixtures were observed in both -IR and +IR IP samples, which were different from input. (B) Imaging of western blot indicating that known R-loops binding factors, XRN2, DHX9, and H3 could be detected in both -IR and +IR S9.6 IP samples.

From proteomics analysis, I found that many well-known R-loops interactors, such as DDH5, XRN2, and PARP1 were detected in the control (-IR) sample (Table 3-1). Next, I compared the differences between -IR and +IR samples from two different biological mass spectrometry repeats and identified proteins that were significantly enriched in S9.6 IP samples specifically upon DNA damage (Figure 3-3). As a result, I listed identified potential R-loops interactors in Table 3-2.

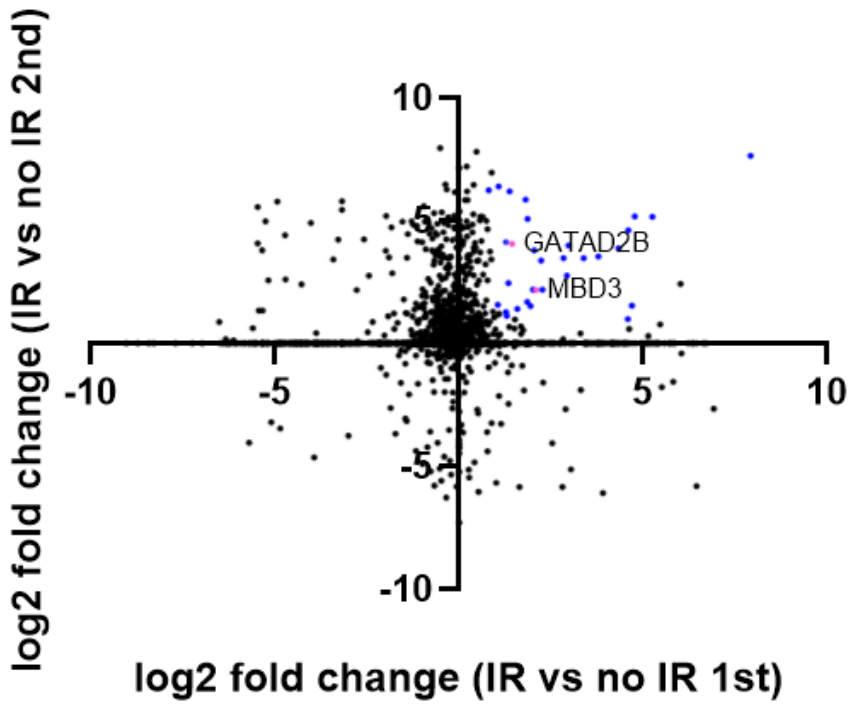


Figure 3-3 Screening of novel R-loops binding factors related to DDR. Volcano plot showing significantly enriched S9.6 binders after IR treatment in two biological replicates of S9.6 IP-Mass Spectrometry samples. Potential candidates with log2 relative fold change compared +IR to -IR samples bigger than 1 in both repeats were labled in blue color, while MBD3 and GATAD2B, both of which are components of NuRD complex, were labeled in pink color to be distinguished.

Table 3-1 Known R-loops binding factors screened from the -IR S9.6 IP Mass spectrometry samples

Name	Intensity
DDX5	6.12E+10
DDX21	5.81E+10
RBM14	3.07E+10
SMARCA5	1.81E+10
XRN2	1.14E+10
PARP1	1.12E+10
ILF3	6.14E+09
CHD4	4.84E+09
RBMX;RBMXL1	1.97E+09
TOP1	1.55E+09
SRSF7	1.22E+09
SRPK1	8.21E+08
WHSC1	6.26E+08
RAD50	4.94E+08
DNMT1	2.8E+08

Table 3-2 Potential novel R-loops binding factors identified from S9.6 IP-Mass spectrometry related to Figure 3-3

Gene name	Average Log2 Fold changes (+IR VS -IR)
IGFN1	10.75378799
TRIM4	7.780150414
PUF60	4.597714424
NOP10	3.916346073
HNRNPL	3.782220364
RUVBL2	3.518584728
RAN	3.48355341
SAFB2	3.428174496
ZNF189	3.157113552
LUC7L3	2.918427467
CRNKL1	2.841762066
BYSL	2.800688267
PCMT1	2.786775112
RBMX	2.751998425
HNRNPDL	2.715929508
PRPF31	2.357191563
PDS5B	2.226240635
SF3A3	2.145429134
MBD3	2.127829075
LMNB2	2.095678329
GATAD2B	1.500137329
HNRNPR	1.27636528
LARP7	1.211964607
PWP2	1.142299652

3.4 Components of NuRD complex were identified as novel R-loops interactors relevant to DDR

Multiple previous reports have suggested that R-loops may regulate transcription and remodel chromatin structure under normal conditions(107-109, 175-177). To determine whether R-loops perform these functions in response to DSBs, I conducted GO and STRING analyses on the screened R-loops interactors listed in Table 3-2. Interestingly, the GO analysis for biological processes indicated that these factors play important roles in RNA processing and gene expression regulation. Additionally, the GO analysis for cellular components and the. STRING analysis revealed an enrichment of proteins involved in histone deacetylase and the NuRD complex (Figure 3-4). Furthermore, I noticed that MBD3 and GATAD2B, both of which are components of the NuRD complex, were enriched in the +IR samples. Hence, these findings suggest that components of the NuRD complex may potentially interact with R-loops in response to DNA damage, thereby identifying them as novel interactors.

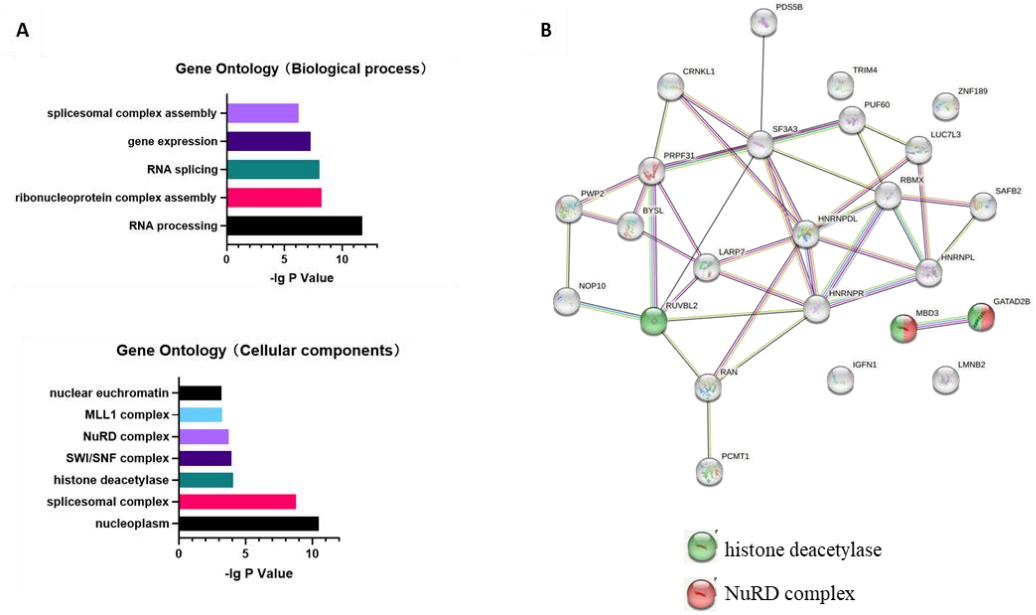


Figure 3-4 Components of NuRD complex were identified as novel R-loops interactors relevant to

DDR. (A) GO analysis proteins listed in Table 3-2, and overrepresented biological processes and cellular components were listed in bar charts, while the x axis indicates the statistical significance of overrepresentation. (B) STRING analysis of proteins from Table 3-2 showing strong interaction between MBD3 and GATAD2B, both of which are components of NuRD complex. NuRD complex and histone deacetylase, which were overrepresented cellular components were marked in red and green respectively.

3.5 Components of NuRD complex interact with R-loops *in vivo*

Mass spectrometry-based proteomics analysis suggested that MBD3 and GATAD2B specifically interact with R-loops in response to DNA damage. To further validate the binding of NuRD components to R-loops in living cells, I employed a proximity ligation assay (PLA). This antibody-based technique enables the detection of interactions between two different proteins or structures that are recognized by primary antibodies in situ with a proximity of less than 40 nm (178, 179). In this assay, primary antibodies from two distinct species were used to recognize the proteins of interest, followed by the addition of oligonucleotide-labeled secondary antibodies (known as PLA probes) that bind to the primary antibodies. If the two recognized proteins are in close proximity (<40 nm), the two probes can be ligated by a ligase, resulting in the generation of circular DNA. The circular DNA can then be amplified by a DNA polymerase and detected using fluorescently labeled complementary oligonucleotide probes. The resulting quantifiable signals can be visualized using microscopy (Figure 3-5A).

Using antibodies against endogenous GATAD2B or MBD3 and S9.6, I detected a significant increase in PLA foci following IR treatment, indicating enhanced interaction between GATAD2B or MBD3 and R-loops (Figure 3-5B and C). Notably,

when RNase H, which can degrade RNA in DNA: RNA hybrids and reduce the levels of R-loops, was overexpressed, the number of GATAD2B-S9.6 or MBD3-S9.6 PLA foci decreased. This confirmed the specificity of the PLA assay and demonstrated that GATAD2B and MBD3 preferentially interact with R-loops *in vivo*. Since subunits HDAC1 or HDAC2 of the NuRD complex possess histone deacetylase activity(180), I also conducted PLA experiments using HDAC1 and S9.6 antibodies. Interestingly, I observed increased co-localization between HDAC1 and DNA: RNA hybrids upon DNA damage, while RNaseH overexpression resulted in a decreased number of HDAC1-S9.6 PLA foci (Figure 3-5D). These results suggest that components of the NuRD complex exhibit a preferential binding to R-loops *in vivo* in response to DNA damage.

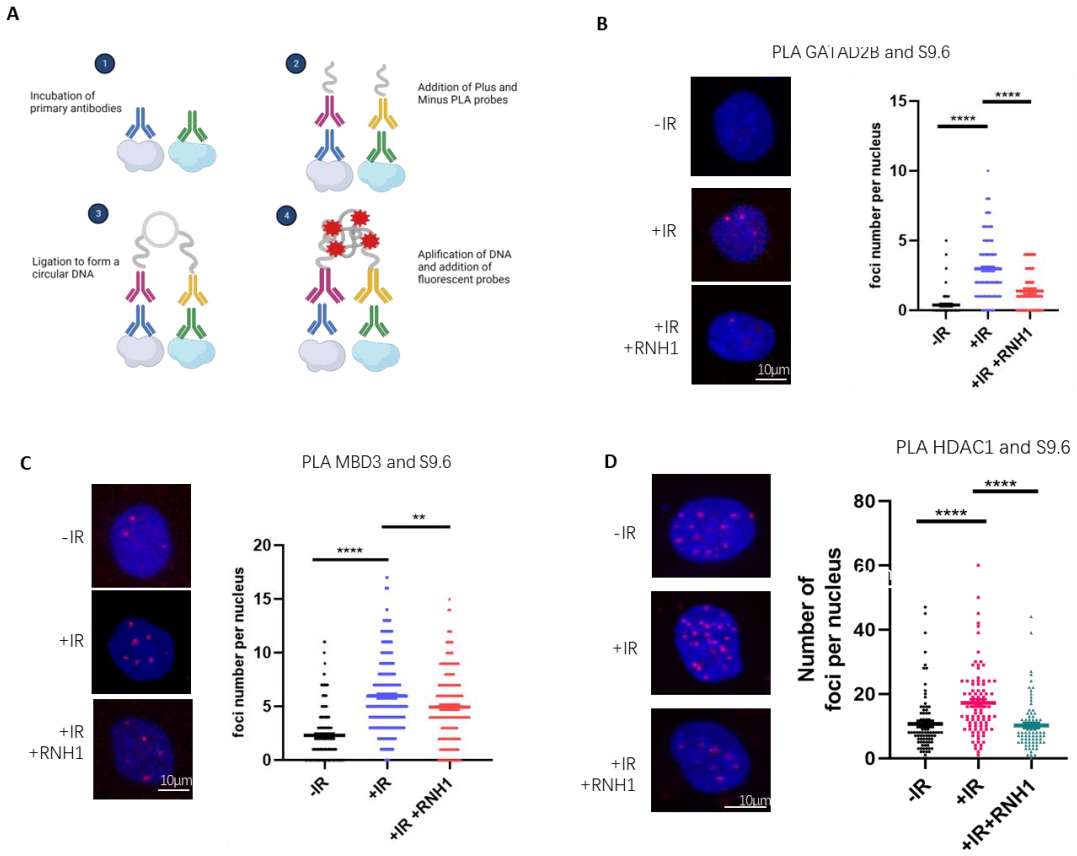


Figure 3-5 Components of GATAD2B-NuRD complex interact with R-loops upon DNA damage in vivo. (A) Diagram showing the basic principle of PLA. (B) Left: quantification of Right, error bar = mean ± SEM, significance was determined using non-parametric Mann-Whitney test. ****p ⩽ 0.0001. Right: representative confocal microscopy images of GATAD2B-S9.6 PLA. (C) Left: quantification of Right, error bar = mean ± SEM, significance was determined using non-parametric Mann-Whitney test. ****p ⩽ 0.0001, **p ⩽ 0.01. Right: representative confocal microscopy images of MBD3-S9.6 PLA (D) Left: quantification of Right, error bar = mean ± SEM, significance was determined using non-parametric Mann-Whitney test. ****p ⩽ 0.0001. Right: representative confocal microscopy images of HDAC1-S9.6 PLA.

3.6 GATAD2B and MBD3 are recruited to DSBs in transcription and R-loop dependent manner

The above data identified components of the NuRD complex as novel DNA damage-specific R-loop binders. Transcription is the source of R-loops and the importance of transcription in DDR has been widely reported. Therefore, I was interested in testing whether transcription and R-loops were important for the DSB localization of MBD3 and GATAD2B. To investigate this, I applied laser micro-irradiation to examine the potential recruitment of GATAD2B and MBD3 to DSBs. Specifically, HeLa cells were transfected with GATAD2B-GFP or MBD3-GFP plasmids, followed by DNA damage induced by laser micro-irradiation and time-lapse microscope imaging. Using this approach, I observed that both proteins could be rapidly recruited to DSBs within ~30s after laser induction. Interestingly, upon transcription inhibition by either DRB or triptolide treatment (181), the recruitment of MBD3 or GATAD2B to DSBs was significantly impaired (Figure 3-6a and b), indicating that their localization to DSBs was transcription-dependent. Next, to test the effect of R-loops on the recruitment of MBD3 and GATAD2B to DSBs, I co-transfected RNase H1-mCherry plasmids with GATAD2B-GFP or MBD3-GFP plasmids, followed by DNA damage induced by laser

micro irradiation. Live cell imaging revealed that localization of GATAD2B and MBD3 at DSBs was suppressed by the overexpression of RNaseH1 (Figure 3-6 c and d), suggesting the recruitment of these two proteins to damaged loci is also R-loop dependent.

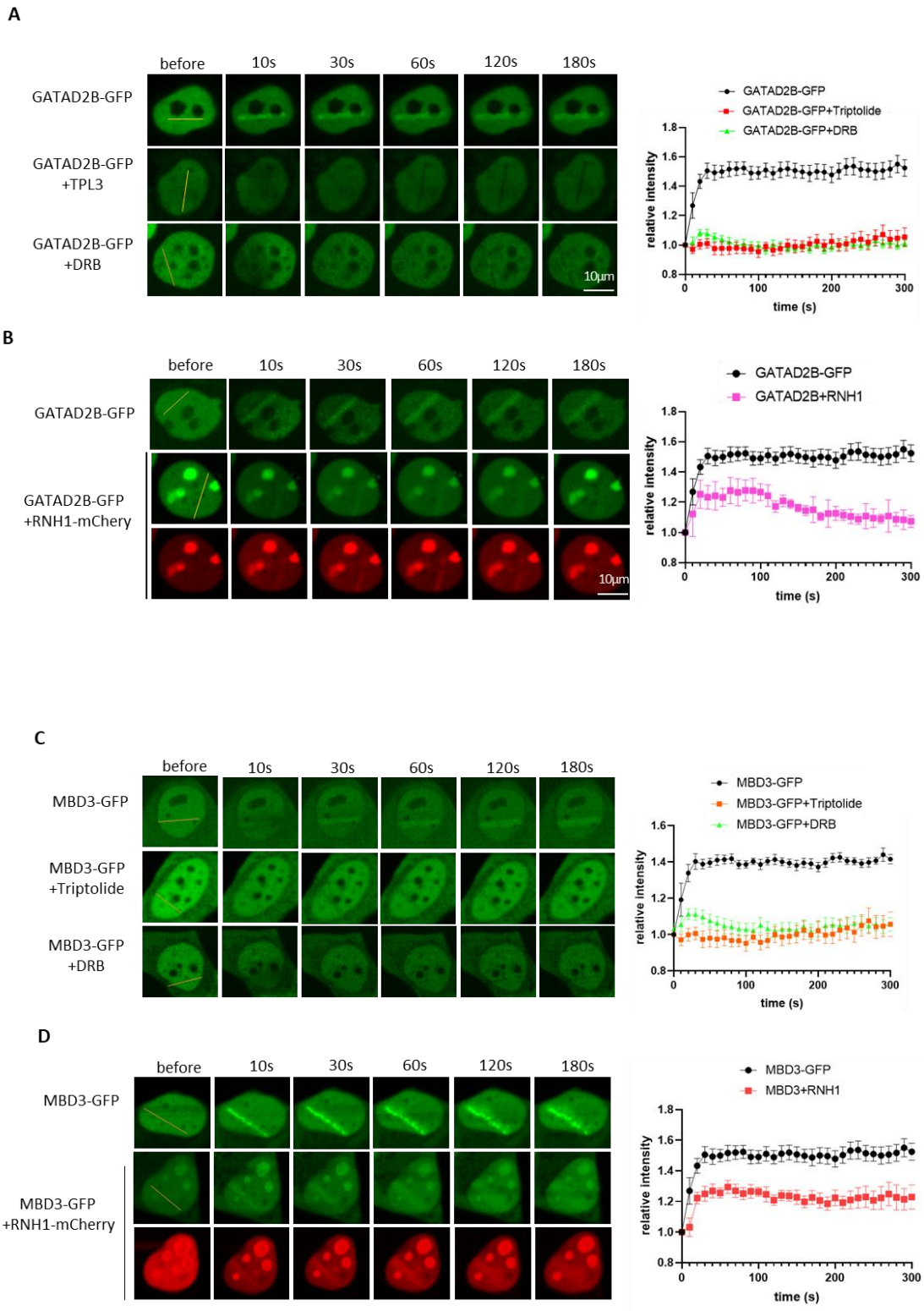


Figure 3-6 GATAD2B and MBD3 could be localized to DNA damage sites in a transcription- and R-loops-dependent manner. (A) Laser stripping of GATAD2B-GFP cells with or without treatment with transcription inhibitors triptolide (TPL3) and DRB. Top: Representative spinning disk confocal microscopy images before and after laser-stripping. Bottom: quantification (n⩾10) showing GFP

signals before and after laser striping at indicated time points; error bar = mean ± SEM. (B) Laser stripping of GATAD2B-GFP cells with or without transiently expression of RNAseH1-mCherry plasmid. Top: Representative spinning disk confocal microscopy images before and after laser-stripping. Bottom: quantification (n⩾10) showing GFP and RFP signals before and after laser striping at indicated time points; error bar = mean ± SEM. (C) Laser stripping of MBD3-GFP cells with or without treatment with transcription inhibitors triptolide (TPL3) and DRB. Top: Representative spinning disk confocal microscopy images before and after laser-stripping. Bottom: quantification (n⩾10) showing GFP signals before and after laser striping at indicated time points; error bar = mean ± SEM. (D) Laser stripping of MBD3-GFP cells with or without transiently expression of RNAseH1-mCherry plasmid. Top: Representative spinning disk confocal microscopy images before and after laser-stripping. Bottom: quantification (n⩾10) showing GFP and RFP signals before and after laser striping at indicated time points; error bar = mean ± SEM.

To further validate these findings, I also employed a PLA using MBD3 or GATAD2B and γH2AX antibodies. As expected, an increased number of MBD3-γH2AX or GATAD2B-γH2AX PLA foci was detected upon IR treatment when compared to control cells. Additionally, MBD3-γH2AX or GATAD2B-γH2AX PLA foci were sensitive to transcription inhibition by DRB or triptolide and overexpression of RNase H1 (Figure 3-7a and b). These data indicate that the localization of endogenous MBD3 and GATAD2B to DSBs is also associated with transcription and R-loops. Thus, my results show that these two subunits of the NuRD complex are recruited to damaged DNA in transcription and R-loop dependent manner, possibly indicating their roles in the early stages of DDR.

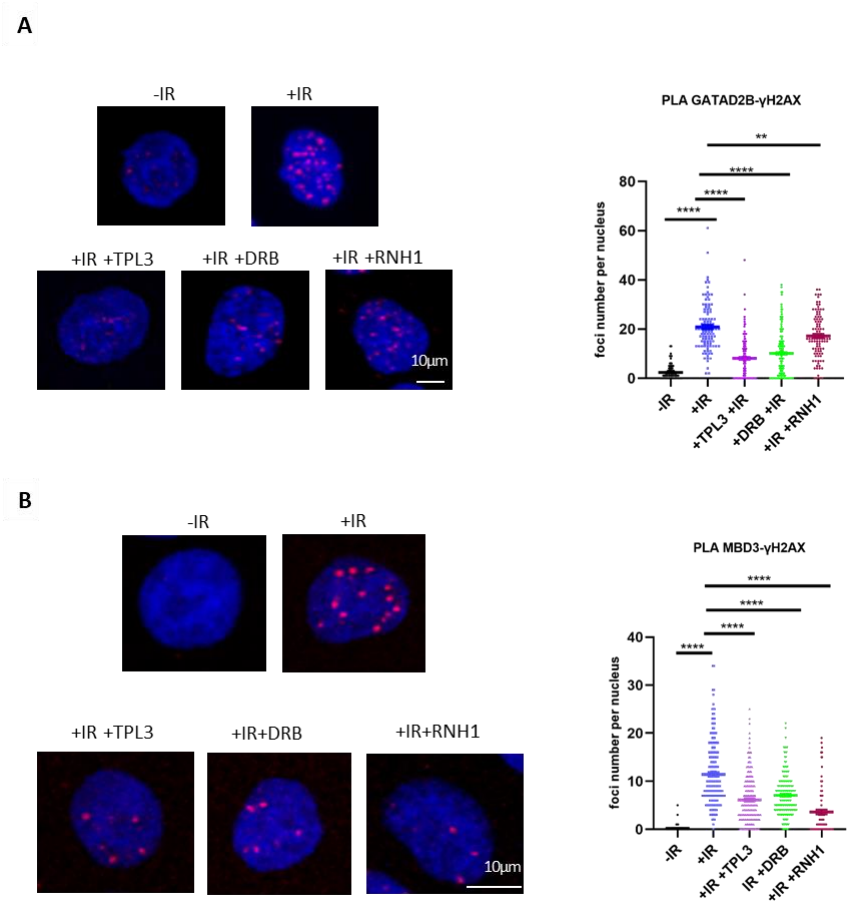


Figure 3-7 Endogenous GATAD2B and MBD3 could be localized to DNA damage sites in a transcription- and R-loops-dependent manner. (A) PLA of GATAD2B and γH2AX in cells with or without IR and transcription inhibition (TPL3 or DRB) or overexpression of RNAseH1. IR=5Gy. Left: representative confocal microscopy images; right: quantification of left, error bar = mean ± SEM, significance was determined using non-parametric Mann-Whitney test. ****p ≤ 0.0001, ** $p \leq 0.01$. (B) PLA of MBD3 and γH2AX in cells with or without IR and transcription inhibition (TPL3 or DRB) or overexpression of RNAseH1. IR=10Gy. Left: representative confocal microscopy images; right: quantification of left, error bar = mean ± SEM, significance was determined using non-parametric Mann-Whitney test. ****p ⩽ 0.0001.

3.7 GATAD2B controls HDAC1 recruitment to DSBs

As mentioned above, HDAC1 is a subunit of the NuRD complex that possesses histone deacetylase activity. To investigate whether MBD3 and GATAD2B play a role in recruiting HDAC1 to DSBs, I conducted PLA assay using antibodies against HDAC1 and γH2AX. Upon treatment with IR, I observed PLA foci, indicating an

interaction between HDAC1 and γH2AX. Similar to the findings with MBD3 and GATAD2B, the transcription inhibition using DRB or triptolide, as well as the overexpression of RNase H1, resulted in a decreased number of HDAC1-γH2AX PLA foci. These results suggest that both transcription and the presence of R-loops are important for the recruitment of HDAC1. Interestingly, when MBD3 or GATAD2B was knocked down using siRNA, there was also a reduction in the number ofHDAC1-γH2AX PLA foci (Figure 3-8). This finding suggests that the recruitment of HDAC1 to DSBs is regulated by MBD3 and GATAD2B.

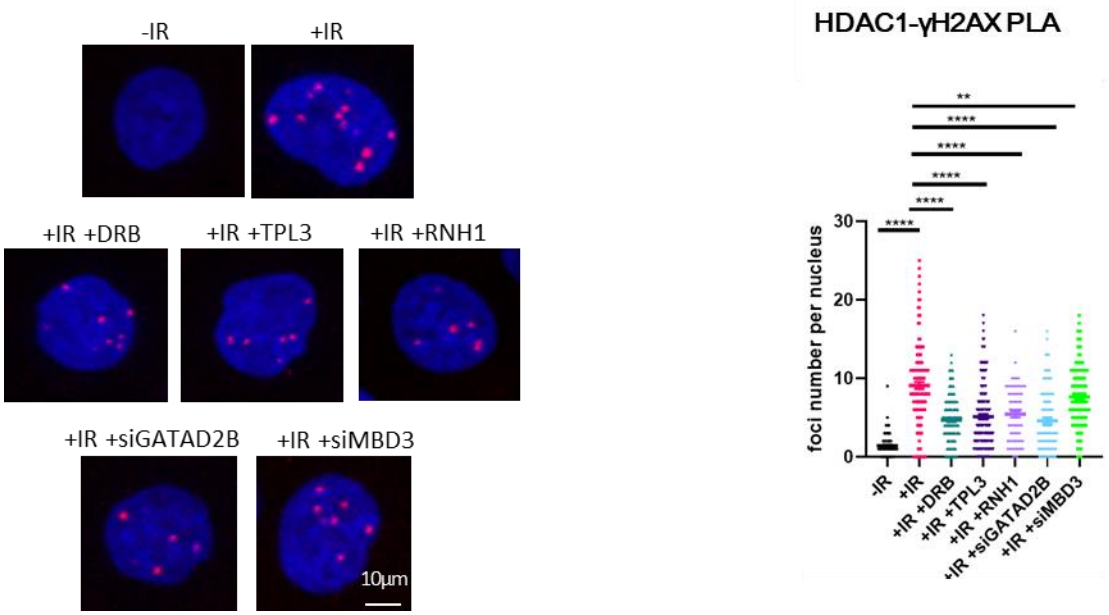


Figure 3-8 DSB localization of HDAC1 is regulated by transcription, R-loops, MBD3 and GATAD2B. PLA of HDAC1 and γH2AX in cells with or without IR and transcription inhibition (TPL3 or DRB), overexpression of RNAseH1 or depletion of GATAD2B and MBD3. IR=5 Gy. Left: representative confocal microscopy images; right: quantification of left, error bar = mean ± SEM, significance was determined using non-parametric Mann-Whitney test. ****$p \leq 0.0001$, **$p \leq 0.01$.

To further investigate the role of GATAD2B in the recruitment of HDAC1, I utilized a cell line with inducible sequence specific DSB called AsiSI (DIvA). This cell line, derived from U2OS cells, contains an integrated gene encoding the endonuclease AsiSI fused to the estrogen receptor ligand-binding domain (AsiSI-ER), which prevents its 1ocalization to the nucleus until activated by 4-hydroxytamoxifen (4-

OHT). Upon the addition of 4-OHT, the fusion protein translocates rapidly to the nucleus and generates site-specific double-strand breaks (DSBs) by digesting genomic DNA. This cellular system allows for the study of DSBs in a sequence-specific manner, as AsiSI has approximately 80 cutting sites in the human genome (182, 183).

Using the DIvA cell line, I performed HDAC1 chromatin immunoprecipitation (ChIP) followed by quantitative PCR (ChIP-qPCR). This assay allowed me to assess the enrichment of HDAC1 at two specific AsiSI cutting sites upon 4-OHT activation. I observed a significant increase in HDAC1 enrichment at these cutting sites following 4-OHT treatment. However, when GATAD2B was knocked down, the ChIP-qPCR signal was reduced (Figure 3-9). These results provide further confirmation of the involvement of GATAD2B in the recruitment of HDAC1 to DSBs.

In summary, these results indicate that GATAD2B and MBD3, along with transcription and R-loops, play a role in regulating the localization of HDAC1 to sites of double-strand breaks.

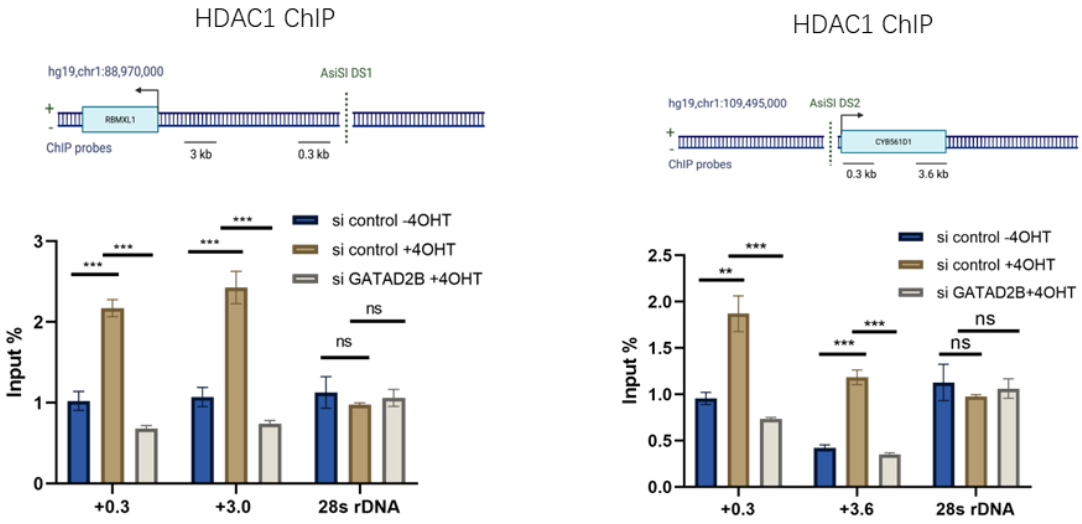


Figure 3-9 HDAC1 recruitment to DSBs is dependent on GATAD2B. Left Part: Top: drawing showing DS1 genomic region with AsiSI cut site and position of ChIP probes. Bottom: Bar chart

showing HDAC1 ChIP levels at indicated sites next to AsiSI cut in cells with or without 4-OHT and depletion of GATAD2B, error bar = mean ± SEM, significance was determined using non-parametric Mann-Whitney test. ***p ≤ 0.001, n.s. not significant. Right Part: Top: drawing showing DS2 genomic region with AsiSI cut site and position of ChIP probes. Bottom: Bar chart showing HDAC1 ChIP levels at indicated sites next to AsiSI cut in cells with or without 4OH and depletion of GATAD2B, error bar = mean ± SEM, significance was determined using non-parametric Mann-Whitney test. ***p ⩽ 0.001, **p ⩽ 0.01,n.s. not significant.

3.8 GATAD2B and HDAC1 occupancy at DSBs overlaps with that of R-loops

investigate the distribution and profile of the GATAD2B-NuRD complex in the vicinity of DSBs throughout the genome, I performed GATAD2B and HDAC1 ChIP in the DIvA cell line. Subsequently, I performed next-generation sequencing (ChIP-seq) to assess the occupancy of these two proteins at DSB loci. Interestingly, the ChIP-seq analysis revealed a significant enrichment of both GATAD2B and HDAC1 at DSBs following 4-OHT treatment. The accumulation of these proteins was particularly prominent at DSBs and extended approximately 2.5-kb around the AsiSI cutting sites. In contrast, no significant enrichment of these proteins was detected at uncut loci (Figures 3-10 A-C). Furthermore, a previous study employing DNA: RNA hybrids immunoprecipitation (DRIP) demonstrated the accumulation of R-loops in the vicinity of DSBs within a 2.5-kb window(112, 169). Interestingly, this accumulation of R-loops perfectly overlapped with the occupancy of GATAD2B and HDAC1 at DSBs. These findings suggest a correlation between the presence of R-loops, the recruitment of GATAD2B and HDAC1, and the formation of the GATAD2B-NuRD complex at DSB sites.

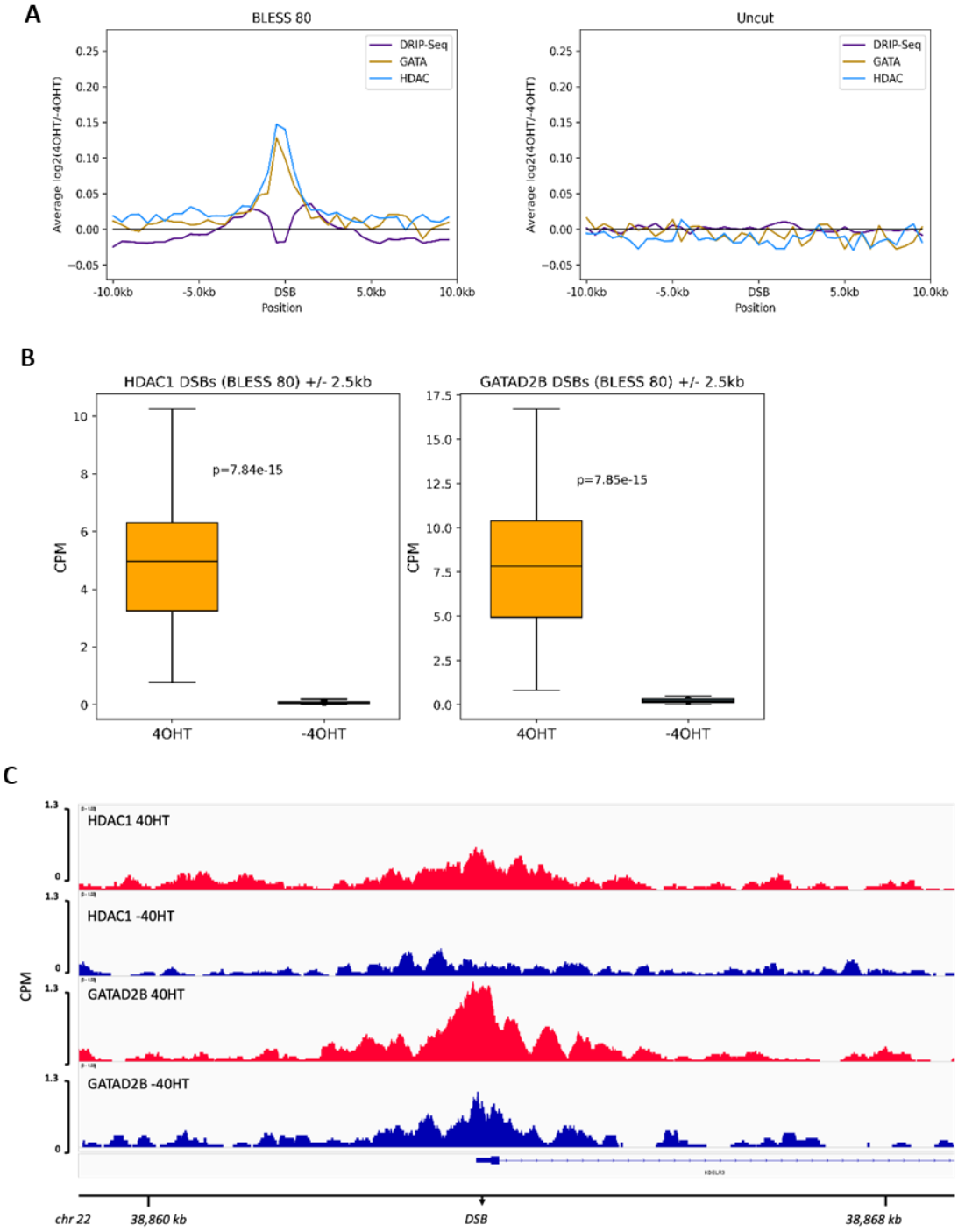


Figure 3-10 GATAD2B and HDAC1 occupancy at DSBs overlaps with that of R-loops. (A) Metagene profile showing ChIP-seq enrichment of GATAD2B, HDAC1 and R-loops at AsiSI cut (left), but not uncut (right) sites (as defined by BLESS technique). The metagene profiles showed on a 10-kb window centered at 80 cutting DSBs as defined by BLESS (left) or centered at uncut AsiSI recognition sites (right). (B) Box plot graph showing levels of HDAC1 and GATAD2B ChIP-seq reads mapping to AsiSI sites in presence or absence of 4OHT. Wilcoxon two sample test was used to determine statistical significance with p-value cut-off set at 0.01, and calculated significances were labeled. (C) Screenshots showing HDAC1 and GATAD2B ChIP-Seq reads count of no damage and damage induction(+4OHT) conditions at representative AsiSI cutting sites. Snapshot showed a 5-bb window centered at the

representative DSB.

To assess the cutting efficiency of different AsiSI digestion sites, I utilized data generated from a previously published technique called "direct in situ breaks labeling, enrichment on streptavidin, and next-generation sequencing" (BLESS). This technique involves direct labeling of blunt DSB ends using biotinylated DNA linkers containing a barcode DNA sequence (184). After ligating these DNA linkers to the blunt DSB ends, the samples are sheared, and the biotin-labeled DSB ends are enriched by adding streptavidin beads. Subsequently, additional linkers containing a different barcode sequence are added to the free end of the purified DNA, followed by another round of streptavidin bead enrichment to remove the biotin marker. The enriched DNA fragments are then amplified and subjected to next-generation sequencing for the identification of DSBs. Based on the BLESS sequencing data the cutting efficiency of the various AsiSI restriction sites are ranked. Heatmap analysis of this data revealed a correlation between the recruitment of GATAD2B and HDAC1 and the cutting efficiency of the AsiSI sites as ranked by BLESS signals(185). Specifically, the GATAD2B and HDAC1 complexes showed a preference for being recruited to more accessible AsiSI sites, which are likely located near transcriptionally active regions (Figure 3-11).

In summary, these findings indicate that HDAC1 and GATAD2B are enriched at DSBs within a 2.5-kb window and suggest that they co-localize with R-loops around the DSBs. This suggests that the recruitment of HDAC1 and GATAD2B is influenced by the accessibility and cutting efficiency of the AsiSI sites, potentially in relation to nearby transcriptionally active regions.

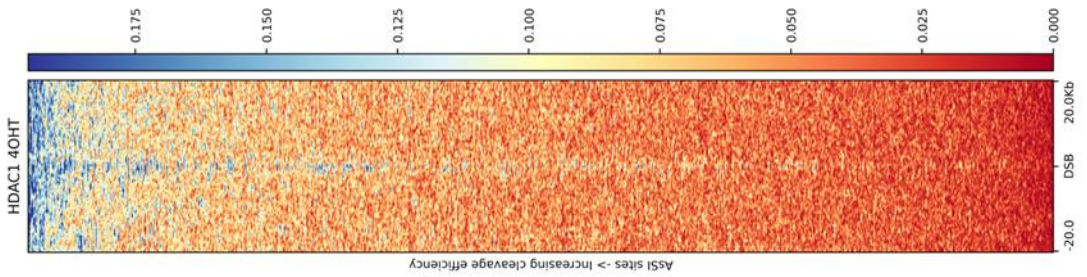


Figure 3-11 The recruitment of the GATAD2B and HDAC1 correlated with AsiSI cutting efficiency as ranked by BLESS signals. Heat maps representing GATAD2B and HDAC1 ChIP-seq count over a 20 kb window centered on the DSB before(−4OHT) and after(+4OHT) DSB induction. DSBs are sorted according to decreasing cutting efficiency.

3.9 GATAD2B and HDAC1 occupancy at DSBs is prone to high transcription activity and HR-prone loci

The data presented above demonstrate that GATAD2B and HDAC1 are rapidly recruited to DSBs in a transcription and R-loops-dependent manner. Additionally, the recruitment of the GATAD2B and HDAC1 correlates with the AsiSI cutting efficiency as determined by BLESS signals. To further explore the influence of transcription activity on the localization of GATAD2B and HDAC1 at DSBs, I investigated whether the transcriptional status of the broken loci affects the recruitment of these proteins. To investigate this, the AsiSI cutting sites were categorized into high transcriptional and low transcriptional loci based on mapping the RNA Polymerase II CTD S2P ChIP-seq data and RNA-seq −4OHT as described in a previous study(99). Subsequently, the ChIP-seq data from section 3.8 was further analyzed. The analysis revealed a significant increase in the DSB-induced enrichment of HDAC1 and GATAD2B at loci with high transcriptional activity (Figures 3-12a and b). This finding suggests that the GATAD2B-NuRD complex plays a more critical role in responding to damage induced at loci with high transcription activity.

In summary, these results indicate that the recruitment of GATAD2B and HDAC1 to DSBs is influenced by the transcriptional activity of the loci. The GATAD2B-NuRD complex appears to have a greater functional significance in the response to damage occurring at loci with high transcriptional activity.

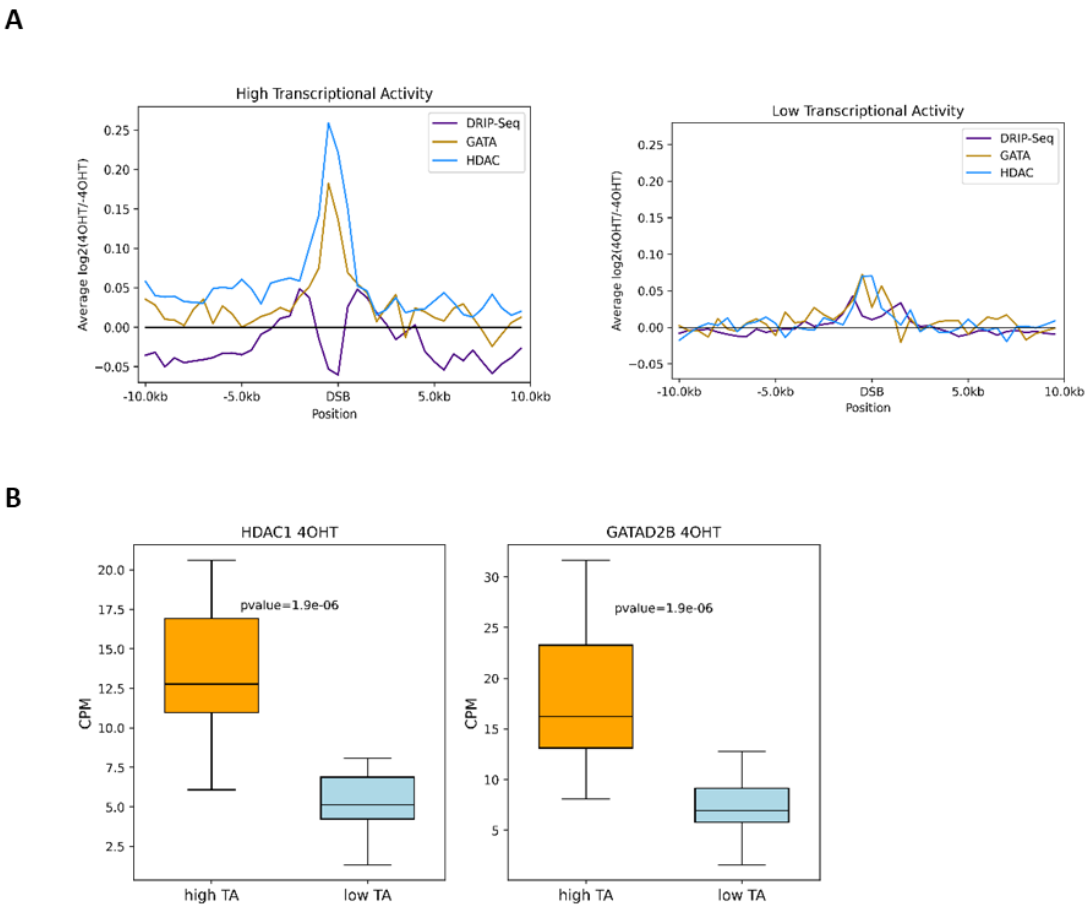


Figure 3-12 GATAD2B and HDAC1 occupancy at DSBs is prone to high transcription activity. (A) Metagene profile showing ChIP-seq enrichment of GATAD2B, HDAC1 and R-loops at AsiSI cut sites in high (left) or low transcribed regions (right). The metagene profiles showed on a 10-kb window centered at DSBs. high transcriptional and low transcriptional loci indicated by RNA PolII S2P ChIP-seq mapping and RNA-seq −4OHT according to a previous study. (B) Box plot graph showing levels of HDAC1 and GATAD2B ChIP-seq reads mapping to AsiSI sites at high or low transcription regions. Wilcoxon two sample test was used to determine statistical significance with p-value cut-off set at 0.01, and calculated significances were labeled.

Previous studies have demonstrated that transcription can promote DSB repair through the HR pathway(99). I sought to investigate whether the occupancy of HDAC1 and GATAD2B at DSBs exhibited a preference for the loci repaired by HR

pathway. To address this, the AsiSI cutting sites were categorized as HR- or NHEJ-prone sites based on a ChIP-seq coverage ratio between RAD51 (within 4 kb window from a DSB) and XRCC4 (within a 1 kb window from a DSB) as described in a previous publication(135). By analyzing the ChIP-seq data for GATAD2B and HDAC1, I observed a significant enrichment of both proteins at HR-prone AsiSI cut sites (Figures 3-13 a and b).

In summary, the analysis of the GATAD2B and HDAC1 ChIP-seq data revealed their co-localization with R-loops induced at DSBs. Furthermore, their enrichment at DSBs was notably higher in regions of high transcriptional activity and at loci prone to HR-mediated repair. These findings suggest a potential association between the recruitment of GATAD2B and HDAC1, R-loops formation, transcriptional activity, and a preference for the HR pathway in DSB repair.

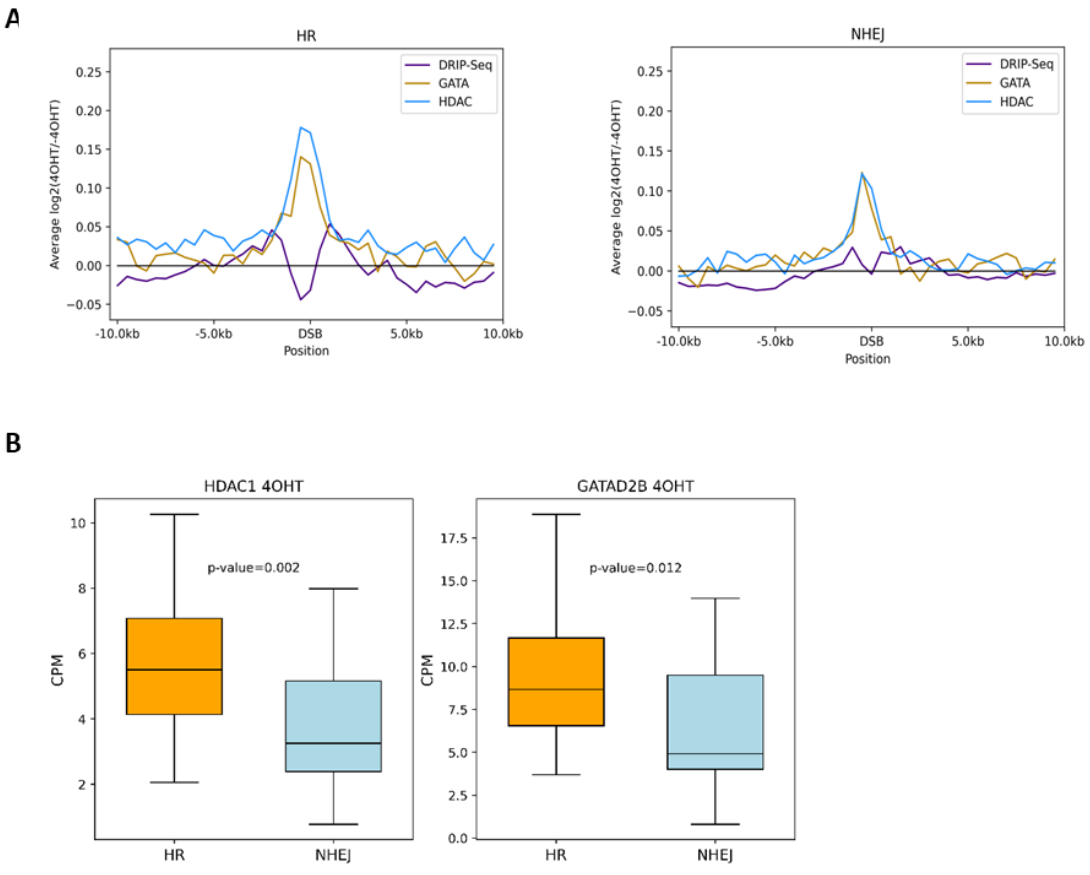


Figure 3-13 GATAD2B and HDAC1 occupancy at DSBs is more enriched at HR-prone loci. (A) Metagene profile showing ChIP-seq enrichment of GATAD2B, HDAC1 and R-loops at AsiSI cut sites in HR-prone (left) or NHEJ-prone regions (right). The metagene profiles showed on a 10-kb window centered at DSBs. The AsiSI cutting sites were divided into HR- or NHEJ-prone sites based on a ChIP-seq coverage ratio between RAD51 (4 kb window) and XRCC4 (1 kb window) from a previous publication (B) Box plot graph showing levels of HDAC1 and GATAD2B ChIP-seq reads mapping to AsiSI sites at HR-prone or NHEJ-prone regions. Wilcoxon two sample test was used to determine statistical significance with p-value cut-off set at 0.01, and calculated significances were labeled.

3.10 Discussion

In the initial part of this chapter, I successfully identified novel factors that interact with R-loops and are involved in DDR. It is important to note that R-loops formation can be induced by DSBs and the S9.6 antibody specifically recognizes the structure of DNA: RNA hybrids. However, it has been shown that this antibody can also bind to double-stranded RNA (dsRNA)(173), leading to non-specific signals during S9.6 IP and potentially affecting the accuracy of the method. To minimize the effect of non-specific signals, RNaseA was added to S9.6 IP samples in this study. As an additional approach to S9.6 IP, catalytically inactive RNase H1 can be applied to study biology of R-loops. As RNase H1 degrades RNA in DNA: RNA hybrids, the D210N mutant of this enzyme loses its RNA degradation ability, but remains its DNA:RNA hybrid binding property(186, 187). Thus, catalytically inactive RNase H can recognize and bind to DNA: RNA hybrids and be used to detect and isolate R-loop structures and associated proteins. Furthermore, both the hybrid binding and catalytic domains of RNase H1 bind exhibit a stronger affinity for DNA: RNA hybrids compared to dsRNA with a 25–30-fold higher binding affinity (186, 187). These characteristics are particularly advantageous as it can significantly reduce non-specific signals originating from dsRNA. However, the S9.6 antibody only interacts with long DNA:

RNA hybrids that are greater than >40 base pairs in length, whereas RNaseH1 can recognize segments as short as 4 base pairs (188, 189). Consequently, catalytic RNase H1 is also likely to detect short DNA: RNA hybrids that are generated during processes such as transcription or replication. Additionally, utilizing D210N RNase H1 for immunoprecipitation can be labor intensive since each cell line needs to be individually engineered and further optimization may be required(190). Given that DSBs-induced R-loops often consist of relatively long hybrids, the S9.6 IP method was adopted in this study.

Moreover, though S9.6 antibody was found to recognize dsRNA structure, the analysis of my mass spectrometry data revealed that some known dsRNA factors, such as Dicer, were not detected in the S9.6 IP samples. Furthermore, the signals obtained for GATAD2B-S9.6 or MBD3-S9.6 signals were sensitive to RNase H overexpression. Thus, factors screened from S9.6 IP followed by Mass spectrometry specifically bind with DNA: RNA hybrids.

Overall, the combination of S9.6 IP and mass spectrometry provides a valuable approach for identifying factors that specifically interact with DNA: RNA hybrids, enabling a deeper understanding of their functional roles.

R-loops were reported to regulate several biological processes under normal conditions, including maintenance of centromere and telomere, histone modification, recruitment of chromatin remodeler, DNA demethylation, and either positive or negative regulation of transcription. Chromatin remodeling and transcription are important steps in DDR. Interestingly, the analysis of S9.6 IP mass spectrometry identified components of NuRD complex, MBD3 and GATAD2B as novel R-loops binding factors upon DNA damage. NuRD complex has both histone deacetylase and

ATP-dependent chromatin remodeling activities, which allows this complex to change the chromatin structure and consequently to regulate transcription. Moreover, the localization of this complex to DSBs is dependent on R-loops. Based on these findings, I speculate that R-loops could remodel chromatin structure and regulate transcription through the recruitment of GATAD2B-NuRD complex and positively function in DDR.

Both the S9.6 antibody and RNase H1 recognize DNA: RNA hybrids. It remains unclear whether the GATAD2B-NuRD complex preferentially interacts with two-stranded DNA: RNA hybrids or three-stranded R-loops structures. As both structures could be formed at DSBs(112, 113), two-stranded DNA: RNA hybrids were observed to be formed at DNA ends after end resection. I detected that MBD3 and GATAD2B could be rapidly recruited to DSBs in less than 30 seconds after laser micro irradiation, suggesting these proteins function at the early stage of DDR. However, end resection occurs at late stage of DDR process, I hypothesize that GATAD2B-NuRD complex preferentially binds with the three-stranded R-loops structure upon DNA damage *in vivo.* However, whether DNA: RNA hybrids are sufficient for the localization of the GATAD2B-NuRD complex, or whether the unpaired ssDNA is necessary for the recruitment of this complex needs to be further clarified.

Next-generation sequencing analysis suggested HDAC1 and GATAD2B co-localize with R-loops around DSBs. The analysis of DRIP-seq data show a dip in DNA: RNA hybrids level at DSBs, and this might because processing of broken DNA would lead to the transient loss of the cleaved loci, and this might occur reduce the reads of these sequences and so could be the explanation for the DRIP-Seq profile. RNA immunoprecipitated by the S9.6 antibody could also be sequenced, and those

molecules would not be cleaved or resected during broken-end processing. Thus, the enrichment of DNA: RNA hybrids exactly around cleavage sites might be detected by RNA sequencing of DRIP samples. In addition, although general enrichment of damage-induced DNA: RNA hybrids could be detected within a 2.5-kb window. R-loops were shown to facilitate the recruitment of HR factors, suggesting that HR-prone regions might have higher levels of R-loops. The canonical HR pathway requires homologous DNA sequences from sister chromatid as templates. Because of this, trimming of one DNA strand at DSB ends, the end resection, is important for the generation of ssDNA overhang, which will transiently remove the sequences at the broken DNA end. For the preparation of DRIP-seq samples performed by Cohen et al., DNA: RNA hybrids from damaged (+4OHT) or control (-4OHT) DIvA cells were pulled down by S9.6 antibody, followed by purification of immunoprecipitated DNA, and those purified DNA samples were then sequenced. In this previous study, DIvA cells were incubated with 4-OHT for 4 hours to induce DSBs. Though AsiSI-ER in DIvA cells could be rapidly translocated to the nucleus upon 4-OHT addition, DSBs produced in this system were not immediate nor synchronized among different gene loci or cell populations. Furthermore, accurately repaired DSBs could be re-cleaved and therefore another round of DDR was initiated(191). Consequently, resolutions for specific DDR events are limited in DIvA system.

I observed the recruitment of the GATAD2B-NuRD complex is dependent on transcription and R-loops. It has been shown that DSBs could induce *de novo* transcription around broken DNA. Both *de novo* transcription and pre-existing transcription could form R-loops at DSBs(2, 97, 113). Thus, it is not clear which transcription is important for the recruitment of the GATAD2B-NuRD complex to DSBs. The enrichment of GATAD2B and HDAC1 at regions with high transcription

activity, suggests that pre-existing transcription may be important for the localization of these two proteins to DSBs. However, it is not clear whether there was a correlation between *de novo* transcription level and pre-existing transcription activity. Thus, it is still difficult to understand whether *de novo* transcription is crucial for the recruitment of the GATAD2B-NuRD complex. C Terminal Domain of RNAPII phosphorylated at tyr1 (Y1P) was found to facilitate *de novo* transcription(2). Therefore, investigating interactions or co-localizations between the NuRD complex and RNAPII Y1P and whether dephosphorylation of Y1P may affect the recruitment of GATAD2B-NuRD complex to DSBs could further our understanding of the roles of *de novo* transcription in this pathway.

Overall, my data show that the GATAD2B-NuRD complex preferentially binds to R-loops upon DNA damage and its rapid recruitment to HR-Prone DSBs is dependent on transcription and R-loops.

4. The role of R-loops and GATAD2B-NuRD complex in DNA Damage Response

4.1 Introduction

In Chapter 3, I identified GATAD2B and MBD3 as novel R-loop binding factors related to DDR. Furthermore, I found that the recruitment of the GATAD2B-NuRD complex is dependent on transcription and R-loops. Based on these findings, I hypothesized that the GATAD2B-NuRD complex plays coordinating roles in DDR. Here, I would like to identify novel functions of R-loops as well as GATAD2B-NuRD in DDR.

4.2 R-loops repress transcription *in cis* to DSBs

It was reported that DSBs can promote transcription repression *in cis* to DSBs(78, 82). However, the role of R-loops in this biological process remains unclear. As mentioned earlier, R-loops can regulate transcription either positively or negatively, as well as facilitate transcription termination. To verify whether R-loops could affect transcription *in cis* near to damaged sites, I induced site-specific DSBs in DIvA cells and isolated chromatin-bound nascent RNA in wild-type, MBD3 knock-down, and GATAD2B knock-down conditions. In agreement with published data, I detected lower levels of nascent RNA within the first neighboring gene CCNB1, located approximately 10kb away from the DSBs, upon 4-OHT treatment (+4-OHT). Similarly, at another DSB locus, I observed a decrease in nascent RNA levels derived from the RBMXL1 gene (~10kb away from the DSB) in cells treated with 4-OHT.

Interestingly, overexpression of RNase H rescued DSBs induced repression of nascent transcription at both loci (Figure 4-1 A), suggesting that R-loops could contribute to repression transcription *in cis* to DSBs. Moreover, the overexpression of RNase H did not inhibit transcription of GAPDH, which is not in proximity to the AsiSI cut site, upon the addition of 4-OHT (Figure 4-1A). As reduced nascent transcription could lead to lower mRNA levels, I also extracted total RNA from DIvA cells to further confirm the roles of R-loops in transcription repression upon DNA damage. Consistent with the nascent RNA results, also mRNA levels of RBMXL1 and CCNB1, both of which are genes located near the DSBs, were reduced upon 4-OHT treatment, and this reduction was rescued by the overexpression of RNase H (Figure 4-1B). However, the expression of Dicer, which is not a gene in proximity to DSBs, was not affected in these conditions (Figure 4-1B). To validate this hypothesis in a different system and in different chromatin contexts, I generated site-specific DSBs using IPpoI, another restriction enzyme(192). Similarly, mRNA levels within genes in proximity to I-PpoI cut sites (RYR2 and ANKRD30BL) were reduced upon nuclear translocation of this enzyme, while this reduction was rescued by the overexpression of RNase H. However, the expression of DROSHA and actin, both of which are distal from IPpoI recognition sites, was not affected by IPpoI cleavage or the overexpression of RNase H (Figure 4-1C). Thus, these results indicated that DNA damage-induced R-loops specifically repress transcription *in cis* to DSBs.

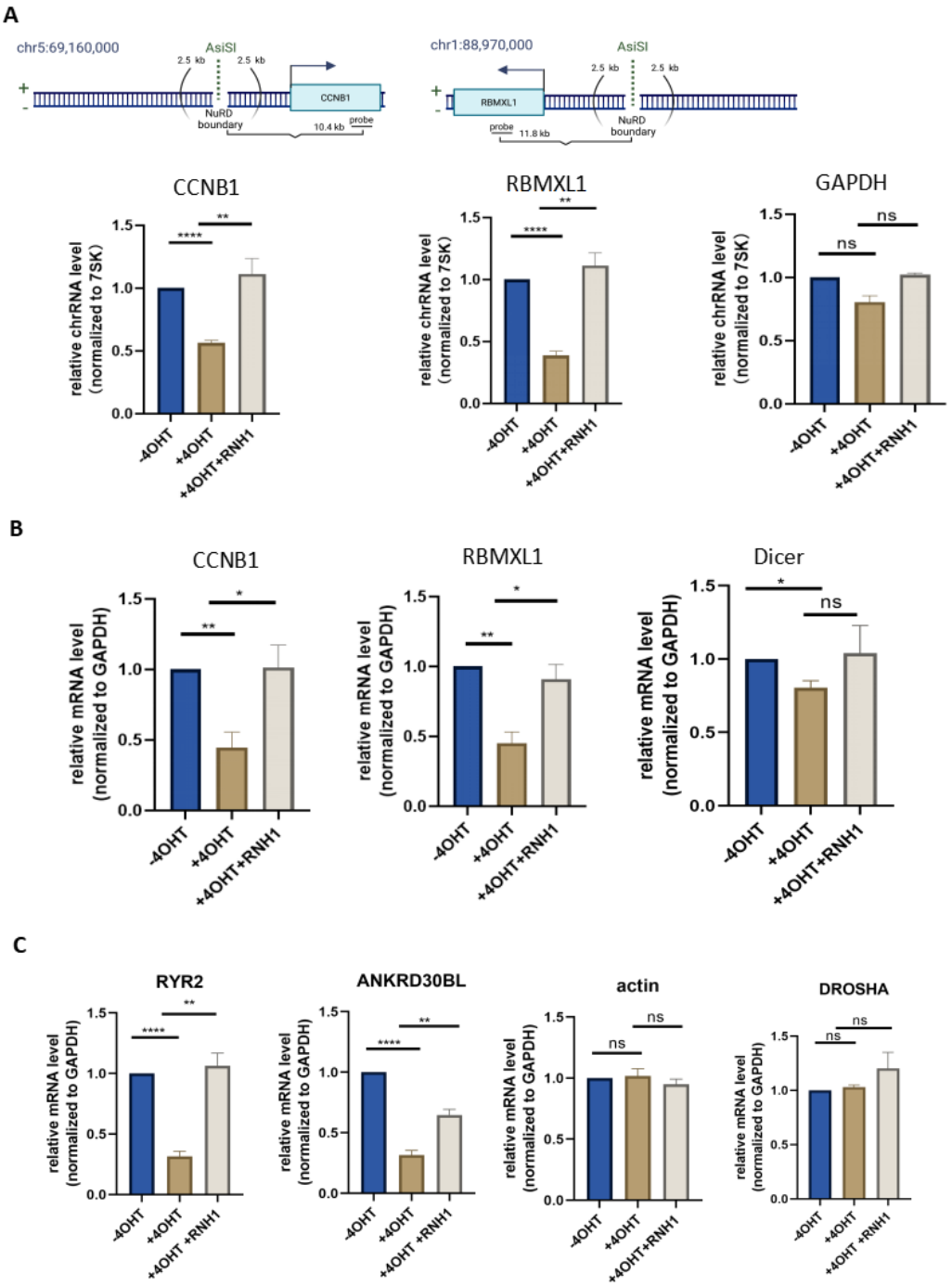


Figure 4-1 R-loops repress transcription *in cis* to DSBs. (A) Top: Drawing showing the position of two different AsiSI cut sites and their neighboring genes. Positions of qRT-PCR probes are indicated below the genes. Bottom: Bar chart showing levels of nascent RNA at CCNB1, RBMXL1, and GAPDH genes, in the absence or presence of 4OHT and overexpression of RNH1. (B) Bar chart showing levels of mRNA at CCNB1, RBMXL1, and Dicer genes, in the absence or presence of 4OHT and overexpression of RNH1. (C) Bar chart showing levels of mRNA at RYR2 and ANKRD30BL, which are genes in proximity to IPpoI cutting sites, as well as actin and DROSHA genes, in the absence or presence of 4OHT and overexpression of RNH1.

4.3 GATAD2B-NuRD complex represses transcription *in cis* to DSBs

Above I showed that MBD3 and GATAD2B are potential R-loops binding factors related to DDR. It was reported that the NuRD complex could repress transcription in no damage condition. Therefore, I hypothesized that R-loops may repress transcription *in cis* to DSBs through the involvement of the NuRD complex. To test this hypothesis, I transfected DIvA cells with either control siRNA or siRNA targeting MBD3 or GATAD2B, followed by the addition of 4-OHT and isolation of chromatin-bound RNA. In control cells, expression of CCNB1 and RBMXL1 was decreased upon 4-OHT treatment. Interestingly, I observed that the depletion of MBD3 or GATAD2B partially rescued reduced nascent transcription around DSBs (Figure 4-2A). Similarly, the mRNA levels of CCNB1 and RBMXL1 were also decreased upon the induction of site-specific DSBs, but transfection of siMBD3 or siGATAD2B could rescue this reduction (Figure 4-2B). These findings suggest that the GATAD2B-NuRD complex may work in coordination with R-loops to repress transcription *in cis* to DSBs.

Overall, these data support the hypothesis that the GATAD2B-NuRD complex plays a role in the repression of transcription in proximity to DSBs, potentially through its interaction with R-loops.

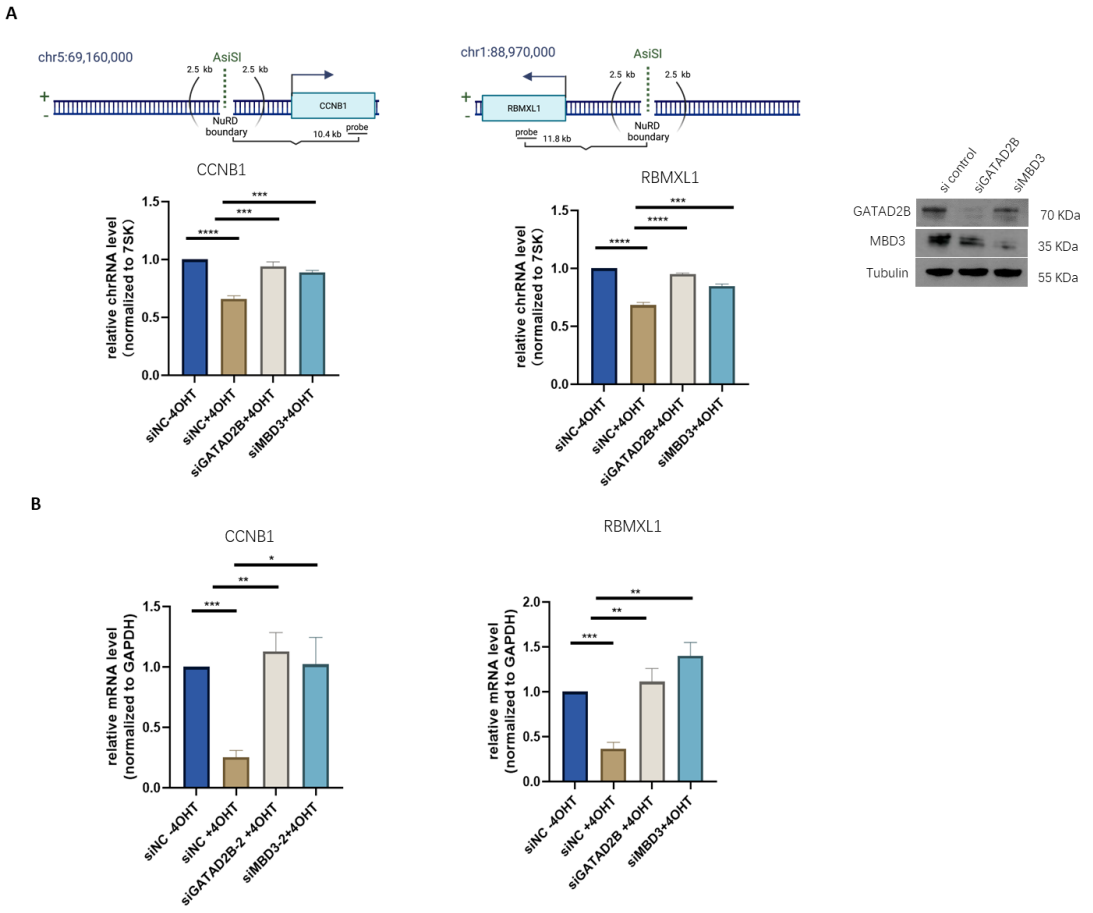


Figure 4-2 The GATAD2B-NuRD complex represses transcription *in cis* to DSBs. (A) Top: Drawing showing the position of two different AsiSI cut sites and their neighboring genes. Positions of qRT-PCR probes are indicated below the genes. Bottom left: Bar chart showing levels of nascent RNA at CCNB1 and RBMXL1 in the absence or presence of 4OHT and knockdown of MBD3 or GATAD2B. Bottom Right: Western blot analysis showing knock down efficiency of MBD3 and GATAD2B (B) Bar chart showing levels of mRNA at CCNB1 and RBMXL1, in the absence or presence of 4OHT and knockdown of MBD3 or GATAD2B.

4.4 R-loops and GATAD2B-NuRD complex reduce H4K12 acetylation level within their chromatin boundary

The NuRD complex is involved in ATP-dependent chromatin remodeling and histone deacetylation activities. Additionally, R-loops have been found to regulate histone modification and chromatin structure. In my research, I discovered that the localization of HDAC1, the deacetylase subunit in the GATAD2B-NuRD

complex(145), at DSBs is dependent on R-loops. Therefore, I investigated whether R-loops and the GATAD2B-NuRD complex could impact histone acetylation levels around DSBs. A previously published ChIP-seq analysis revealed that the signals for H4K12 acetylation, which was reported to facilitate transcription(193), were present across uncut AsiSI restriction sites, but were reduced upon the addition of 4-OHT(135). The enrichment of this histone modification at DSBs is opposite to that of DNA: RNA hybrids and the GATAD2B-NuRD complex that were shown to repress transcription *in cis* to DSBs. I then aligned my HDAC1 and GATAD2B ChIP-seq profiles with the previously published ChIP-seq profile of acetylated H4K12. Interestingly, I observed a negative correlation between the level of H4K12 acetylation and the levels of HDAC1 or GATAD2B around DSBs (Figure 4-3A). Surprisingly, this negative correlation was more pronounced at HR-prone AsiSI restriction sites or at DSBs within highly transcribed gene loci (Figures 4-3B and C). These analyses revealed that H4K12 acetylation may be deacetylated by the GATAD2B-NuRD complex around DSBs to repress transcription in proximity to the damaged sites.

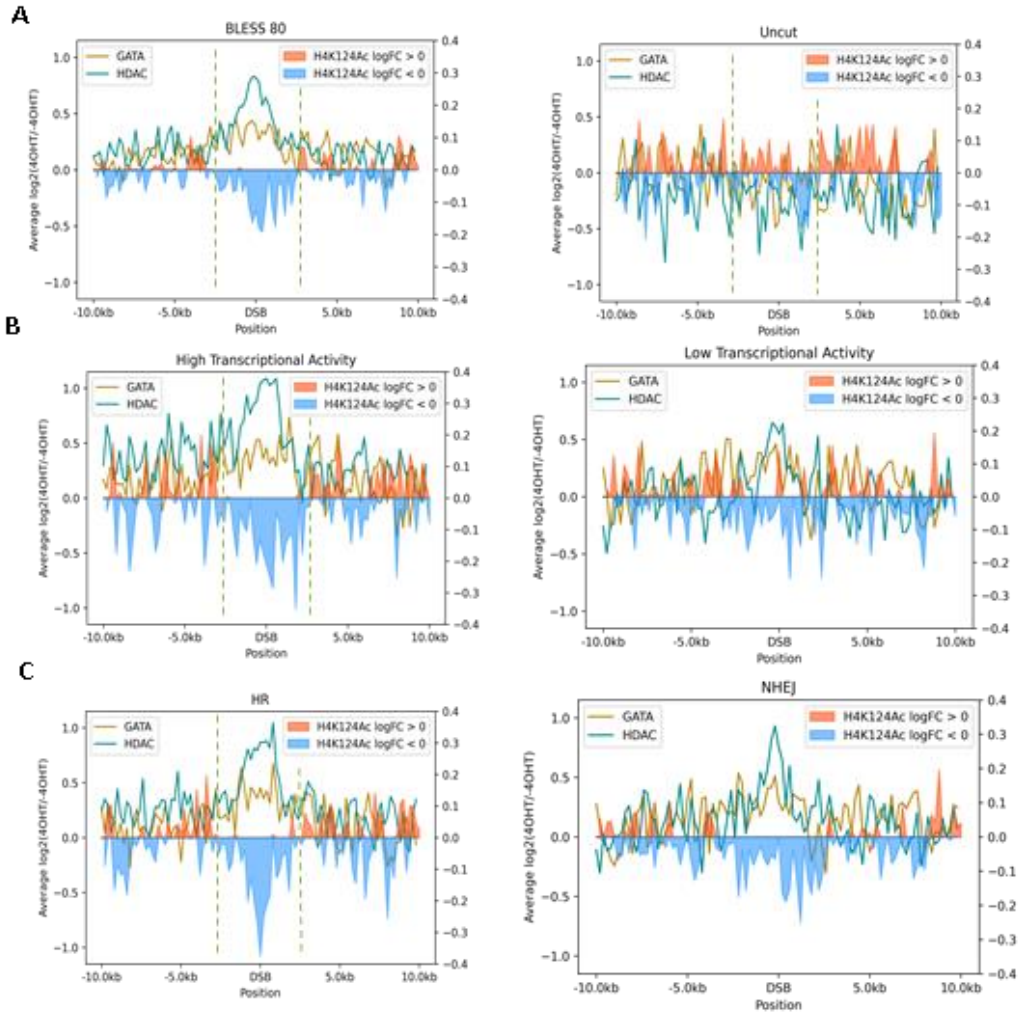


Figure 4-3 R-loops and GATAD2B-NuRD complex reduce H4K12 acetylation level within their chromatin boundary. (A) Metagene profile showing ChIP-seq enrichment of GATAD2B, HDAC1, and H4K12ac at AsiSI cut and uncut sites (as defined by BLESS technique). (B) Metagene profile showing ChIP-seq enrichment of GATAD2B, HDAC1, and H4K12ac at AsiSI cut sites in highly transcribed regions and low transcripted regions respectively. (C) Metagene profile showing ChIP-seq enrichment of GATAD2B, HDAC1, and H4K12ac at AsiSI cut sites in HR-prone and NHEJ-prone regions.

4.5 R-loops and GATAD2B-NuRD complex facilitate histone deacetylation around DSBs

Next, I was eager to investigate whether R-loops and the GATAD2B-NuRD complex could regulate general histone acetylation around DSBs. To test this, I transfected

HeLa cells with expression vectors encoding RNase H1 and siRNA against MBD3 or GATAD2B and performed PLA using antibodies against γH2AX and pan-acetyl H3 or pan-acetyl H4. As expected, the γH2AX-pan-acetyl-H3 PLA signal was detected upon 10 Gy IR treatment, and interestingly, I found that knockdown of MBD3 or GATAD2B and overexpression of RNase H1 significantly increased the number of PLA foci (Figure 4-4A). Similarly, I observed H4 acetylation around DSBs by performing γH2AX-pan-acetyl-H4 PLA, and transfection of siMBD3, siGATAD2B, or RNase H increased the level of histone H4 acetylation (Figure 4-4B). These results suggest that R-loops and the GATAD2B-NuRD complex facilitate histone deacetylation around DSBs.

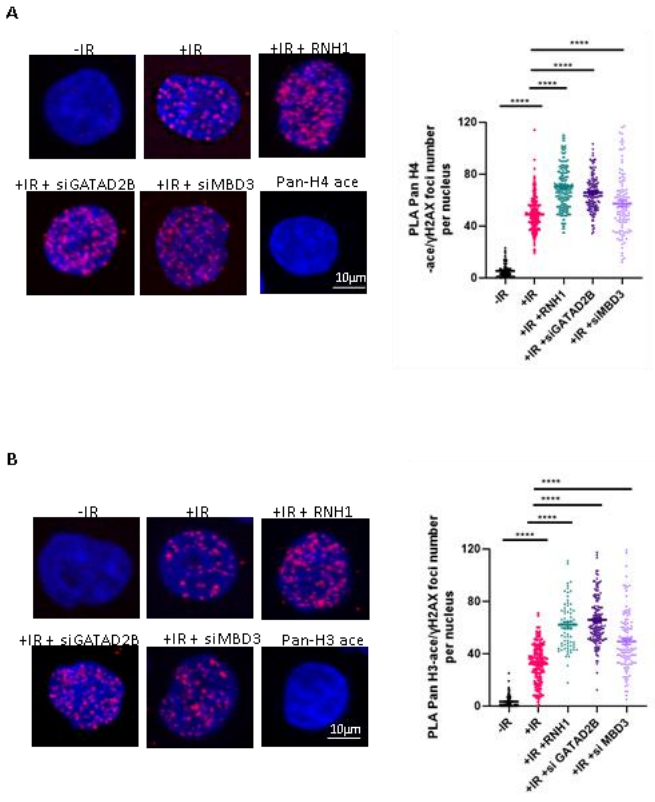


Figure 4-4 PLA of pan-acetyl H3 or H4 and γH2AX in cells with or without IR, and overexpression of RNAseH1 or depletion of GATAD2B and MBD3. IR=10Gy. (A) Left: representative confocal microscopy images of PLA of pan-acetyl H3 and γ H2AX; right: quantification of the left, error bar = mean ± SEM, significance was determined using a non-parametric Mann-Whitney test. (B) Left: representative confocal microscopy images pan-acetyl H4 and γ H2AX; right: quantification of the left, error bar = mean ± SEM, significance was determined using a non-

parametric Mann-Whitney test. ****p ⩽ 0.0001.

To further explore the relationship between histone acetylation and the chromatin boundary of the GATAD2B-NuRD complex, I transfected DIvA cells with siRNA against GATAD2B, followed by the addition of 4-OHT before harvesting the cells and performing histone H4 and pan-acetyl H4 ChIP-qPCR. When compared to control cells, I observed that relative histone H4 acetylation levels remained unchanged within 2.0 kb from two different AsiSI cutting sites upon 4-OHT treatment, although lower H4 occupancy was detected within 1 kb from DSBs. However, reduced levels of histone H4 acetylation were observed at distances greater than 3.0 kb from DSBs, which are beyond the chromatin boundary of the GATAD2B-NuRD complex (approximately 2.5 kb from DSBs, as shown in the ChIP-seq results from the Chapter 3), upon DNA damage. More interestingly, GATAD2B depletion led to significantly increased levels of H4 acetylation and lower histone H4 intensity around the two DSBs upon 4-OHT treatment (Figures 4-5A-C). These results revealed that R-loops and GATAD2B could facilitate histone deacetylation beyond their chromatin boundaries upon DNA damage.

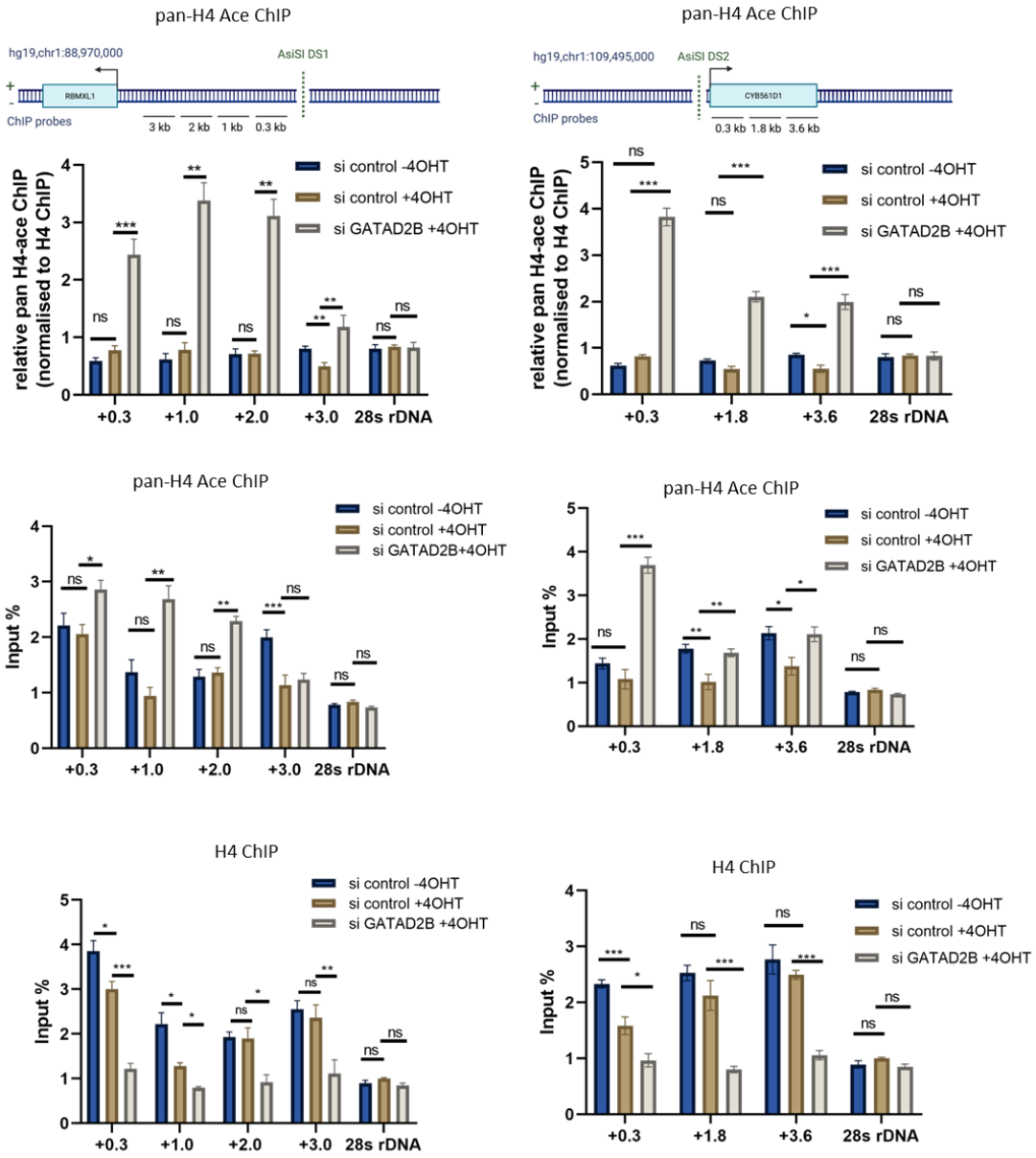


Figure 4-5 The GATAD2B-NuRD complex and R-loops promote histone de-acetylation at DSBs. (A) Top: drawing showing DS1 and DS2 genomic region with AsiSI cut site and position of ChIP-qPCR probes. Bottom: Bar chart showing relative pan-acetyl H4 ChIP levels (normalized to H4 ChIP levels) at indicated sites next to AsiSI cut in cells with or without 4-OHT and depletion of GATAD2B, error bar = mean ± SEM, significance was determined using non-parametric Mann-Whitney test. (B) Bar chart showing raw pan-acetyl H4 ChIP levels at indicated sites (Left: DS1, right: DS2) next to AsiSI cut in cells with or without 4-OHT and depletion of GATAD2B, error bar = mean ± SEM, significance was determined using non-parametric Mann-Whitney test. (C) Bar chart showing raw pan-acetyl H4 ChIP levels at indicated sites (Left: DS1, right: DS2) next to AsiSI cut in cells with or without 4-OHT and depletion of GATAD2B, error bar = mean ± SEM, significance was determined using non-parametric Mann-Whitney test. ***p ⩽ 0.001, **p ⩽ 0.01, *p ⩽ 0.05 n.s. not significant.

4.6 R-loops and GATAD2B-NuRD complex limit chromatin accessibility upon DSBs

Above, I showed that R-loops and the GATAD2B-NuRD complex could repress transcription *in cis* to DSBs. R-loops, together with the GATAD2B-NuRD complex, were also found to play important roles in histone modification and chromatin remodeling, which could affect chromatin accessibility to several proteins, such as transcription factors and RNA polymerases, consequently affecting transcription. To verify whether R-loops and the GATAD2B-NuRD complex could affect chromatin accessibility upon DSBs, I applied an MNase-based chromatin accessibility assay(126). MNase is a non-specific endo-exonuclease that can cleave naked, unprotected DNA, while protein-bound chromatin regions, such as histone-bound nucleosomes, will remain undigested. Thus, more accessible regions in open chromatin will be more digested by MNase, resulting in a ladder of DNA fragments that can be visualized by agarose gel electrophoresis. Each band corresponds to DNA protected by units of nucleosomes. The lowest band represents DNA fragments forming a single nucleosome (mono-nucleosome, ~147bp), and the upper bands represent DNA segments forming multiple nucleosomes. Consequently, relatively more mono-nucleosomes could be detected after MNase digestion of accessible open chromatin. By performing this MNase-based chromatin accessibility assay, I observed that an increased number of mono-nucleosomes could be detected in cells treated with 10 Gy of IR. Interestingly, overexpression of RNase H significantly increased MNase accessibility and digestion upon DNA damage (Figure 4-6A), indicating that the removal of R-loops could lead to higher chromatin accessibility and consequently to a more opened and relaxed chromatin structure at the early stages of DDR.

I then tested whether the GATAD2B-NuRD complex could have a similar function upon DNA damage. Accordingly, higher chromatin accessibility could be detected in control cells upon 10 Gy IR treatment as measured by the increased DNA band intensity at 147bp. Surprisingly, GATAD2B depletion led to a dramatically increased number of mono-nucleosome when compared to control cells upon IR treatment (Figure 4-6B), indicating that knock-down of GATAD2B also led to a more accessible chromatin structure. Thus, these results suggested that the GATAD2B-NuRD complex and R-loops could limit chromatin accessibility upon DNA damage.

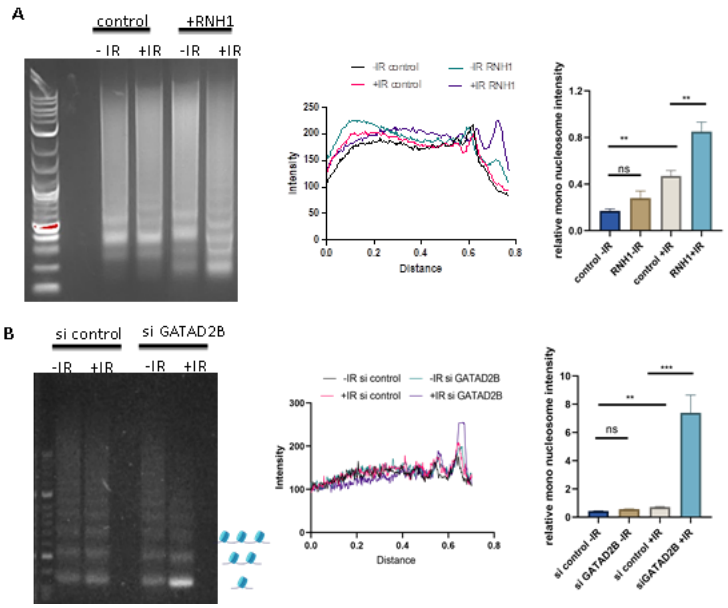


Figure 4-6 R-loops and GATAD2B-NuRD complex limit chromatin accessibility upon DSBs. (A) Left: DNA gel showing nucleosome profile of wild-type and cells overexpressing RNaseH after MNase treatment and DNA extraction. Middle: Intensities profile showing DNA densities profile from the top to bottom of each lane as indicated. Right: Bar chart showing the relative mono-nucleosome intensity of each lane. **p ⩽ 0.01, n.s. not significant. (B) Left: DNA gel showing nucleosome profile of wild type and cells lacking GATAD2B after MNase treatment and DNA extraction. Middle: Intensities profile showing DNA densities profile from the top to bottom of each lane as indicated. Right: Bar chart showing the relative mono-nucleosome intensity of each lane. **p ⩽ 0.01, n.s. not significant.

4.7 GATAD2B-NuRD complex prevents chromatin hyper-relaxation upon DSBs

It was reported that DNA damage could lead to a more relaxed chromatin structure around DSBs to allow the access of DDR factors to the broken DNA(172). Chromatin accessibility is typically associated with its structure, where more relaxed chromatin usually exhibits higher accessibility(194). While I observed that the GATAD2B-NuRD complex could limit chromatin accessibility upon DNA damage, I then asked whether GATAD2B could regulate chromatin relaxation upon DNA damage. To examine this, I utilized plasmids encoding core histone H2B fused to the PAGFP proteins, which undergo a transition from a dark state to a fluorescent state upon illumination at 405 nm(86, 195). By transfecting these plasmids and employing live-cell imaging combined with laser micro-irradiation, I could study the kinetics of chromatin decondensation following DNA damage by measuring the thickness and intensity of GFP stripes. Consistent with previous studies, I observed rapid chromatin relaxation upon laser micro-irradiation in control cells. Surprisingly, I discovered that knockdown of GATAD2B resulted in significantly increased chromatin relaxation upon laser-induced DNA damage (Figure 4-7). Hence, my results suggest that the GATAD2B-NuRD complex negatively regulates chromatin decondensation and prevents excessive chromatin relaxation in response to DNA damage.

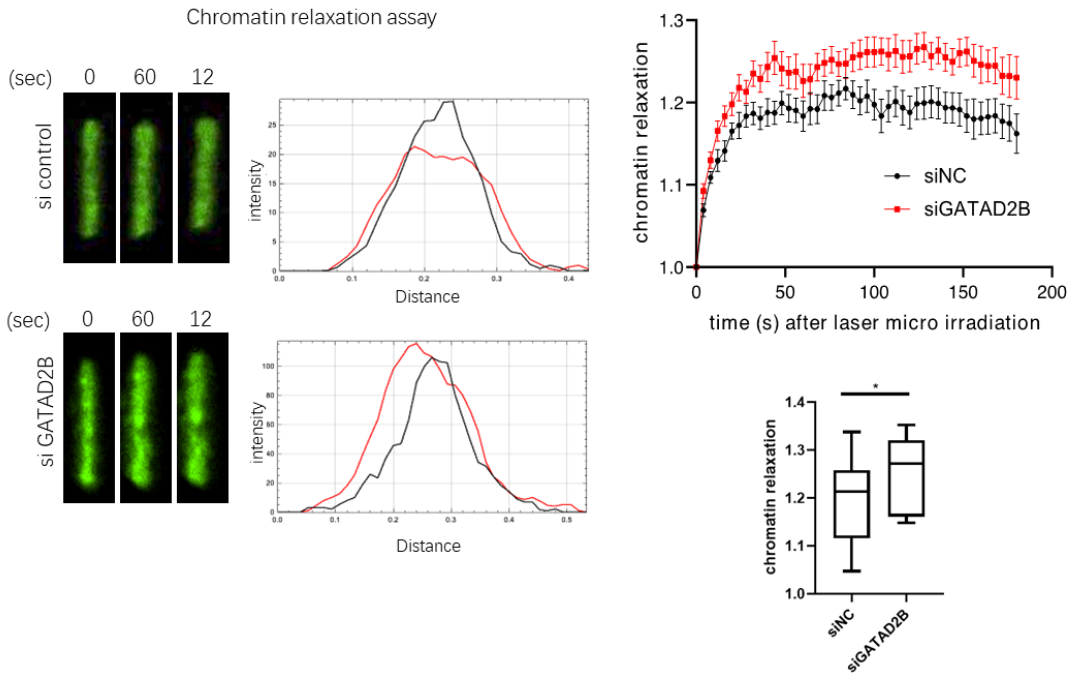


Figure 4-7 GATAD2B-NuRD complex prevents chromatin hyper-relaxation upon DSBs. Left: Representative confocal images of the chromatin line that is simultaneously damaged by irradiation at 405 nm in U2OS wt or GATAD2B KD cells, and intensity profiles showing thickness of the irradiated lines at 0 s (black) and 120 s (red) after damage induction. Top right: Graph showing the kinetics of chromatin relaxation in wt U2OS and GATAD2B KD cells after DNA damage induction. Bottom right: Box plot showing the levels of chromatin relaxation at 120 s after laser irradiation in wt and GATAD2B KD cells.

4.8 R-loops and GATAD2B-NuRD complex prevent hyper DNA end resection upon DSBs

Transcription can drive the repair of double-strand breaks (DSBs) towards the homologous recombination (HR) pathway. I showed that GATAD2B and HDAC1 are significantly associated with HR-prone loci upon DSBs. Additionally, it has been demonstrated that chromatin remodeling can influence the process of end resection, which is a crucial initial step of HR(139, 196, 197). Specifically, chromatin relaxation can increase the accessibility of exonucleases to the broken DNA ends, facilitating the end resection process and generation of single-stranded DNA overhangs. I have

provided evidence that R-loops and the GATAD2B-NuRD complex can limit chromatin accessibility and prevent excessive chromatin relaxation upon DNA damage. Therefore, I hypothesized that R-loops and the GATAD2B-NuRD complex could facilitate the termination of the end resection process and prevent hyper-resection of the broken DNA ends. To test this hypothesis, I performed immunofluorescence using an antibody against phospho-S4/S8 RPA32, which binds to single-stranded DNA (ssDNA) overhangs at DSBs. As expected, I observed the formation of phospho-S4/S8 RPA32 foci upon treatment with IR. Interestingly, treatment with transcription inhibitors (DRB or triptolide), overexpression of RNase H1, or transfection of siRNA targeting MBD3 or GATAD2B resulted in significantly higher levels of phosphorylated RPA32 (Figure 4-8A). To further investigate the effect of R-loops and the GATAD2B-NuRD complex on the end resection process, I treated HeLa cells with 5-bromo-2'-deoxyuridine (BrdU) before IR and performed immunofluorescence staining for BrdU under native conditions. BrdU is incorporated into DNA during replication, and typically, DNA needs to be denatured for the BrdU antibody to detect any BrdU incorporated into the DNA. However, during the end resection step, damaged DNA is cleaved into single-stranded DNA, providing access for antibody binding. Thus, the number of BrdU foci can indicate the levels of single-stranded DNA(198). Using BrdU immunofluorescence, I discovered that transcription inhibition, overexpression of RNase H1, or depletion of GATAD2B or MBD3 resulted in higher levels of BrdU signal when compared to wild-type cells upon IR treatment (Figure 4-8B). These findings suggest that R-loops and GATAD2B can limit DNA end resection upon DSBs.

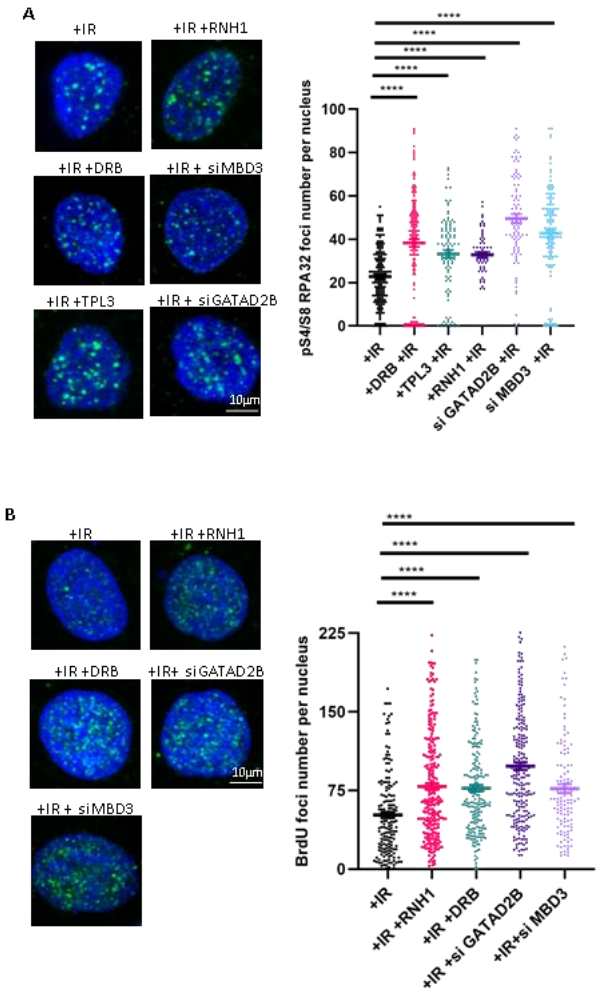


Figure 4-8 R-loops and GATAD2B-NuRD complex prevent hyper DNA end resection upon DSBs. (A) Left: representative confocal images showing immunofluorescence signals of phospho S4/S8 RPA32 in irradiated cells with overexpression of RNAseH1 or transcription inhibition (TLP3 or DRB) or depletion of GATAD2B and MBD3. Right: quantification of left, error bar = mean ± SEM, significance was determined using non-parametric Mann-Whitney test. (B) Left: representative confocal images showing immunofluorescence signals of BrdU in irradiated cells with transcription inhibition (TLP3 or DRB), overexpression of RNAseH1 or depletion of GATAD2B and MBD3. Right: quantification of left, error bar = mean ± SEM, significance was determined using non-parametric Mann-Whitney test. ****p $\leqslant$ 0.0001.

Uncontrolled DNA end resection can lead to the generation of longer single-stranded DNA overhangs, which may be susceptible to exonuclease attack or trigger alternative DSB repair pathways such as single-strand annealing (SSA) or micro-homology-mediated end joining (MMEJ). Consequently, this can result in the loss of genetic information, especially in regions with repetitive sequences(64, 115). To further verify the roles of R-loops and the GATAD2B-NuRD complex in the DNA end resection

process, I utilized the IPpOI-ER restriction enzyme to induce site-specific DSBs at the 28s rDNA region, which consists of repetitive sequences (199). Interestingly, overexpression of RNase H1 or knockdown of GATAD2B led to a loss of 28s rDNA copy number (Figure 4-9). These findings provide further support for the role of R-loops and the GATAD2B-NuRD complex in the termination of end resection and the prevention of genetic information loss.

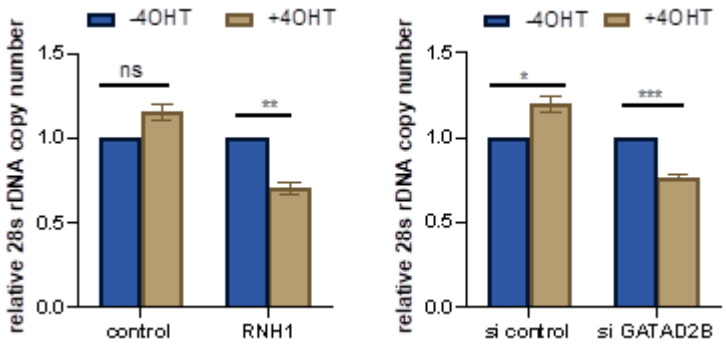


Figure 4-9 R-loops and GATAD2B-NuRD complex prevent loss of 28s rDNA copy number upon DSBs. Bar charts showing the change of 28s rDNA copy number upon 4OHT induction compared to no damage condition in cells expressing IPpOI, and overexpression of RNaseH (left) or knockdown of GATAD2B (right)

4.9 The GATAD2B-NuRD complex regulates HR repair efficiency

Correct end resection is crucial for the HR pathway, and GATAD2B has been shown to accumulate at HR-prone regions upon DSBs. To test whether the GATAD2B-NuRD complex is required for efficient HR repair, I employed U2OS DR-GFP and EJ5-GFP cells, which bear HR and NHEJ reporter cassettes respectively(56, 200). In the DR-GFP system, the first copy of the GFP gene is disrupted by inserted external DNA sequences, while the downstream repeat is a 5' and 3' truncated GFP fragment that lacks the start and stop codons under normal conditions. Consequently, no green fluorescence is detected. However, upon induction of DSBs by I-SceI cleavage, the

first copy of GFP utilizes the downstream GFP fragment as a repair template, leading to HR repair and reconstitution of the functional GFP gene (Figure 4-10A). Similarly, in the EJ5-GFP system, the expression of GFP genes on the NHEJ cassette is interrupted by inserted puromycin genes, resulting in no green fluorescence signal under normal conditions. However, upon induction of site-specific DSBs by I-SceI, the two broken DNA ends can be rejoined, removing the inserted segments and restoring the function of the GFP gene (Figure 4-10B). Using these reporter assays, I observed that knockdown of GATAD2B and MBD3 decreased HR efficiency, while NHEJ efficiency remained unaffected (Figure 4-10A and B). These findings strongly suggest that the GATAD2B-NuRD complex is crucial for efficient HR repair.

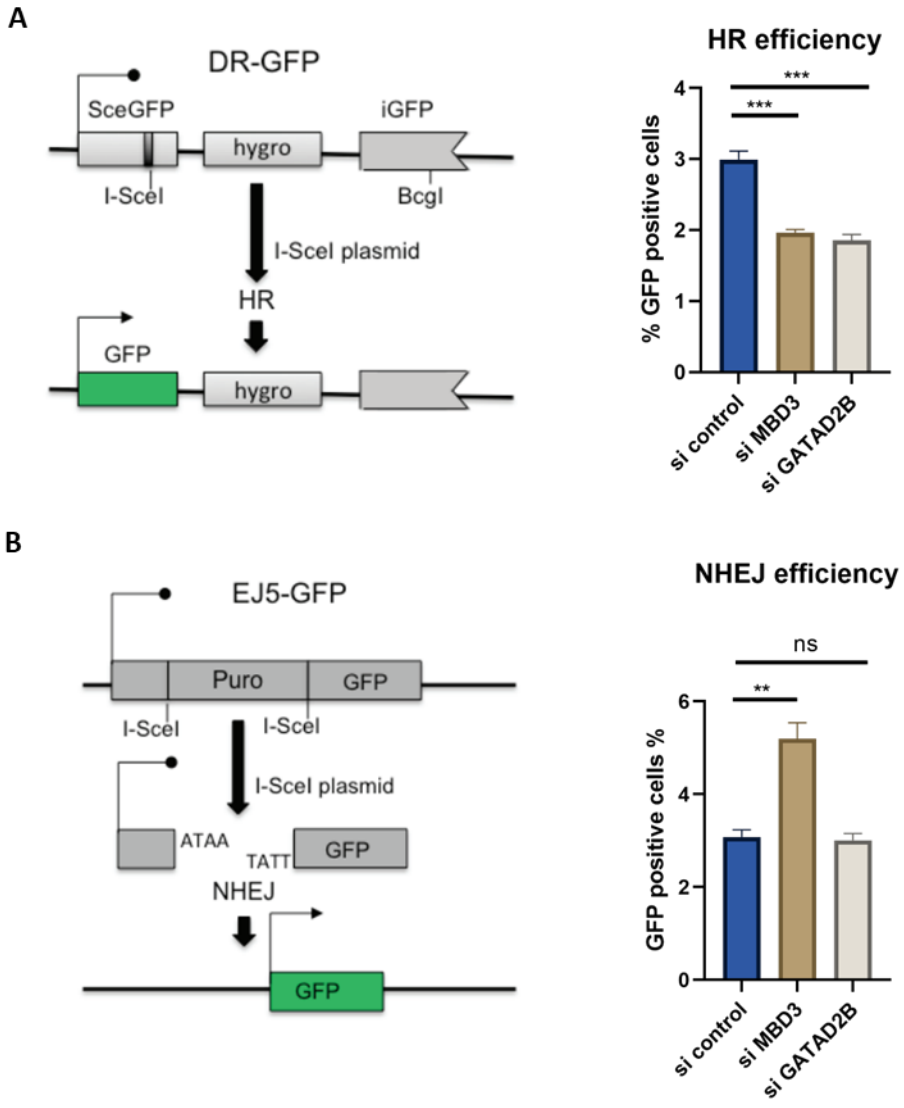


Figure 4-10 The GATAD2B-NuRD complex regulates HR repair efficiency. (A) Left: Drawing indicating the structure of HR reporter cassette, Sce GFP: the first copy of GFP in un-rearranged cassette, iGFP, the second copy of GFP in un-rearranged HR cassette. Right: bar charts showing HR repair efficiency under DSB inducted by I-SceI in U2OS cells containing HR reporter, and knockdown of MBD3 and GATAD2B, inhibition of DNA-PK and ATR. (B) Left: Drawing indicating the structure of NHEJ reporter cassette, Puro, the inserted puromycin gene. Right: bar charts showing NHEJ repair efficiency under DSB inducted by I-SceI in U2OS cells containing NHEJ reporter, and knockdown of MBD3 and GATAD2B.

4.10 The GATAD2B-NuRD complex facilitates the kinetics of DSB repair

To further investigate the importance of the GATAD2B-NuRD complex in efficient completion of DSB repair, I performed immunofluorescence staining for γH2AX to monitor the clearance of this DSB marker after IR treatment. After a 1-hour recovery following 2 Gy IR, a similar number of γH2AX foci was detected in the control group and cells transfected with siRNA against MBD3 or GATAD2B. However, at 12 hours after IR, I observed a delayed clearance of γH2AX in cells lacking GATAD2B and MBD3 (Figure 4-11A). This indicates that the DSB repair process was negatively affected in these deficient cells. To directly measure the DSB repair process, I employed the comet assay, which allows for the quantification of DNA damage. In this assay, more DNA damage leads to the release of smaller DNA segments, which generate tails upon 2D-gel electrophoresis. By measuring tail moments, I could directly assess the level of DSBs. Similar to the immunofluorescence results, depletion of GATAD2B and MBD3 did not induce more DNA damage immediately after IR. However, after a 6-hour recovery, a significant accumulation of DNA tails was observed in GATAD2B- and MBD3-deficient cells compared to wild-type cells (Figure 4-11B). These findings suggest that the GATAD2B-NuRD complex plays a role in facilitating the kinetics of DSB repair.

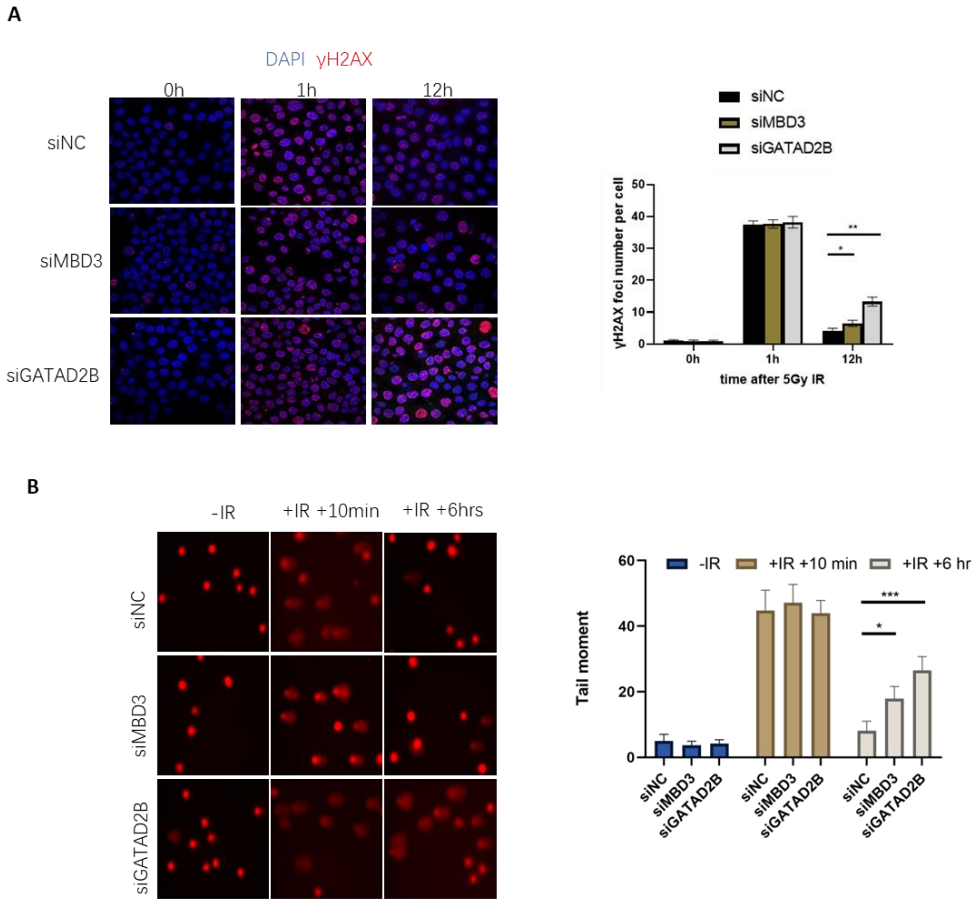


Figure 4-11 The GATAD2B-NuRD complex facilitates DSB repair kenetics. (A) Immunofluorescence of γH2AX in cells with IR, and depletion of GATAD2B and MBD3. Left: representative confocal microscopy images; right: quantification of left, error bar = mean ± SEM, significance was determined using non-parametric Mann-Whitney test. ***p ⩽ 0.001, ** p ⩽ 0.01, * p ⩽ 0.05. (B) Left: representative microscopy images showing comet assay of control (siNC), or GATAD2B and MBD3 knock down cells without IR, or irradiated with 5 Gy with 10 min recovery and 6 hr recovery. Right: quantification of left, error bar = mean ± SEM, significance was determined using non-parametric Mann-Whitney test.

4.11 Hypothetical model of chromatin boundaries between open and condensed chromatin

Taken together, we propose a model where R-loops coordinate the GATAD2B-NuRD complex to regulate chromatin remodeling, transcription, and DNA repair process upon DNA damage. These results drive the hypothesis that R-loops recruit

GATAD2B-NuRD complex to DSBs to establish chromatin boundaries between open and condensed chromatin, which is required for transcriptional repression of genes in proximity to DSBs and termination of end resection of damaged DNA ends (Figure 4-12).

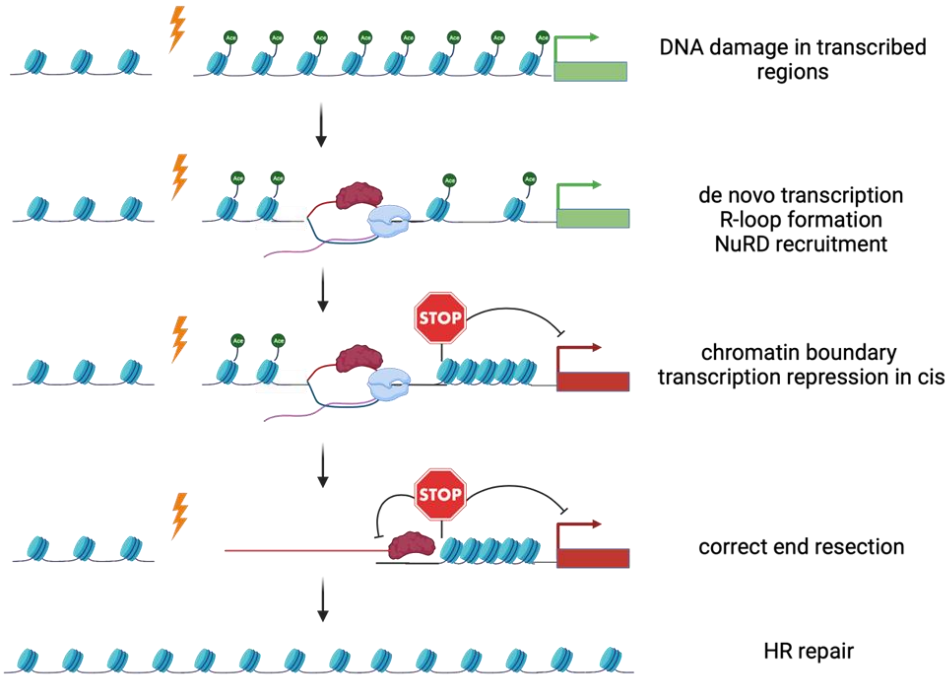


Figure 4-12 The Model of chromatin boundary around DSBs established by GATAD2B-NuRD complex and R-loops. GATAD2B-NuRD complex associates with DSBs in a transcription and R-loop-dependent manner, creating a boundary and facilitating histone deacetylation and chromatin condensation around DSBs. Its presence near damaged loci is required for transcriptional repression in cis. The lack of the GATAD2B-NuRD complex leads to chromatin hyper-relaxation and extended DNA end resection, causing failure in HR repair.

4.12 Discussion

In this chapter, I investigated the roles of R-loops and GATAD2B in DDR, in particular their roles in chromatin remodeling, transcription regulation, and efficient DSB repair.

Previous research has shown that R-loops and the NuRD complex are involved in

transcription regulation under non-damage conditions. By inducing site-specific DSBs in DIvA cells, I observed that R-loops and the GATAD2B-NuRD complex repress nascent transcription in the vicinity of DSBs. These findings were further supported by analyzing H4K12ac ChIP-seq data from a previous study(135). H4K12 acetylation is associated with actively transcribed regions, and a decrease in H4K12 acetylation levels were observed around DSBs. Interestingly, when aligning GATAD2B and HDAC1 ChIP-seq data with the H4K12ac profile, a negative correlation between H4K12ac levels and GATAD2B or HDAC1 levels around DSBs was detected. This suggests that acetylated H4K12 may serve as a potential substrate for the GATAD2B-NuRD complex during DNA damage. Furthermore, it has been observed that RNA polymerase II (RNAPII) pausing occurs around DSBs(82), and DSB-induced *de novo* transcription at these sites requires regulated termination. Therefore, it is plausible that the HDAC1-containing NuRD complex deacetylates H4K12 to facilitate transcription termination, which in turn prevents transcription elongation and represses transcription *in cis* to DSBs. Indeed, R-loops were reported to regulate transcription termination(107). However, further investigation is required to determine whether the GATAD2B-NuRD complex plays a role in transcription termination and whether R-loops coordinate with the GATAD2B-NuRD complex to facilitate this process, particularly in the context of DSBs.

R-loops were found to regulate chromatin remodeling by either relaxing or condensing chromatin structures. Using MNase-based chromatin accessibility assay and PAGFP-H2B-based laser micro-irradiation, I found R-loops and the GATAD2B-NuRD complex limit chromatin decondensation at the early stage of DDR. Chromatin remodeling is an important step in DDR(172). Although relaxed chromatin is required for increased accessibility for DDR factors to broken DNA ends, it is worth noting

that heterochromatin markers, such as H3K9me3, are often observed to be enriched next to DSBs(144), and several proteins involved in chromatin condensation, such as HP1 and G9a, are also found to be localized around DSBs(142, 143). Interestingly, these two proteins have been reported to be recruited to transcription termination loci to establish heterochromatin formation after R-loops dependent H3K9me2 deposition(144). Additionally, a delicate balance of various proteins and histone modifications associated with heterochromatin and euchromatin has been observed at sequence-independent heterochromatin borders(201, 202). Therefore, it is plausible that R-loops formed at DSBs act as boundary elements, facilitating the recruitment of the GATAD2B-NuRD complex to promote histone deacetylation. This deacetylation allows for the availability of lysine residues on histones for the deposition of other modifications, such as methylation by G9a. Consequently, this facilitates the loading of HP1, which in turn recruits SUV39H to methylate neighboring histones to establish and propagate heterochromatin structure.

In Chapter 3 I showed that the GATAD2B-NuRD complex co-localizes with R-loops at 2.5 kb around DSBs, creating a boundary between the damaged locus and surrounding chromatin. Interestingly, I detected histone H4 deacetylation beyond 2.5kb from damaged DNA ends, which are chromatin boundaries formed by the GATAD2B-NuRD complex. Thus, it is worth noting that the GATAD2B-NuRD complex and R-loops may also play a role in controlling the spread of heterochromatin unidirectionally away from DSBs, potentially serving as a mechanism to repress transcription *in cis* to DSBs and terminate end resection of broken DNA end, while ensuring sufficient *de novo* transcription and accessibility for DDR factors at DSBs.

Another component of the NuRD complex, CHD4, has been found to be recruited to DSBs and is involved in transcriptional repression *in cis* to DSBs(203). Though I found that the GATAD2B-NuRD complex could limit chromatin relaxation and establish the boundary between open and condensed chromatin, CHD4 was reported to promote chromatin relaxation upon DNA damage(86, 204). CHD4 has ATP-dependent chromatin remodeling activities, which enables it to facilitate nucleosome assembly, sliding, ejection, or histone exchange(205). Furthermore, reduced nucleosome intensity was found at DSBs to promote efficient HR repair(206). Thus, it is plausible that CHD4-dependent local chromatin relaxation is necessary for *de novo* transcription and R-loop formation around DSBs. This chromatin relaxation process likely clears the nucleosomes around DSBs and creates a nucleosome-free region, which prevents the spread of heterochromatin toward DSBs and thereby facilitates the establishment of R-loops dependent heterochromatin boundaries.

DSBs-induced R-loops formation has been primarily observed in transcriptionally active regions(97, 112, 169). Therefore, the GATAD2B-NuRD complex- and R-loop-dependent heterochromatin borders may be linked to DSB repair within gene loci that require precise repair through HR. This association is crucial for avoiding pathogenic mutations in these regions and maintaining genomic integrity.

One crucial aspect of HR is end resection, which is facilitated by chromatin decondensation(196). However, excessive end resection can result in long ssDNA overhangs that are prone to be cleaved by endonucleases and exonucleases. Long ssDNA overhang can also activate the single-strand annealing (SSA) and microhomology-mediated end-joining (MMEJ) pathways(64). These pathways can lead to significant loss of DNA, particularly in repetitive regions. Thus, termination of

end resection is crucial for effective HR repair. Interestingly, it was shown that end resection was terminated prior to the chromatin boundary formed by the GATAD2B-NuRD complex and restricted to approximately 2 kb from DSBs(36). My data suggest that the GATAD2B-NuRD complex-dependent chromatin boundary has important functions in the termination of end resection and efficient HR. This boundary helps to maintain the appropriate range of end resection, preventing excessive loss of genetic material and ensuring accurate and effective DNA repair.

Overall, these results suggested that R-loops and the GATAD2B-NuRD complex facilitate the establishment of the chromatin boundary between open and condensed chromatin. This boundary represses transcription *in cis* to DSBs, promotes the termination of end resection, and ensures efficient HR, especially at highly transcribed genomic loci.

5. The role of DROSHA in RNA-dependent DDR

5.1 Introduction

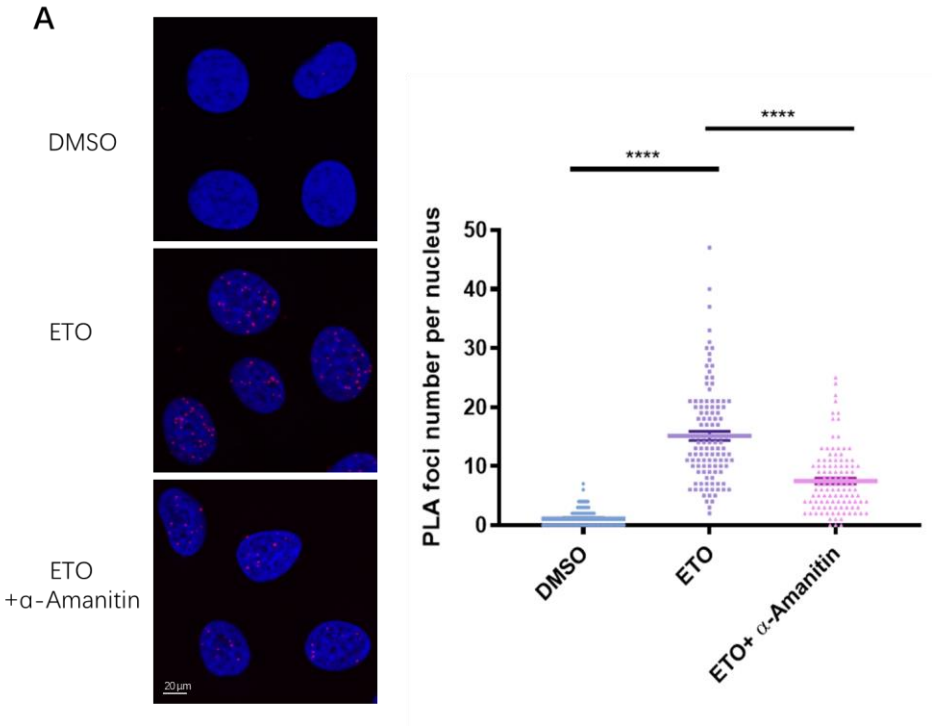
As mentioned before, DSBs could induce *de novo* transcription at damaged loci, which could produce DNA damage-induced long non-coding RNA (dilncRNA)(2, 3). This long non-coding RNA could hybridize with DNA and form DNA: RNA hybrid structures around DSBs(113).

Interestingly, it was reported that DROSHA could be recruited to DSBs, and facilitate the formation of DNA: RNA hybrids at broken DNA loci in an RNAi-independent manner(161, 165). However, the functions of DROSHA at DSB breaks and RNA-dependent DDR need to be further investigated. DROSHA was reported to have several non-canonical functions, including mRNA destabilisation and alternative splicing(160, 207-209). Furthermore, this protein was also found to facilitate or terminate transcription(157, 158). These non-canonical roles of DROSHA suggested that this protein may directly regulate DSBs-induced *de novo* transcription in an RNAi-independent manner. Intrigued by these previous studies, I was then keen on investigating the molecular mechanisms of DROSHA in regulating RNA-dependent DDR.

5.2 DROSHA is localized to DSBs in a transcription-dependent manner

As it was reported before that DROSHA could be recruited to DSBs and facilitate DNA: RNA hybrids formation around DSBs, I then asked whether the DSBs localization of DROSHA was dependent on transcription. To verify this hypothesis, I performed PLA using antibodies against DROSHA and γH2AX. In agreement with the previous studies, etoposide treatment could significantly increase number of DROSHA-γH2AX PLA foci. However, this increase was inhibited upon treatment with transcription inhibitor, α-amanitin (Figure 5-1A), suggesting that the recruitment of DROSHA to DSBs is dependent on RNA Pol II activity.

To further verify this, site-specific DSBs were induced in the DIvA system. By performing ChIP-qPCR experiments, I observed that DROSHA was enriched at the AsiSI cutting site DS1 upon 4-OHT treatment, while this enrichment was decreased upon transcription inhibition (Figure 5-1B). Thus, these results confirmed that DROSHA could be recruited to DSBs in a transcription-dependent manner



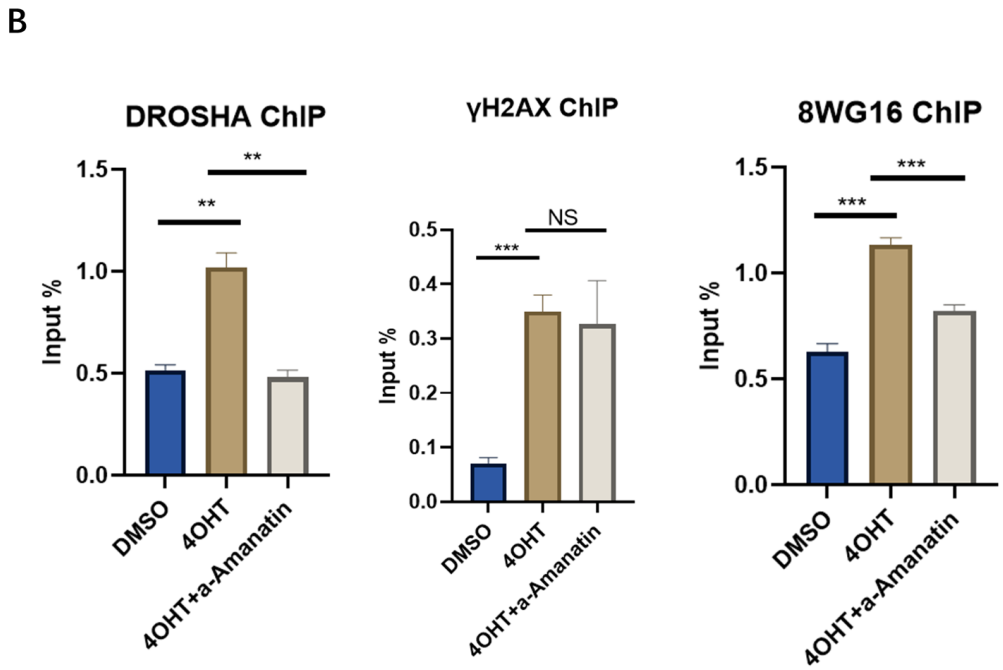


Figure 5-1 DROSHA could be recruited to DSBs in a transcription-dependent manner. (A) Left: Representative confocal microscopy imaging of DROSHA-γH2AX PLA under DMSO, etoposide (ETO), and etoposide/ α-Amanitin combined treatment. Right: quantification of Left, error bar = mean ± SEM, significance was determined using non-parametric Mann-Whitney test. ****p ⩽ 0.0001. (B) Bar chart showing DROSHA ChIP (left), γH2AX ChIP (middle), and RNA Pol II (right) levels at an AsiSI cutting site in cells with or without 4-OHT and treatment of α-Amanitin, error bar = mean ± SEM, significance was determined using non-parametric Mann-Whitney test. ***p ≤ 0.001, **p ⩽ 0.01, NS. not significant.

5.3 DROSHA interacts with RNA Pol II upon DNA damage

After I found that DROSHA could be recruited to DSBs in a transcription-dependent manner, I then asked whether DROSHA could interact with RNA Pol II upon DNA damage. In order to test this, I performed PLA by using antibodies against DROSHA and RNA Pol II. In no damage condition, DROSHA-RNA Pol II PLA foci could be detected, suggesting its roles in miRNA processing as well as transcription regulation. Surprisingly, etoposide treatment significantly increased number of PLA foci (Figure 5-2), suggesting that DNA damage stimulates interactions between DROSHA and RNA Pol II.

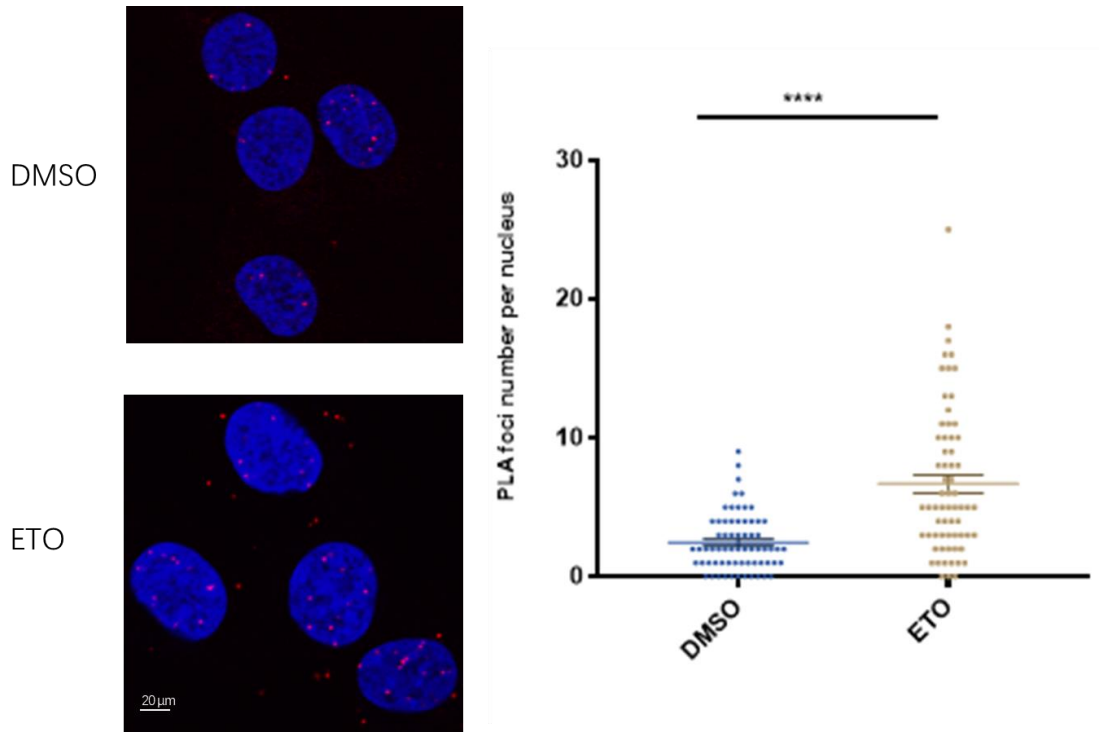


Figure 5-2 DROSHA preferentially interacts with RNA Pol II upon DNA damage. (A) Left: Representative confocal microscopy imaging of DROSHA-RNA Pol II PLA under DMSO, etoposide treatment. Right: quantification of Left, error bar = mean ± SEM, significance was determined using non-parametric Mann-Whitney test. ****$p \leqslant 0.0001$.

The C-terminal domain (CTD) of the largest subunit of RNA Polymerase II has multiple hepta-peptid repeats consisting of YSPTSPS(210). RNA Pol II activity is

regulated by the phosphorylation of its CTD(211, 212). Specifically, phosphorylation of the fifth serine in this domain (S5P) was found to be linked with transcription initiation(213), while phosphorylation of the second serine (S2P) in CTD regions was reported to be crucial for transcription elongation(214). Interestingly, a previous study revealed that the phosphorylation of tyrosine 1 residue in RNA Pol II CTD (CTD Y1P) is required for DSBs-induced *de novo* transcriptions(2). To further test whether DROSHA could interact with this specifically modified RNA Pol II upon DNA damage, I employed PLA assay using antibodies against DROSHA and Y1P CTD. Colocalization between DROSHA and RNA Pol II CTD Y1P was detected in no damage condition. Etoposide treatment resulted in significant increase in number of DROSHA-CTD Y1P PLA foci, and this DROSHA-CTD Y1P PLA signal was reduced upon transcription inhibition by triptolide (Figure 5-3). These results suggest that DROSHA could preferentially interact with Y1P CTD of RNA Pol II upon DNA damage. Overall, these data revealed that DROSHA could preferentially interact with RNA Pol II as well as CTD Y1P RNA Pol II upon DNA damage.

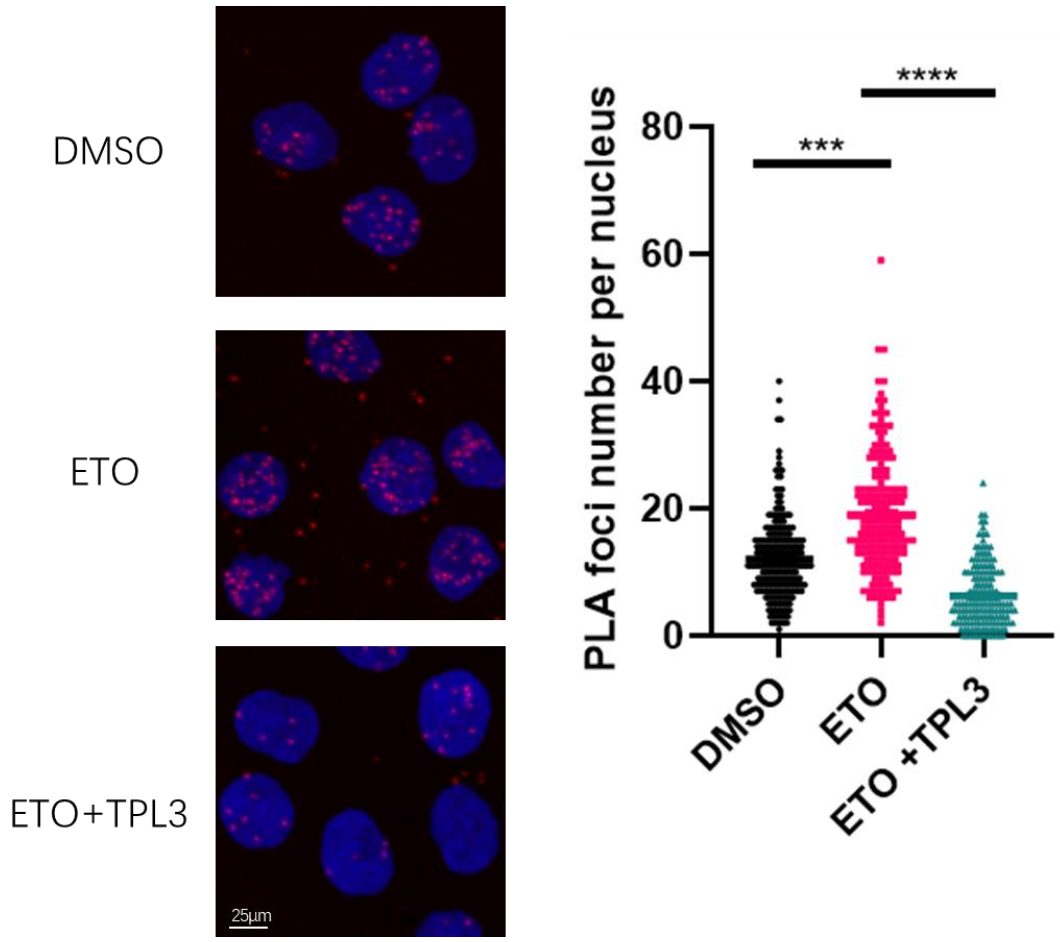


Figure 5-3 DROSHA preferentially interacts with RNA Pol II CTD Y1P upon DNA damage. Left: Representative confocal microscopy imaging of DROSHA-RNA Pol II CTD Y1P PLA under DMSO, etoposide treatment. Right: quantification of Left, error bar = mean ± SEM, significance was determined using non-parametric Mann-Whitney test. ****p ⩽ 0.0001, ***p ⩽ 0.001.

5.4 DROSHA KD leads to enrichment of active Pol II in proximity to DSB ends

It has been reported that DROSHA could facilitate the formation of DNA: RNA hybrids around DNA double-strand breaks (DSBs) and regulate transcription (157,

158, 161). Transcription is the main source of DNA: RNA hybrids and I have shown that DROSHA preferentially interacts with RNA polymerase II, especially with Y1P CTD RNA Pol II. Therefore, I investigated next whether DROSHA could regulate DSBs-induced *de novo* transcription.

To test this, I transfected DIvA cells with siRNAs against DROSHA, followed by treatment with DMSO or 4-OHT. Subsequently, I performed ChIP-qPCR using antibodies against RNA Pol II and its CTD modifications such as Y1P and S2P. Interestingly, RNA Pol II with CTD Y1P and S2P was significantly enriched in proximity to the DSB ends (approximately 0.3 kb) at two different AsiSI cutting sites after DROSHA knockdown following 4OHT treatment. However, the enrichment of RNA Pol II CTD Y1P and S2P was not significantly changed beyond these regions compared to the no-damage conditions. Moreover, the signal of RNA Pol II CTD Y1P and S2P at uncut AsiSI loci in cells treated with 4-OHT was similar to that of cells with no damage (Figure 5-4). These results suggest that DROSHA knockdown could lead to stalling or pausing of active RNA Pol II in close proximity to DSB end.

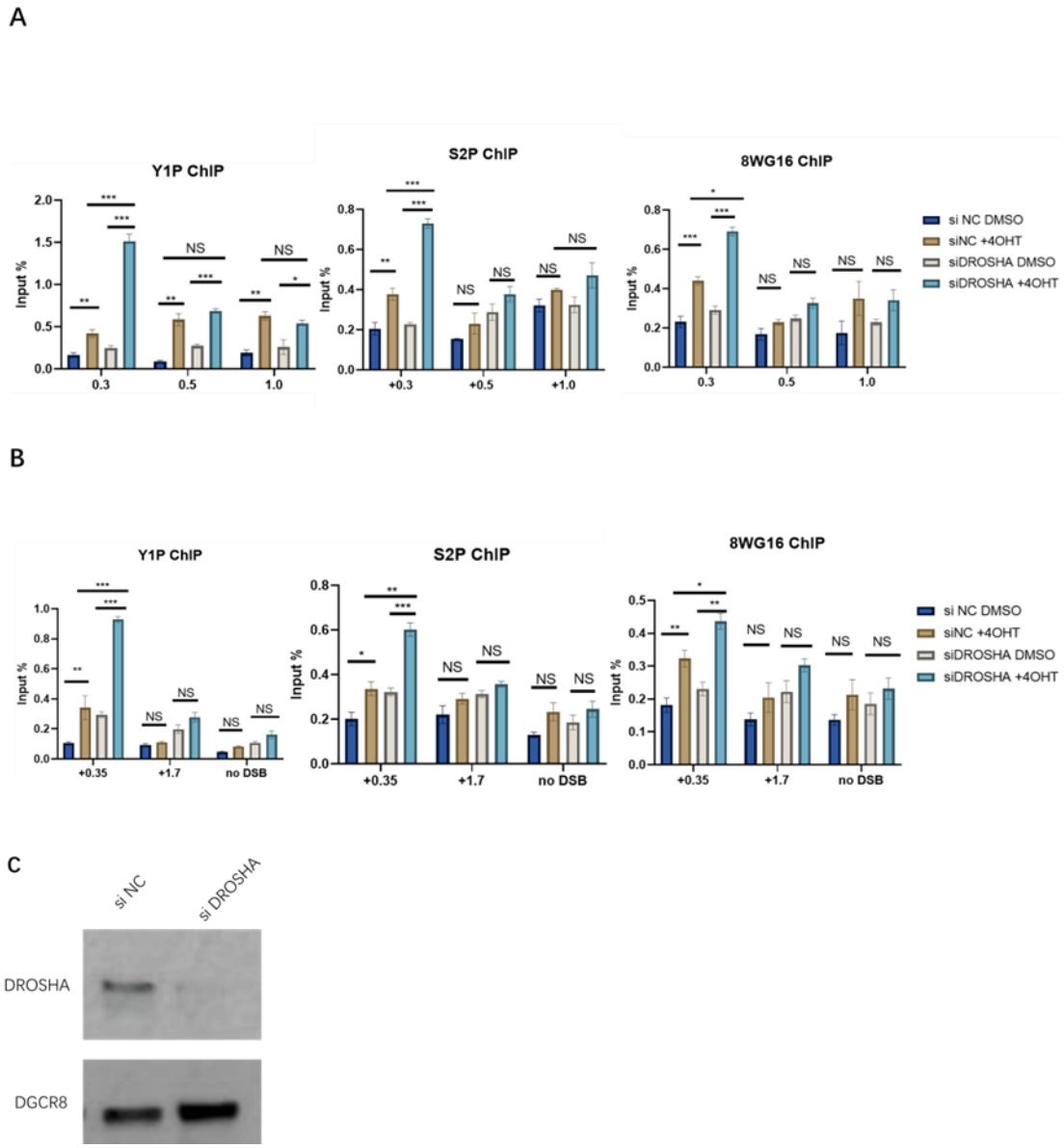


Figure 5-4 DROSHA KD could lead to stalled RNA Pol II CTD Y1P and S2P in proximity to DSB ends. (A) Bar chart showing RNA Pol II CTD Y1P ChIP (left), RNA Pol II CTD S2P ChIP (middle), and RNA Pol II (right) levels at indicated sites next to AsiSI cut (DS1, mentioned in Figure 4-5) in WT or DROSHA KD DIvA cells with or without 4-OHT, error bar = mean ± SEM, significance was determined using non-parametric Mann-Whitney test. ***$p \leq 0.001$, **$p \leqslant 0.01$, *$p \leqslant 0.05$ NS. not significant. (B) Bar chart showing RNA Pol II CTD Y1P ChIP (left), RNA Pol II CTD S2P ChIP (middle), and RNA Pol II (right) levels at indicated sites next to AsiSI cut (DS2, mentioned in Figure 4-5) in WT or DROSHA KD DIvA cells with or without 4-OHT, error bar = mean ± SEM, significance was determined using non-parametric Mann-Whitney test. ***$p \leq 0.001$, **$p \leqslant 0.01$, *$p \leqslant 0.05$ NS. not significant. (C) Imaging of western blot showing the KD efficiency of siRNA against DROSHA.

5.5 DROSHA interacts with CBP80 upon DNA damage

It was reported that DROSHA could interact with CBP80 to activate transcription of protein coding genes (157), I then asked whether stronger interaction between these two proteins could be detected upon DNA damage. To test this, I first performed co-IP by using antibodies against GFP to pull down interactomes of GFP-tagged DROSHA and its variants, followed by western blot. Specifically, plasmids encoding N terminal 1-390 of DROSHA (the minimum nuclear localization domain) and 1-850 (which lacks RNaseIII and dsRNA binding domains) were used for these analyses (215). As expected, imaging of western blot showed that the interaction between DROSHA and DGCR8 (known DROSHA binding factor involved in miRNA processing) was not significantly changed upon DNA damage, while interestingly, stronger interaction between CBP80 and full length DROSHA, but not its truncated variants, could be detected upon etoposide treatment (Figure 5-5 A). To verify the interaction between CBP80 and DROSHA upon DNA damage *in vivo* and clarify whether their interaction is dependent on transcription, I then performed PLA by using antibodies against these two proteins. Data generated from PLA revealed that DROSHA could interact with CBP80 upon DMSO treatment, while etoposide treatment significantly strengthens this interaction. Interestingly, triptolide-induced transcription inhibition could significantly inhibits the colocalization between CBP80 and DROSHA upon DNA damage (Figure 5-5B). Thus, these results suggested that DROSHA preferentially interacts with CBP80 upon DNA damage in a transcription-dependent manner.

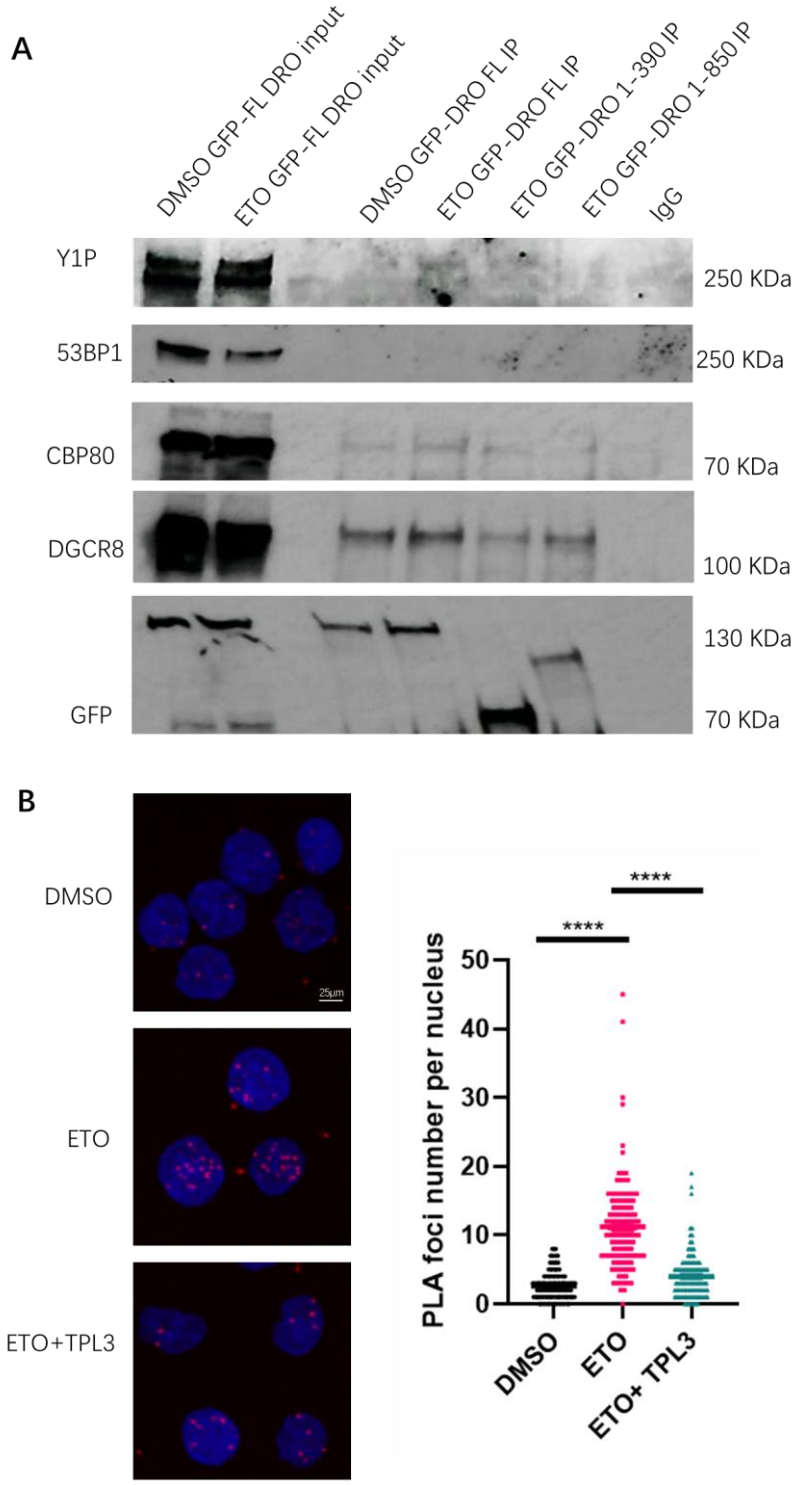


Figure 5-5 DROSHA preferentially interacts with CBP80 upon DNA damage. (A) Imaging of western blot of GFP-IP using indicated antibodies. HEK293T cells were transfected with plasmids encoding GFP-tagged different variants of DROSHA as indicated prior to treatment, FL DRO, full length DROSHA, DRO 1-390, 1-390 aa of DROSHA, DRO 1-850, 1-850 aa of DROSHA. (B) Left: Representative confocal microscopy imaging of DROSHA-CBP80 PLA under DMSO, etoposide, and etoposide/triptolide combined treatment. Right: quantification of Left, error bar = mean ± SEM,

significance was determined using non-parametric Mann-Whitney test. ****p ⩽ 0.0001.

5.6 CBP80 could be localized to DSBs in a DROSHA-dependent manner

Since DROSHA can be recruited to DSBs, and it preferentially interacts with CBP80 following DNA damage, I then asked whether CBP80 could also localize to damaged DNA. To address this question, I induced site-specific DSBs in DIvA cells and performed ChIP-qPCR by using the antibody against CBP80. Indeed, the ChIP signal was detectable at an AsiSI cutting locus. Furthermore, a significantly stronger signal was observed after 4-OHT treatment, suggesting that CBP80 might indeed be recruited to DSBs. Interestingly, the α-Amanitin treatment inhibited this elevation (Figure 5-6A), indicating that the recruitment of CBP80 is dependent on transcription. Given the observed preferential interaction between DROSHA and CBP80 upon DNA damage, I proceeded to investigate whether DROSHA could affect the CBP80 localisation to DSBs. To test this, I applied antibodies recognizing CBP80 and γH2AX to perform a PLA. The resulting images indicated significant increase in the CBP80-γH2AX PLA foci number upon etoposide treatment (Figure 5-6B). However, upon transfection of siRNA against DROSHA, a reduced number of CBP80-γH2AX PLA foci was detected following etoposide treatment (Figure 5-6B). Thus, these results collectively suggest that CBP80 could be recruited to DSBs in a manner dependent on both DROSHA and transcription.

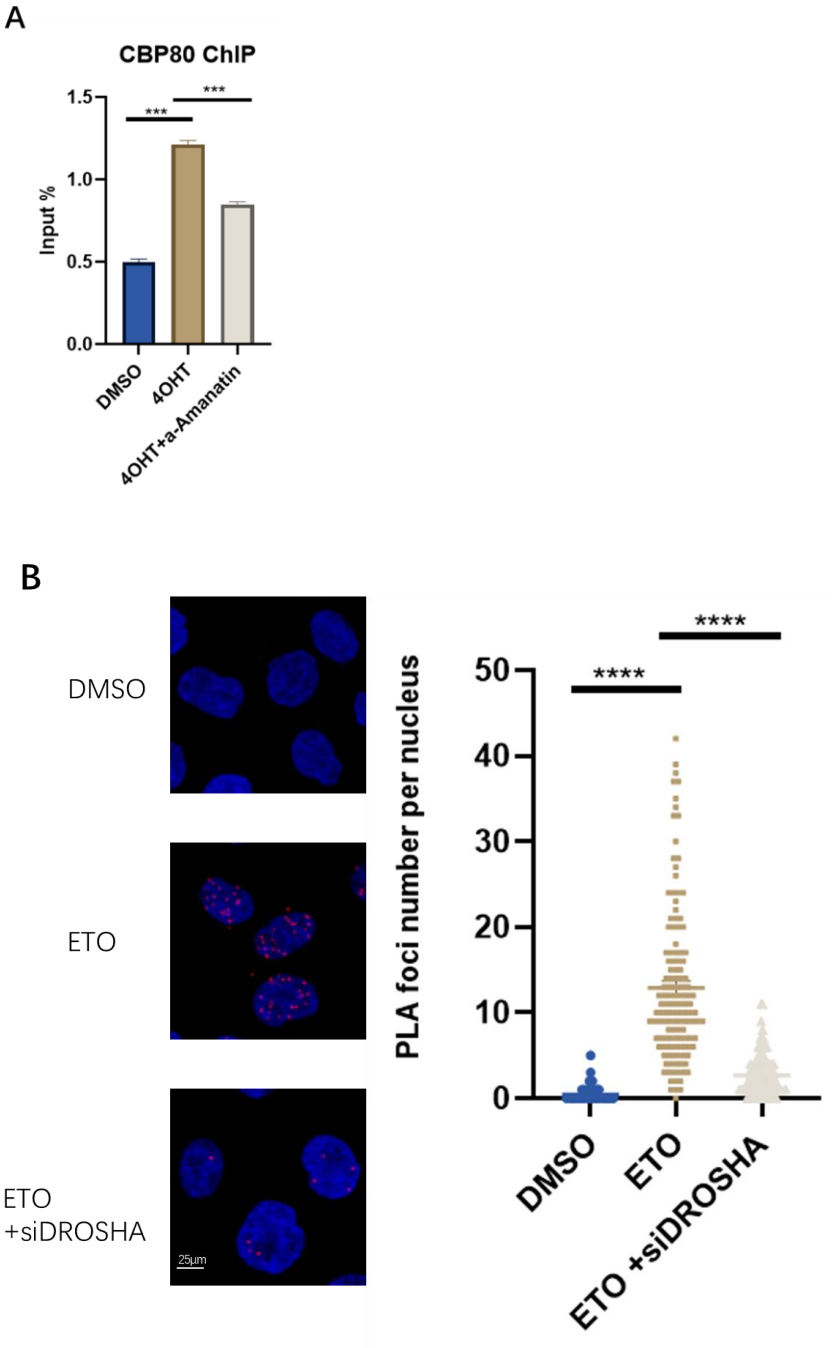


Figure 5-6 CBP80 could be recruited to DSBs in a transcription- and DROSHA-dependent manner. (A) Bar chart showing CBP80 ChIP levels at an AsiSI cutting site (DS1 +0.3 kb) in cells with or without 4-OHT and treatment of α-Amanitin, error bar = mean ± SEM, significance was determined using non-parametric Mann-Whitney test. ***p ≤ 0.001. (B) Left: Representative confocal microscopy imaging of CBP80-γH2AX PLA under DMSO, etoposide (ETO), and etoposide/ siDROSHA combined treatment. Right: quantification of Left, error bar = mean ± SEM, significance was determined using non-parametric Mann-Whitney test. ****p ⩽ 0.0001.

5.7 CBP80 interacts with RNA Pol II CTD Y1P upon DNA damage

The Y1P modification on the RNA Pol II CTD (C-terminal domain) is necessary for de novo transcription in response to double-strand breaks (DSBs). In my research, I've observed that DROSHA has a higher affinity for this specific form of RNA Pol II, alongside CBP80, following DNA damage. This led me to investigate whether CBP80 could also bind to RNA Pol II CTD Y1P, particularly in the context of DNA damage. To validate this hypothesis, I conducted a co-immunoprecipitation (co-IP) experiment aimed at capturing proteins that interact with this specific version of RNA Pol II.

The co-IP analysis revealed an association between CBP80 and RNA Pol II CTD Y1P even in the absence of DNA damage. However, the strength of this interaction increased upon treatment with etoposide, a DNA-damaging agent (Figure 5-7). These findings collectively demonstrate that CBP80 is capable of binding to RNA Pol II CTD Y1P, with this interaction becoming notably pronounced under DNA damage conditions.

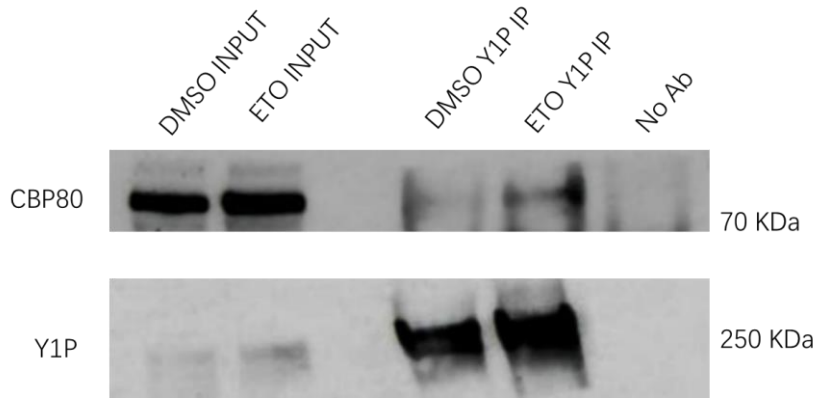


Figure 5-7 CBP8 interacts with RNA Pol II CTD Y1P upon DNA damage. Imaging of western blot of RNA Pol II CTD Y1P using antibodies against CBP80 or RNA Pol II CTD Y1P.

5.8 Discussion

In this chapter, I explored the potential roles of DROSHA in RNA-dependent DDR.

It was reported that DROSHA could facilitate DNA: RNA hybrid formation around DSBs in a miRNA-independent manner. Broken DNA ends were also reported to act as promoters to induce RNA Pol II CTD Y1P-dependent *de novo* transcription(2, 92). Furthermore, DROSHA was proven to either activate or terminate transcription in a non-canonical manner(157, 158). I detected DROSHA interacion of RNA Pol II CTD Y1P, especially upon DNA damage, suggesting DROSHA might play important roles in directly regulating DSBs-induced *de novo* transcription. Moreover, previously published DROSHA ChIP-seq and ChIP-qPCR data revealed that DROSHA could be localized in proximity to DSBs, and in my study I further proved that recruitment of DROSHA is dependent on transcription activity. Thus, these studies suggest that DROSHA may directly regulate *de novo* transcription at DSBs in an RNAi-independent manner.

To further explore the functions of DROSHA in regulating *de novo* transcription around DSBs, I transfected siRNA against DROSHA in DIvA cells. ChIP-qPCR results showed DROSHA knockdown significantly increases the enrichment of RNA Pol II CTD Y1P and CTD S2P enrichment in proximity to two different AsiSI cut sites but not at other loci. This suggests that DROSHA KD leads to stalling of those specific forms of RNA Pol II. Stalled RNA Pol II could be triggered by pausing, arrest, or termination of transcription. DROSHA KD only leads to Pol II enrichment near DSBs, which act as functional promoters upon DSBs. Thus, this stalled Pol II might be the consequence of RNA polymerase pausing or arrest and DROSHA might have crucial functions in the release of such stalled RNA Pol II.

DROSHA was found to interact with CBP80. Furthermore, this interaction was also found to be important for transcription activation of protein coding genes. Interestingly, I detected enhanced interaction between DROSHA and CBP80 upon DNA damage. This suggested that DROSHA may function together with CBP80 to activate *de novo* transcription. Additionally, results of Co-IP experiments revealed only full length DROSHA has a stronger interaction with CBP80 upon DNA damage, suggesting either dsRNA binding or RNase III domain of DROSHA plays important roles in the regulation of interaction between this protein and CBP80. Furthermore, CBP80 was also shown to preferentially interact with RNA Pol II CTD Y1P upon DNA damage, which further supports the possibility that CBP80 and DROSHA facilitate dilncRNA transcription potentially by releasing paused RNA Pol II.

CBP80 is a component of the cap-binding complex(216). This suggests that dilncRNA is capped during transcription initiation. dilncRNA was reported to lack of polyA structure, and it is interesting to verify whether and how these non-coding transcripts could be capped. Future works should explore whether caps are important for DROSHA function and the regulation of dilncRNA in the future.

6. Conclusions and perspectives

6.1 Conclusions

In my DPhil study, I screened for novel R-loops binding factors that preferentially bind upon DNA damage and verified the functions of these proteins and R-loops in DDR. Moreover, I explored the potential roles of DROSHA in DDR.

Firstly, by using the S9.6 antibody which recognises DNA: RNA hybrids structure, I performed IP followed by mass spectrometry analysis, and identified the R-loops interactome upon IR treatment. Interestingly, I found MBD3 and GATAD2B, both components of the NuRD complex that preferentially interact with R-loops upon DNA damage. By performing PLA, I confirmed components of the NuRD complexbind to R-loops *in vivo.* Furthermore, by performing PLA and laser micro irradiation, I found that MBD3 and GATAD2B are recruited to DSBs in a transcription- and R-loops- dependent manner.

Next, I generated site-specific DSBs in DIvA cell genomic DNA and performed ChIP-seq experiments using antibodies against GATAD2B and HDAC1. NGS results revealed enrichments of GATAD2B and HDAC1 overlapped with DSB-induced R-loops regions. This suggests that these two proteins together with R-loops form chromatin boundaries.

In Chapter 4, I further explored the roles of GATAD2B/R-loops dependent-chromatin boundaries in DDR. Knockdown of GATAD2B and MBD3 or overexpression of RNase H could significantly reduce the transcription of genes *in cis* to DSBs. Interestingly, GATAD2B KD and overexpression of RNase H increased histone acetylation levels around DSBs, indicating that these chromatin boundaries could

limit the spread of acetylated histones or facilitate histone deacetylation around DSBs. Considering that chromatin relaxation is necessary to provide access for DDR factors and histone acetylation is thought to positively regulate chromatin relaxation, I hypothesized that GATAD2B and R-loops could establish boundaries between open and condensed chromatin structures. GATAD2B knockdown and R-loops removal by RNase H overexpression could increase histone acetylation levels around DSBs, as DNA damage-induced chromatin relaxation cannot be unlimited and unregulated. By applying MNase sensitivity assays and laser micro irradiation, I observed that the downregulation of GATAD2B and R-loops levels further promoted DSB-induced chromatin relaxation, which confirms the roles of GATAD2B-NuRD complex and R-loops in establishing boundaries between open and condensed chromatin upon DNA damage. Furthermore, GATAD2B KD and R-loops removal were also found to promote hyper DNA end-resection as well as impair HR efficiency, indicating GATAD2B/R-loops dependent chromatin boundaries can also regulate termination of DNA end resection to ensure accurate HR repair.

In Chapter 5, I investigated the potential functions of DROSHA in DDR. Through ChIP-qPCR and PLA experiments, I verified DROSHA could be localized to DSBs in a transcription-dependent manner. This RNase III was also found to preferentially interact with RNA Pol II and in participates its CTD Y1P isoform upon DNA damage. Notably, CTD Y1P of RNA Pol II is known to activate DSBs-induced *de novo* transcription. I further investigated whether DROSHA could regulate this DSB-related transcription. Interestingly, DROSHA KD led to significant enrichment of RNA Pol II CTD Y1P and S2P in proximity to broken DSBs (~0.3kb), but not in other regions. This indicates that DROSHA facilitates the release of stalled RNA pol II at DSBs. Moreover, I found that CBP80, which is known to interact with DROSHA to activate

transcription, was localized to DSBs in a transcription- and DROSHA-dependent manner. Additionally, CBP80 preferentially interact with RNA Pol II CTD Y1P upon DNA damage. Thus, CBP80 might function in the same pathway as DROSHA to regulate DSB-induced *de novo* transcription.

6.2 Future work

Although I observed that components of the GATAD2B-NuRD complex preferentially interact with R-loops upon DNA damage, the underlying mechanisms of these interactions remain unclear. Specifically, it is not yet understood how these interactions preferentially occur upon DNA damage and how R-loops contribute to the recruitment of the GATAD2B-NuRD complex. One interesting aspect to explore is whether the DNA modification 5-hydroxymethylcytosine (5hmC), which is recognized by MBD3(217), could be induced around DNA double-strand breaks (DSBs) to the binding of the GATAD2B-NuRD complex. Additionally, it would be worthwhile to investigate whether the GATAD2B-NuRD comple preferentially interacts with DNA harboring this modification. RNA m6A was also observed on DSB-induced R-loops(218), and this raises the possibility that DSBs facilitate specific RNA modifications, which might further contribute to the recruitment of the GATAD2B-NuRD complex. These areas of investigation hold great potential to shed light on the precise mechanisms underlying interactions between the GATAD2B-NuRD complex and R-loops in the context of DNA damage response.

Though R-loop formation induced by DSBs has been widely reported(97, 113, 161), clarification still needed as to how those three-strand structures are formed upon DNA

damage. Are the preferentially formed in GC-rich regions? Additionally, it is essential to ascertain whether the RNA molecules in these hybrids derive from de novo transcription, or pre-existing transcripts or even transcription *in trans*(219). Furthermore, understanding the detailed molecular mechanisms of how these RNA molecules anneal with their template DNA is of great interest and importance.

Notably, other components of the NuRD complex, CHD3, and CHD4, have been reported to promote chromatin relaxation while repressing transcription in cis to DSBs(86, 203, 204). It will be intriguing to investigate how the CHD3/CHD4-dependent open chromatin structure is related to GATAD2B/R-loops chromatin boundaries. It is also essential to explore whether GATAD2B and CHD3/CHD4 form the same complex upon DNA damage. This may provide insights into their functional interplay in the DNA damage response.

Another question left unanswered is how condensed chromatin structures are spread beyond GATAD2B/R-loops-dependent chromatin boundaries unidirectionally. Several heterochromatin factors, including HP1, G9A, and SUV39H1, have been reported to be involved in the DNA damage response (DDR)(142-144). Therefore, performing ChIP-seq experiments to verify whether these proteins spread from the chromatin boundaries established by the GATAD2B-NuRD complex is critical. This could provide valuable insight into their roles in the regulation of chromatin organization and DDR. Additionally, since the spread of γH2AX, a marker of DNA damage, is limited to within topologically associated domain (TAD) boundaries(220), it would be interesting to verify whether the spread of heterochromatin is also terminated at TAD boundaries. Understanding how heterochromatin spreads and is restricted in relation to TAD boundaries may provide important information about the spatial organization

of chromatin in the context of the DNA damage response.

In my study, I found that knockdown of DROSHA leads to the stalling of RNA Pol II CTD Y1P and CTD S2P in proximity to DSB ends. However, it is currently unclear whether this stalling is due to the pausing of RNA polymerase II or increased recruitment of RNA polymerase II. To address this question, chrRNA-seq experiments need to be performed to determine whether there is nascent recruitment of RNA polymerase II or if the existing RNA polymerase II is paused at DSBs.

If DROSHA indeed facilitates the release of paused RNA polymerase II, it would be extremely interesting to explore the molecular mechanism by which DROSHA is involved in this process. Moreover, it would be valuable to investigate whether the RNase III activity of DROSHA is critical for this function. Recent reports have shown that the histone modification H3K4me3 can promote the release of paused RNA Pol II(221). Therefore, examination of the relationship between DROSHA and H3K4me3 is critical as is the determination of whether DROSHA is linked to this histone modification.

Additionally, I discovered that CBP80 can be localized to DSBs. Since CBP80 is a factor from the cap-binding complex, its recruitment to DSBs suggests that de novo transcripts around DSBs might be capped. To investigate this further, it is essential to explore whether cap structures can be detected at the 5’ end of these lncRNAs. Furthermore, it would be intriguing to uncover the functions of these potential cap structures and CBP80 in the context of RNA-dependent DDR.

Finally, the RNA-dependent DNA damage response (DDR) is gaining increased importance In not only enhancing our understanding of fundamental molecular mechanisms underlying DDR but also in potentially opening up new avenues for the

treatment of various serious diseases. Thus, it is interesting to investigate the relationship between RNA-dependent DDR and diseases, including age-related disease and cancer.

7. Bibliography

1. Michelini F, Jalihal AP, Francia S, Meers C, Neeb ZT, Rossiello F, et al. From "Cellular" RNA to "Smart" RNA: Multiple Roles of RNA in Genome Stability and Beyond. Chem Rev. 2018;118(8):4365-403.
2. Burger K, Schlackow M, Gullerova M. Tyrosine kinase c-Abl couples RNA polymerase II transcription to DNA double-strand breaks. Nucleic Acids Res. 2019;47(7):3467-84.
3. Michelini F, Pitchiaya S, Vitelli V, Sharma S, Gioia U, Pessina F, et al. Damage-induced lncRNAs control the DNA damage response through interaction with DDRNAs at individual double-strand breaks. Nat Cell Biol. 2017;19(12):1400-11.
4. Long Q, Liu Z, Gullerova M. Sweet Melody or Jazz? Transcription Around DNA Double-Strand Breaks. Front Mol Biosci. 2021;8:655786.
5. Marnef A, Legube G. R-loops as Janus-faced modulators of DNA repair. Nat Cell Biol. 2021;23(4):305-13.
6. Thada V, Greenberg RA. Unpaved roads: How the DNA damage response navigates endogenous genotoxins. DNA Repair (Amst). 2022;118:103383.
7. Jackson SP, Bartek J. The DNA-damage response in human biology and disease. Nature. 2009;461(7267):1071-8.
8. Chatterjee N, Walker GC. Mechanisms of DNA damage, repair, and mutagenesis. Environ Mol Mutagen. 2017;58(5):235-63.
9. Ciccia A, Elledge SJ. The DNA damage response: making it safe to play with knives. Mol Cell. 2010;40(2):179-204.
10. Burrell RA, McClelland SE, Endesfelder D, Groth P, Weller MC, Shaikh N, et al. Replication stress links structural and numerical cancer chromosomal instability. Nature. 2013;494(7438):492-6.
11. Berti M, Vindigni A. Replication stress: getting back on track. Nat Struct Mol Biol. 2016;23(2):103-9.
12. Kunkel TA. Evolving views of DNA replication (in)fidelity. Cold Spring Harb Symp Quant Biol. 2009;74:91-101.
13. Viguera E, Canceill D, Ehrlich SD. Replication slippage involves DNA polymerase pausing and dissociation. EMBO J. 2001;20(10):2587-95.
14. Pommier Y, Barcelo JM, Rao VA, Sordet O, Jobson AG, Thibaut L, et al. Repair of topoisomerase I-mediated DNA damage. Prog Nucleic Acid Res Mol Biol. 2006;81:179-229.
15. Cadet J, Douki T, Ravanat JL. Oxidatively generated base damage to cellular DNA. Free Radic Biol Med. 2010;49(1):9-21.
16. Woods DS, Sears CR, Turchi JJ. Recognition of DNA Termini by the C-Terminal Region of the Ku80 and the DNA-Dependent Protein Kinase Catalytic Subunit. PLoS One. 2015;10(5):e0127321.
17. Andres SN, Schellenberg MJ, Wallace BD, Tumbale P, Williams RS. Recognition and repair of chemically heterogeneous structures at DNA ends. Environ Mol Mutagen. 2015;56(1):1-21.
18. Sung S, Li F, Park YB, Kim JS, Kim AK, Song OK, et al. DNA end recognition by the Mre11 nuclease dimer: insights into resection and repair of damaged DNA. EMBO J. 2014;33(20):2422-35.
19. Blackford AN, Jackson SP. ATM, ATR, and DNA-PK: The Trinity at the Heart of the DNA Damage Response. Mol Cell. 2017;66(6):801-17.
20. Ribezzo F, Shiloh Y, Schumacher B. Systemic DNA damage responses in aging and diseases. Semin

Cancer Biol. 2016;37-38:26-35.
21. Huang R, Zhou PK. DNA damage repair: historical perspectives, mechanistic pathways and clinical translation for targeted cancer therapy. Signal Transduct Target Ther. 2021;6(1):254.
22. Latham A, Shia J, Patel Z, Reidy-Lagunes DL, Segal NH, Yaeger R, et al. Characterization and Clinical Outcomes of DNA Mismatch Repair-deficient Small Bowel Adenocarcinoma. Clin Cancer Res. 2021;27(5):1429-37.
23. Krokan HE, Bjoras M. Base excision repair. Cold Spring Harb Perspect Biol. 2013;5(4):a012583.
24. Marteijn JA, Lans H, Vermeulen W, Hoeijmakers JH. Understanding nucleotide excision repair and its roles in cancer and ageing. Nat Rev Mol Cell Biol. 2014;15(7):465-81.
25. Spivak G. Nucleotide excision repair in humans. DNA Repair (Amst). 2015;36:13-8.
26. Goellner EM, Putnam CD, Kolodner RD. Exonuclease 1-dependent and independent mismatch repair. DNA Repair (Amst). 2015;32:24-32.
27. Kimura Y, Kajimoto S, Yamamoto Y, Tanaka N. Enzymatic characteristics of Nudix hydrolase 2 (Nud2), an 8-oxo-dGTP hydrolase from Myxococcus xanthus. J Gen Appl Microbiol. 2020;66(1):46-50.
28. Wang K, Maayah M, Sweasy JB, Alnajjar KS. The role of cysteines in the structure and function of OGG1. J Biol Chem. 2021;296:100093.
29. Lu H, Davis AJ. Human RecQ Helicases in DNA Double-Strand Break Repair. Front Cell Dev Biol. 2021;9:640755.
30. Khanna KK, Jackson SP. DNA double-strand breaks: signaling, repair and the cancer connection. Nat Genet. 2001;27(3):247-54.
31. San Filippo J, Sung P, Klein H. Mechanism of eukaryotic homologous recombination. Annu Rev Biochem. 2008;77:229-57.
32. Sung P, Klein H. Mechanism of homologous recombination: mediators and helicases take on regulatory functions. Nat Rev Mol Cell Biol. 2006;7(10):739-50.
33. Malkova A, Ira G. Break-induced replication: functions and molecular mechanism. Curr Opin Genet Dev. 2013;23(3):271-9.
34. Lamarche BJ, Orazio NI, Weitzman MD. The MRN complex in double-strand break repair and telomere maintenance. FEBS Lett. 2010;584(17):3682-95.
35. Sartori AA, Lukas C, Coates J, Mistrik M, Fu S, Bartek J, et al. Human CtIP promotes DNA end resection. Nature. 2007;450(7169):509-14.
36. Mimitou EP, Yamada S, Keeney S. A global view of meiotic double-strand break end resection. Science. 2017;355(6320):40-5.
37. Mimitou EP, Symington LS. Nucleases and helicases take center stage in homologous recombination. Trends Biochem Sci. 2009;34(5):264-72.
38. McMahill MS, Sham CW, Bishop DK. Synthesis-dependent strand annealing in meiosis. PLoS Biol. 2007;5(11):e299.
39. Allers T, Lichten M. Differential timing and control of noncrossover and crossover recombination during meiosis. Cell. 2001;106(1):47-57.
40. Kramara J, Osia B, Malkova A. Break-Induced Replication: The Where, The Why, and The How. Trends Genet. 2018;34(7):518-31.
41. Sakofsky CJ, Malkova A. Break induced replication in eukaryotes: mechanisms, functions, and consequences. Crit Rev Biochem Mol Biol. 2017;52(4):395-413.
42. Ruff P, Donnianni RA, Glancy E, Oh J, Symington LS. RPA Stabilization of Single-Stranded DNA Is Critical for Break-Induced Replication. Cell Rep. 2016;17(12):3359-68.

43. Malkova A, Naylor ML, Yamaguchi M, Ira G, Haber JE. RAD51-dependent break-induced replication differs in kinetics and checkpoint responses from RAD51-mediated gene conversion. Mol Cell Biol. 2005;25(3):933-44.
44. Zhang JM, Yadav T, Ouyang J, Lan L, Zou L. Alternative Lengthening of Telomeres through Two Distinct Break-Induced Replication Pathways. Cell Rep. 2019;26(4):955-68 e3.
45. Morrish TA, Greider CW. Short telomeres initiate telomere recombination in primary and tumor cells. PLoS Genet. 2009;5(1):e1000357.
46. Mao Z, Bozzella M, Seluanov A, Gorbunova V. DNA repair by nonhomologous end joining and homologous recombination during cell cycle in human cells. Cell Cycle. 2008;7(18):2902-6.
47. Mao Z, Bozzella M, Seluanov A, Gorbunova V. Comparison of nonhomologous end joining and homologous recombination in human cells. DNA Repair (Amst). 2008;7(10):1765-71.
48. Lieber MR. The mechanism of double-strand DNA break repair by the nonhomologous DNA end-joining pathway. Annu Rev Biochem. 2010;79:181-211.
49. Lieber MR. The mechanism of human nonhomologous DNA end joining. J Biol Chem. 2008;283(1):1-5.
50. Ma Y, Lu H, Tippin B, Goodman MF, Shimazaki N, Koiwai O, et al. A biochemically defined system for mammalian nonhomologous DNA end joining. Mol Cell. 2004;16(5):701-13.
51. Sastre-Moreno G, Pryor JM, Moreno-Onate M, Herrero-Ruiz AM, Cortes-Ledesma F, Blanco L, et al. Regulation of human pollambda by ATM-mediated phosphorylation during non-homologous end joining. DNA Repair (Amst). 2017;51:31-45.
52. Capp JP, Boudsocq F, Besnard AG, Lopez BS, Cazaux C, Hoffmann JS, et al. Involvement of DNA polymerase mu in the repair of a specific subset of DNA double-strand breaks in mammalian cells. Nucleic Acids Res. 2007;35(11):3551-60.
53. Ahnesorg P, Smith P, Jackson SP. XLF interacts with the XRCC4-DNA ligase IV complex to promote DNA nonhomologous end-joining. Cell. 2006;124(2):301-13.
54. Chang HHY, Pannunzio NR, Adachi N, Lieber MR. Non-homologous DNA end joining and alternative pathways to double-strand break repair. Nat Rev Mol Cell Biol. 2017;18(8):495-506.
55. McVey M, Lee SE. MMEJ repair of double-strand breaks (director's cut): deleted sequences and alternative endings. Trends Genet. 2008;24(11):529-38.
56. Bennardo N, Cheng A, Huang N, Stark JM. Alternative-NHEJ is a mechanistically distinct pathway of mammalian chromosome break repair. PLoS Genet. 2008;4(6):e1000110.
57. Wang H, Xu X. Microhomology-mediated end joining: new players join the team. Cell Biosci. 2017;7:6.
58. Truong LN, Li Y, Shi LZ, Hwang PY, He J, Wang H, et al. Microhomology-mediated End Joining and Homologous Recombination share the initial end resection step to repair DNA double-strand breaks in mammalian cells. Proc Natl Acad Sci U S A. 2013;110(19):7720-5.
59. Patterson-Fortin J, D'Andrea AD. Exploiting the Microhomology-Mediated End-Joining Pathway in Cancer Therapy. Cancer Res. 2020;80(21):4593-600.
60. Sfeir A, Symington LS. Microhomology-Mediated End Joining: A Back-up Survival Mechanism or Dedicated Pathway? Trends Biochem Sci. 2015;40(11):701-14.
61. Black SJ, Ozdemir AY, Kashkina E, Kent T, Rusanov T, Ristic D, et al. Molecular basis of microhomology-mediated end-joining by purified full-length Poltheta. Nat Commun. 2019;10(1):4423.
62. Bhargava R, Onyango DO, Stark JM. Regulation of Single-Strand Annealing and its Role in Genome Maintenance. Trends Genet. 2016;32(9):566-75.

63. Grimme JM, Honda M, Wright R, Okuno Y, Rothenberg E, Mazin AV, et al. Human Rad52 binds and wraps single-stranded DNA and mediates annealing via two hRad52-ssDNA complexes. Nucleic Acids Res. 2010;38(9):2917-30.
64. Zhao F, Kim W, Kloeber JA, Lou Z. DNA end resection and its role in DNA replication and DSB repair choice in mammalian cells. Exp Mol Med. 2020;52(10):1705-14.
65. Wang H, Qiu Z, Liu B, Wu Y, Ren J, Liu Y, et al. PLK1 targets CtIP to promote microhomology-mediated end joining. Nucleic Acids Res. 2018;46(20):10724-39.
66. Rzeszutek I, Betlej G. The Role of Small Noncoding RNA in DNA Double-Strand Break Repair. Int J Mol Sci. 2020;21(21).
67. Chowdhury D, Choi YE, Brault ME. Charity begins at home: non-coding RNA functions in DNA repair. Nat Rev Mol Cell Biol. 2013;14(3):181-9.
68. Zhang Y, He Q, Hu Z, Feng Y, Fan L, Tang Z, et al. Long noncoding RNA LINP1 regulates repair of DNA double-strand breaks in triple-negative breast cancer. Nat Struct Mol Biol. 2016;23(6):522-30.
69. Sharma V, Khurana S, Kubben N, Abdelmohsen K, Oberdoerffer P, Gorospe M, et al. A BRCA1-interacting lncRNA regulates homologous recombination. EMBO Rep. 2015;16(11):1520-34.
70. Francia S, Michelini F, Saxena A, Tang D, de Hoon M, Anelli V, et al. Site-specific DICER and DROSHA RNA products control the DNA-damage response. Nature. 2012;488(7410):231-5.
71. Francia S, Cabrini M, Matti V, Oldani A, d'Adda di Fagagna F. DICER, DROSHA and DNA damage response RNAs are necessary for the secondary recruitment of DNA damage response factors. J Cell Sci. 2016;129(7):1468-76.
72. Wei W, Ba Z, Gao M, Wu Y, Ma Y, Amiard S, et al. A role for small RNAs in DNA double-strand break repair. Cell. 2012;149(1):101-12.
73. Bonath F, Domingo-Prim J, Tarbier M, Friedlander MR, Visa N. Next-generation sequencing reveals two populations of damage-induced small RNAs at endogenous DNA double-strand breaks. Nucleic Acids Res. 2018;46(22):11869-82.
74. Gao M, Wei W, Li MM, Wu YS, Ba Z, Jin KX, et al. Ago2 facilitates Rad51 recruitment and DNA double-strand break repair by homologous recombination. Cell Res. 2014;24(5):532-41.
75. Wang Q, Goldstein M. Small RNAs Recruit Chromatin-Modifying Enzymes MMSET and Tip60 to Reconfigure Damaged DNA upon Double-Strand Break and Facilitate Repair. Cancer Res. 2016;76(7):1904-15.
76. Kruhlak M, Crouch EE, Orlov M, Montano C, Gorski SA, Nussenzweig A, et al. The ATM repair pathway inhibits RNA polymerase I transcription in response to chromosome breaks. Nature. 2007;447(7145):730-4.
77. Harding SM, Boiarsky JA, Greenberg RA. ATM Dependent Silencing Links Nucleolar Chromatin Reorganization to DNA Damage Recognition. Cell Rep. 2015;13(2):251-9.
78. Shanbhag NM, Rafalska-Metcalf IU, Balane-Bolivar C, Janicki SM, Greenberg RA. ATM-dependent chromatin changes silence transcription in cis to DNA double-strand breaks. Cell. 2010;141(6):970-81.
79. Ui A, Nagaura Y, Yasui A. Transcriptional elongation factor ENL phosphorylated by ATM recruits polycomb and switches off transcription for DSB repair. Mol Cell. 2015;58(3):468-82.
80. Kakarougkas A, Ismail A, Chambers AL, Riballo E, Herbert AD, Kunzel J, et al. Requirement for PBAF in transcriptional repression and repair at DNA breaks in actively transcribed regions of chromatin. Mol Cell. 2014;55(5):723-32.
81. Hu K, Li Y, Wu W, Xie L, Yan H, Cai Y, et al. ATM-Dependent Recruitment of BRD7 is required for Transcriptional Repression and DNA Repair at DNA Breaks Flanking Transcriptional Active Regions. Adv

Sci (Weinh). 2020;7(20):2000157.
82. Pankotai T, Bonhomme C, Chen D, Soutoglou E. DNAPKcs-dependent arrest of RNA polymerase II transcription in the presence of DNA breaks. Nat Struct Mol Biol. 2012;19(3):276-82.
83. Caron P, Pankotai T, Wiegant WW, Tollenaere MAX, Furst A, Bonhomme C, et al. WWP2 ubiquitylates RNA polymerase II for DNA-PK-dependent transcription arrest and repair at DNA breaks. Genes Dev. 2019;33(11-12):684-704.
84. Min S, Ji JH, Heo Y, Cho H. Transcriptional regulation and chromatin dynamics at DNA double-strand breaks. Exp Mol Med. 2022;54(10):1705-12.
85. Chou DM, Adamson B, Dephoure NE, Tan X, Nottke AC, Hurov KE, et al. A chromatin localization screen reveals poly (ADP ribose)-regulated recruitment of the repressive polycomb and NuRD complexes to sites of DNA damage. Proc Natl Acad Sci U S A. 2010;107(43):18475-80.
86. Smith R, Sellou H, Chapuis C, Huet S, Timinszky G. CHD3 and CHD4 recruitment and chromatin remodeling activity at DNA breaks is promoted by early poly(ADP-ribose)-dependent chromatin relaxation. Nucleic Acids Res. 2018;46(12):6087-98.
87. Dong C, West KL, Tan XY, Li J, Ishibashi T, Yu CH, et al. Screen identifies DYRK1B network as mediator of transcription repression on damaged chromatin. Proc Natl Acad Sci U S A. 2020;117(29):17019-30.
88. Gong F, Clouaire T, Aguirrebengoa M, Legube G, Miller KM. Histone demethylase KDM5A regulates the ZMYND8-NuRD chromatin remodeler to promote DNA repair. J Cell Biol. 2017;216(7):1959-74.
89. Abu-Zhayia ER, Awwad SW, Ben-Oz BM, Khoury-Haddad H, Ayoub N. CDYL1 fosters double-strand break-induced transcription silencing and promotes homology-directed repair. J Mol Cell Biol. 2018;10(4):341-57.
90. Awwad SW, Abu-Zhayia ER, Guttmann-Raviv N, Ayoub N. NELF-E is recruited to DNA double-strand break sites to promote transcriptional repression and repair. EMBO Rep. 2017;18(5):745-64.
91. Vitor AC, Sridhara SC, Sabino JC, Afonso AI, Grosso AR, Martin RM, et al. Single-molecule imaging of transcription at damaged chromatin. Sci Adv. 2019;5(1):eaau1249.
92. Pessina F, Giavazzi F, Yin Y, Gioia U, Vitelli V, Galbiati A, et al. Functional transcription promoters at DNA double-strand breaks mediate RNA-driven phase separation of damage-response factors. Nat Cell Biol. 2019;21(10):1286-99.
93. Sharma S, Anand R, Zhang X, Francia S, Michelini F, Galbiati A, et al. MRE11-RAD50-NBS1 Complex Is Sufficient to Promote Transcription by RNA Polymerase II at Double-Strand Breaks by Melting DNA Ends. Cell Rep. 2021;34(1):108565.
94. Bottcher R, Schmidts I, Nitschko V, Duric P, Forstemann K. RNA polymerase II is recruited to DNA double-strand breaks for dilncRNA transcription in Drosophila. RNA Biol. 2022;19(1):68-77.
95. Burger K, Schlackow M, Potts M, Hester S, Mohammed S, Gullerova M. Nuclear phosphorylated Dicer processes double-stranded RNA in response to DNA damage. J Cell Biol. 2017;216(8):2373-89.
96. Liu S, Hua Y, Wang J, Li L, Yuan J, Zhang B, et al. RNA polymerase III is required for the repair of DNA double-strand breaks by homologous recombination. Cell. 2021;184(5):1314-29 e10.
97. Yasuhara T, Kato R, Hagiwara Y, Shiotani B, Yamauchi M, Nakada S, et al. Human Rad52 Promotes XPG-Mediated R-loop Processing to Initiate Transcription-Associated Homologous Recombination Repair. Cell. 2018;175(2):558-70 e11.
98. Chaurasia P, Sen R, Pandita TK, Bhaumik SR. Preferential repair of DNA double-strand break at the active gene in vivo. J Biol Chem. 2012;287(43):36414-22.

99. Aymard F, Bugler B, Schmidt CK, Guillou E, Caron P, Briois S, et al. Transcriptionally active chromatin recruits homologous recombination at DNA double-strand breaks. Nat Struct Mol Biol. 2014;21(4):366-74.
100. Teng Y, Yadav T, Duan M, Tan J, Xiang Y, Gao B, et al. ROS-induced R loops trigger a transcription-coupled but BRCA1/2-independent homologous recombination pathway through CSB. Nat Commun. 2018;9(1):4115.
101. Ouyang J, Yadav T, Zhang JM, Yang H, Rheinbay E, Guo H, et al. RNA transcripts stimulate homologous recombination by forming DR-loops. Nature. 2021;594(7862):283-8.
102. Wei L, Nakajima S, Bohm S, Bernstein KA, Shen Z, Tsang M, et al. DNA damage during the G0/G1 phase triggers RNA-templated, Cockayne syndrome B-dependent homologous recombination. Proc Natl Acad Sci U S A. 2015;112(27):E3495-504.
103. Skourti-Stathaki K, Proudfoot NJ. A double-edged sword: R loops as threats to genome integrity and powerful regulators of gene expression. Genes Dev. 2014;28(13):1384-96.
104. Aguilera A, Garcia-Muse T. R loops: from transcription byproducts to threats to genome stability. Mol Cell. 2012;46(2):115-24.
105. Garcia-Muse T, Aguilera A. R Loops: From Physiological to Pathological Roles. Cell. 2019;179(3):604-18.
106. Santos-Pereira JM, Aguilera A. R loops: new modulators of genome dynamics and function. Nat Rev Genet. 2015;16(10):583-97.
107. Skourti-Stathaki K, Kamieniarz-Gdula K, Proudfoot NJ. R-loops induce repressive chromatin marks over mammalian gene terminators. Nature. 2014;516(7531):436-9.
108. Chen PB, Chen HV, Acharya D, Rando OJ, Fazzio TG. R loops regulate promoter-proximal chromatin architecture and cellular differentiation. Nat Struct Mol Biol. 2015;22(12):999-1007.
109. Boque-Sastre R, Soler M, Oliveira-Mateos C, Portela A, Moutinho C, Sayols S, et al. Head-to-head antisense transcription and R-loop formation promotes transcriptional activation. Proc Natl Acad Sci U S A. 2015;112(18):5785-90.
110. Grunseich C, Wang IX, Watts JA, Burdick JT, Guber RD, Zhu Z, et al. Senataxin Mutation Reveals How R-Loops Promote Transcription by Blocking DNA Methylation at Gene Promoters. Mol Cell. 2018;69(3):426-37 e7.
111. Arab K, Karaulanov E, Musheev M, Trnka P, Schafer A, Grummt I, et al. GADD45A binds R-loops and recruits TET1 to CpG island promoters. Nat Genet. 2019;51(2):217-23.
112. Cohen S, Puget N, Lin YL, Clouaire T, Aguirrebengoa M, Rocher V, et al. Senataxin resolves RNA:DNA hybrids forming at DNA double-strand breaks to prevent translocations. Nat Commun. 2018;9(1):533.
113. D'Alessandro G, Whelan DR, Howard SM, Vitelli V, Renaudin X, Adamowicz M, et al. BRCA2 controls DNA:RNA hybrid level at DSBs by mediating RNase H2 recruitment. Nat Commun. 2018;9(1):5376.
114. Tan J, Duan M, Yadav T, Phoon L, Wang X, Zhang JM, et al. An R-loop-initiated CSB-RAD52-POLD3 pathway suppresses ROS-induced telomeric DNA breaks. Nucleic Acids Res. 2020;48(3):1285-300.
115. Ohle C, Tesorero R, Schermann G, Dobrev N, Sinning I, Fischer T. Transient RNA-DNA Hybrids Are Required for Efficient Double-Strand Break Repair. Cell. 2016;167(4):1001-13 e7.
116. Matsui M, Sakasai R, Abe M, Kimura Y, Kajita S, Torii W, et al. USP42 enhances homologous recombination repair by promoting R-loop resolution with a DNA-RNA helicase DHX9. Oncogenesis. 2020;9(6):60.

117. Alfano L, Caporaso A, Altieri A, Dell'Aquila M, Landi C, Bini L, et al. Depletion of the RNA binding protein HNRNPD impairs homologous recombination by inhibiting DNA-end resection and inducing R-loop accumulation. Nucleic Acids Res. 2019;47(8):4068-85.
118. Yu Z, Mersaoui SY, Guitton-Sert L, Coulombe Y, Song J, Masson JY, et al. DDX5 resolves R-loops at DNA double-strand breaks to promote DNA repair and avoid chromosomal deletions. NAR Cancer. 2020;2(3):zcaa028.
119. Domingo-Prim J, Endara-Coll M, Bonath F, Jimeno S, Prados-Carvajal R, Friedlander MR, et al. EXOSC10 is required for RPA assembly and controlled DNA end resection at DNA double-strand breaks. Nat Commun. 2019;10(1):2135.
120. Storici F, Bebenek K, Kunkel TA, Gordenin DA, Resnick MA. RNA-templated DNA repair. Nature. 2007;447(7142):338-41.
121. Keskin H, Shen Y, Huang F, Patel M, Yang T, Ashley K, et al. Transcript-RNA-templated DNA recombination and repair. Nature. 2014;515(7527):436-9.
122. Mazina OM, Keskin H, Hanamshet K, Storici F, Mazin AV. Rad52 Inverse Strand Exchange Drives RNA-Templated DNA Double-Strand Break Repair. Mol Cell. 2017;67(1):19-29 e3.
123. Chakraborty A, Tapryal N, Venkova T, Horikoshi N, Pandita RK, Sarker AH, et al. Classical non-homologous end-joining pathway utilizes nascent RNA for error-free double-strand break repair of transcribed genes. Nat Commun. 2016;7:13049.
124. Chandramouly G, Zhao J, McDevitt S, Rusanov T, Hoang T, Borisonnik N, et al. Poltheta reverse transcribes RNA and promotes RNA-templated DNA repair. Sci Adv. 2021;7(24).
125. Chakraborty A, Tapryal N, Islam A, Sarker AH, Manohar K, Mitra J, et al. Human DNA polymerase eta promotes RNA-templated error-free repair of DNA double-strand breaks. J Biol Chem. 2023;299(3):102991.
126. Ziv Y, Bielopolski D, Galanty Y, Lukas C, Taya Y, Schultz DC, et al. Chromatin relaxation in response to DNA double-strand breaks is modulated by a novel ATM- and KAP-1 dependent pathway. Nat Cell Biol. 2006;8(8):870-6.
127. Polo SE, Almouzni G. Chromatin dynamics after DNA damage: The legacy of the access-repair-restore model. DNA Repair (Amst). 2015;36:114-21.
128. Ray Chaudhuri A, Nussenzweig A. The multifaceted roles of PARP1 in DNA repair and chromatin remodelling. Nat Rev Mol Cell Biol. 2017;18(10):610-21.
129. Messner S, Altmeyer M, Zhao H, Pozivil A, Roschitzki B, Gehrig P, et al. PARP1 ADP-ribosylates lysine residues of the core histone tails. Nucleic Acids Res. 2010;38(19):6350-62.
130. Luijsterburg MS, de Krijger I, Wiegant WW, Shah RG, Smeenk G, de Groot AJL, et al. PARP1 Links CHD2-Mediated Chromatin Expansion and H3.3 Deposition to DNA Repair by Non-homologous End-Joining. Mol Cell. 2016;61(4):547-62.
131. Min S, Jo S, Lee HS, Chae S, Lee JS, Ji JH, et al. ATM-dependent chromatin remodeler Rsf-1 facilitates DNA damage checkpoints and homologous recombination repair. Cell Cycle. 2014;13(4):666-77.
132. Nair N, Shoaib M, Sorensen CS. Chromatin Dynamics in Genome Stability: Roles in Suppressing Endogenous DNA Damage and Facilitating DNA Repair. Int J Mol Sci. 2017;18(7).
133. Hossain MB, Shifat R, Johnson DG, Bedford MT, Gabrusiewicz KR, Cortes-Santiago N, et al. TIE2-mediated tyrosine phosphorylation of H4 regulates DNA damage response by recruiting ABL1. Sci Adv. 2016;2(4):e1501290.
134. Ramachandran S, Haddad D, Li C, Le MX, Ling AK, So CC, et al. The SAGA Deubiquitination

Module Promotes DNA Repair and Class Switch Recombination through ATM and DNAPK-Mediated gammaH2AX Formation. Cell Rep. 2016;15(7):1554-65.
135. Clouaire T, Rocher V, Lashgari A, Arnould C, Aguirrebengoa M, Biernacka A, et al. Comprehensive Mapping of Histone Modifications at DNA Double-Strand Breaks Deciphers Repair Pathway Chromatin Signatures. Mol Cell. 2018;72(2):250-62 e6.
136. Xu Y, Ayrapetov MK, Xu C, Gursoy-Yuzugullu O, Hu Y, Price BD. Histone H2A.Z controls a critical chromatin remodeling step required for DNA double-strand break repair. Mol Cell. 2012;48(5):723-33.
137. Clouaire T, Legube G. A Snapshot on the Cis Chromatin Response to DNA Double-Strand Breaks. Trends Genet. 2019;35(5):330-45.
138. Adkins NL, Niu H, Sung P, Peterson CL. Nucleosome dynamics regulates DNA processing. Nat Struct Mol Biol. 2013;20(7):836-42.
139. Costelloe T, Louge R, Tomimatsu N, Mukherjee B, Martini E, Khadaroo B, et al. The yeast Fun30 and human SMARCAD1 chromatin remodellers promote DNA end resection. Nature. 2012;489(7417):581-4.
140. Pfister SX, Ahrabi S, Zalmas LP, Sarkar S, Aymard F, Bachrati CZ, et al. SETD2-dependent histone H3K36 trimethylation is required for homologous recombination repair and genome stability. Cell Rep. 2014;7(6):2006-18.
141. Leung JW, Makharashvili N, Agarwal P, Chiu LY, Pourpre R, Cammarata MB, et al. ZMYM3 regulates BRCA1 localization at damaged chromatin to promote DNA repair. Genes Dev. 2017;31(3):260-74.
142. Yang Q, Zhu Q, Lu X, Du Y, Cao L, Shen C, et al. G9a coordinates with the RPA complex to promote DNA damage repair and cell survival. Proc Natl Acad Sci U S A. 2017;114(30):E6054-E63.
143. Kalousi A, Hoffbeck AS, Selemenakis PN, Pinder J, Savage KI, Khanna KK, et al. The nuclear oncogene SET controls DNA repair by KAP1 and HP1 retention to chromatin. Cell Rep. 2015;11(1):149-63.
144. Ayrapetov MK, Gursoy-Yuzugullu O, Xu C, Xu Y, Price BD. DNA double-strand breaks promote methylation of histone H3 on lysine 9 and transient formation of repressive chromatin. Proc Natl Acad Sci U S A. 2014;111(25):9169-74.
145. Torchy MP, Hamiche A, Klaholz BP. Structure and function insights into the NuRD chromatin remodeling complex. Cell Mol Life Sci. 2015;72(13):2491-507.
146. Miller KM, Tjeertes JV, Coates J, Legube G, Polo SE, Britton S, et al. Human HDAC1 and HDAC2 function in the DNA-damage response to promote DNA nonhomologous end-joining. Nat Struct Mol Biol. 2010;17(9):1144-51.
147. Han J, Lee Y, Yeom KH, Kim YK, Jin H, Kim VN. The Drosha-DGCR8 complex in primary microRNA processing. Genes Dev. 2004;18(24):3016-27.
148. Kwon SC, Nguyen TA, Choi YG, Jo MH, Hohng S, Kim VN, et al. Structure of Human DROSHA. Cell. 2016;164(1-2):81-90.
149. Lee Y, Kim M, Han J, Yeom KH, Lee S, Baek SH, et al. MicroRNA genes are transcribed by RNA polymerase II. EMBO J. 2004;23(20):4051-60.
150. Nguyen TA, Jo MH, Choi YG, Park J, Kwon SC, Hohng S, et al. Functional Anatomy of the Human Microprocessor. Cell. 2015;161(6):1374-87.
151. Yi R, Qin Y, Macara IG, Cullen BR. Exportin-5 mediates the nuclear export of pre-microRNAs and short hairpin RNAs. Genes Dev. 2003;17(24):3011-6.
152. Han J, Lee Y, Yeom KH, Nam JW, Heo I, Rhee JK, et al. Molecular basis for the recognition of

primary microRNAs by the Drosha-DGCR8 complex. Cell. 2006;125(5):887-901.
153. Zeng Y, Yi R, Cullen BR. Recognition and cleavage of primary microRNA precursors by the nuclear processing enzyme Drosha. EMBO J. 2005;24(1):138-48.
154. Auyeung VC, Ulitsky I, McGeary SE, Bartel DP. Beyond secondary structure: primary-sequence determinants license pri-miRNA hairpins for processing. Cell. 2013;152(4):844-58.
155. Mori M, Triboulet R, Mohseni M, Schlegelmilch K, Shrestha K, Camargo FD, et al. Hippo signaling regulates microprocessor and links cell-density-dependent miRNA biogenesis to cancer. Cell. 2014;156(5):893-906.
156. Ha M, Kim VN. Regulation of microRNA biogenesis. Nat Rev Mol Cell Biol. 2014;15(8):509-24.
157. Gromak N, Dienstbier M, Macias S, Plass M, Eyras E, Caceres JF, et al. Drosha regulates gene expression independently of RNA cleavage function. Cell Rep. 2013;5(6):1499-510.
158. Wagschal A, Rousset E, Basavarajaiah P, Contreras X, Harwig A, Laurent-Chabalier S, et al. Microprocessor, Setx, Xrn2, and Rrp6 co-operate to induce premature termination of transcription by RNAPII. Cell. 2012;150(6):1147-57.
159. Dhir A, Dhir S, Proudfoot NJ, Jopling CL. Microprocessor mediates transcriptional termination of long noncoding RNA transcripts hosting microRNAs. Nat Struct Mol Biol. 2015;22(4):319-27.
160. Havens MA, Reich AA, Hastings ML. Drosha promotes splicing of a pre-microRNA-like alternative exon. PLoS Genet. 2014;10(5):e1004312.
161. Lu WT, Hawley BR, Skalka GL, Baldock RA, Smith EM, Bader AS, et al. Drosha drives the formation of DNA:RNA hybrids around DNA break sites to facilitate DNA repair. Nat Commun. 2018;9(1):532.
162. Macias S, Plass M, Stajuda A, Michlewski G, Eyras E, Caceres JF. DGCR8 HITS-CLIP reveals novel functions for the Microprocessor. Nat Struct Mol Biol. 2012;19(8):760-6.
163. Heras SR, Macias S, Plass M, Fernandez N, Cano D, Eyras E, et al. The Microprocessor controls the activity of mammalian retrotransposons. Nat Struct Mol Biol. 2013;20(10):1173-81.
164. Calses PC, Dhillon KK, Tucker N, Chi Y, Huang JW, Kawasumi M, et al. DGCR8 Mediates Repair of UV-Induced DNA Damage Independently of RNA Processing. Cell Rep. 2017;19(1):162-74.
165. Cabrini M, Roncador M, Galbiati A, Cipolla L, Maffia A, Iannelli F, et al. DROSHA is recruited to DNA damage sites by the MRN complex to promote non-homologous end joining. J Cell Sci. 2021;134(6).
166. Cristini A, Groh M, Kristiansen MS, Gromak N. RNA/DNA Hybrid Interactome Identifies DXH9 as a Molecular Player in Transcriptional Termination and R-Loop-Associated DNA Damage. Cell Rep. 2018;23(6):1891-905.
167. Nojima T, Gomes T, Carmo-Fonseca M, Proudfoot NJ. Mammalian NET-seq analysis defines nascent RNA profiles and associated RNA processing genome-wide. Nat Protoc. 2016;11(3):413-28.
168. Ramirez F, Ryan DP, Gruning B, Bhardwaj V, Kilpert F, Richter AS, et al. deepTools2: a next generation web server for deep-sequencing data analysis. Nucleic Acids Res. 2016;44(W1):W160-5.
169. Bader AS, Bushell M. DNA:RNA hybrids form at DNA double-strand breaks in transcriptionally active loci. Cell Death Dis. 2020;11(4):280.
170. Niehrs C, Luke B. Regulatory R-loops as facilitators of gene expression and genome stability. Nat Rev Mol Cell Biol. 2020;21(3):167-78.
171. Petermann E, Lan L, Zou L. Sources, resolution and physiological relevance of R-loops and RNA-DNA hybrids. Nat Rev Mol Cell Biol. 2022;23(8):521-40.
172. Smeenk G, van Attikum H. The chromatin response to DNA breaks: leaving a mark on genome integrity. Annu Rev Biochem. 2013;82:55-80.

173. Phillips DD, Garboczi DN, Singh K, Hu Z, Leppla SH, Leysath CE. The sub-nanomolar binding of DNA-RNA hybrids by the single-chain Fv fragment of antibody S9.6. J Mol Recognit. 2013;26(8):376-81.
174. Boguslawski SJ, Smith DE, Michalak MA, Mickelson KE, Yehle CO, Patterson WL, et al. Characterization of monoclonal antibody to DNA.RNA and its application to immunodetection of hybrids. J Immunol Methods. 1986;89(1):123-30.
175. Nakama M, Kawakami K, Kajitani T, Urano T, Murakami Y. DNA-RNA hybrid formation mediates RNAi-directed heterochromatin formation. Genes Cells. 2012;17(3):218-33.
176. Castellano-Pozo M, Santos-Pereira JM, Rondon AG, Barroso S, Andujar E, Perez-Alegre M, et al. R loops are linked to histone H3 S10 phosphorylation and chromatin condensation. Mol Cell. 2013;52(4):583-90.
177. Sun Q, Csorba T, Skourti-Stathaki K, Proudfoot NJ, Dean C. R-loop stabilization represses antisense transcription at the Arabidopsis FLC locus. Science. 2013;340(6132):619-21.
178. Alagia A, Ketley RF, Gullerova M. Proximity Ligation Assay for Detection of R-Loop Complexes upon DNA Damage. Methods Mol Biol. 2022;2528:289-303.
179. Alam MS. Proximity Ligation Assay (PLA). Curr Protoc Immunol. 2018;123(1):e58.
180. Basta J, Rauchman M. The nucleosome remodeling and deacetylase complex in development and disease. Transl Res. 2015;165(1):36-47.
181. Bensaude O. Inhibiting eukaryotic transcription: Which compound to choose? How to evaluate its activity? Transcription. 2011;2(3):103-8.
182. Iacovoni JS, Caron P, Lassadi I, Nicolas E, Massip L, Trouche D, et al. High-resolution profiling of gammaH2AX around DNA double strand breaks in the mammalian genome. EMBO J. 2010;29(8):1446-57.
183. Coward P, Lee D, Hull MV, Lehmann JM. 4-Hydroxytamoxifen binds to and deactivates the estrogen-related receptor gamma. Proc Natl Acad Sci U S A. 2001;98(15):8880-4.
184. Crosetto N, Mitra A, Silva MJ, Bienko M, Dojer N, Wang Q, et al. Nucleotide-resolution DNA double-strand break mapping by next-generation sequencing. Nat Methods. 2013;10(4):361-5.
185. Aymard F, Aguirrebengoa M, Guillou E, Javierre BM, Bugler B, Arnould C, et al. Genome-wide mapping of long-range contacts unveils clustering of DNA double-strand breaks at damaged active genes. Nat Struct Mol Biol. 2017;24(4):353-61.
186. Nowotny M, Gaidamakov SA, Ghirlando R, Cerritelli SM, Crouch RJ, Yang W. Structure of human RNase H1 complexed with an RNA/DNA hybrid: insight into HIV reverse transcription. Mol Cell. 2007;28(2):264-76.
187. Nowotny M, Cerritelli SM, Ghirlando R, Gaidamakov SA, Crouch RJ, Yang W. Specific recognition of RNA/DNA hybrid and enhancement of human RNase H1 activity by HBD. EMBO J. 2008;27(7):1172-81.
188. Cerritelli SM, Crouch RJ. Ribonuclease H: the enzymes in eukaryotes. FEBS J. 2009;276(6):1494-505.
189. Williams JS, Lujan SA, Kunkel TA. Processing ribonucleotides incorporated during eukaryotic DNA replication. Nat Rev Mol Cell Biol. 2016;17(6):350-63.
190. Crossley MP, Brickner JR, Song C, Zar SMT, Maw SS, Chedin F, et al. Catalytically inactive, purified RNase H1: A specific and sensitive probe for RNA-DNA hybrid imaging. J Cell Biol. 2021;220(9).
191. Vitor AC, Huertas P, Legube G, de Almeida SF. Studying DNA Double-Strand Break Repair: An Ever-Growing Toolbox. Front Mol Biosci. 2020;7:24.
192. Berkovich E, Monnat RJ, Jr., Kastan MB. Roles of ATM and NBS1 in chromatin structure

modulation and DNA double-strand break repair. Nat Cell Biol. 2007;9(6):683-90.
193. Ito T, Umehara T, Sasaki K, Nakamura Y, Nishino N, Terada T, et al. Real-time imaging of histone H4K12-specific acetylation determines the modes of action of histone deacetylase and bromodomain inhibitors. Chem Biol. 2011;18(4):495-507.
194. Klemm SL, Shipony Z, Greenleaf WJ. Chromatin accessibility and the regulatory epigenome. Nat Rev Genet. 2019;20(4):207-20.
195. Patterson GH, Lippincott-Schwartz J. A photoactivatable GFP for selective photolabeling of proteins and cells. Science. 2002;297(5588):1873-7.
196. Pai CC, Deegan RS, Subramanian L, Gal C, Sarkar S, Blaikley EJ, et al. A histone H3K36 chromatin switch coordinates DNA double-strand break repair pathway choice. Nat Commun. 2014;5:4091.
197. Kollarovic G, Topping CE, Shaw EP, Chambers AL. The human HELLS chromatin remodelling protein promotes end resection to facilitate homologous recombination and contributes to DSB repair within heterochromatin. Nucleic Acids Res. 2020;48(4):1872-85.
198. Kilgas S, Kiltie AE, Ramadan K. Immunofluorescence microscopy-based detection of ssDNA foci by BrdU in mammalian cells. STAR Protoc. 2021;2(4):100978.
199. van Sluis M, McStay B. A localized nucleolar DNA damage response facilitates recruitment of the homology-directed repair machinery independent of cell cycle stage. Genes Dev. 2015;29(11):1151-63.
200. Pierce AJ, Jasin M. Measuring recombination proficiency in mouse embryonic stem cells. Methods Mol Biol. 2005;291:373-84.
201. Wang J, Lawry ST, Cohen AL, Jia S. Chromosome boundary elements and regulation of heterochromatin spreading. Cell Mol Life Sci. 2014;71(24):4841-52.
202. Kimura A, Horikoshi M. Partition of distinct chromosomal regions: negotiable border and fixed border. Genes Cells. 2004;9(6):499-508.
203. Gong F, Chiu LY, Cox B, Aymard F, Clouaire T, Leung JW, et al. Screen identifies bromodomain protein ZMYND8 in chromatin recognition of transcription-associated DNA damage that promotes homologous recombination. Genes Dev. 2015;29(2):197-211.
204. Hou T, Cao Z, Zhang J, Tang M, Tian Y, Li Y, et al. SIRT6 coordinates with CHD4 to promote chromatin relaxation and DNA repair. Nucleic Acids Res. 2020;48(6):2982-3000.
205. Farnung L, Ochmann M, Cramer P. Nucleosome-CHD4 chromatin remodeler structure maps human disease mutations. Elife. 2020;9.
206. Chen Y, Zhang H, Xu Z, Tang H, Geng A, Cai B, et al. A PARP1-BRG1-SIRT1 axis promotes HR repair by reducing nucleosome density at DNA damage sites. Nucleic Acids Res. 2019;47(16):8563-80.
207. Pong SK, Gullerova M. Noncanonical functions of microRNA pathway enzymes - Drosha, DGCR8, Dicer and Ago proteins. FEBS Lett. 2018;592(17):2973-86.
208. Lee D, Shin C. Emerging roles of DROSHA beyond primary microRNA processing. RNA Biol. 2018;15(2):186-93.
209. Knuckles P, Vogt MA, Lugert S, Milo M, Chong MM, Hautbergue GM, et al. Drosha regulates neurogenesis by controlling neurogenin 2 expression independent of microRNAs. Nat Neurosci. 2012;15(7):962-9.
210. Hsin JP, Manley JL. The RNA polymerase II CTD coordinates transcription and RNA processing. Genes Dev. 2012;26(19):2119-37.
211. Jeronimo C, Collin P, Robert F. The RNA Polymerase II CTD: The Increasing Complexity of a Low-Complexity Protein Domain. J Mol Biol. 2016;428(12):2607-22.
212. Zaborowska J, Egloff S, Murphy S. The pol II CTD: new twists in the tail. Nat Struct Mol Biol.

2016;23(9):771-7.
213. Wong KH, Jin Y, Struhl K. TFIIH phosphorylation of the Pol II CTD stimulates mediator dissociation from the preinitiation complex and promoter escape. Mol Cell. 2014;54(4):601-12.
214. Heidemann M, Hintermair C, Voss K, Eick D. Dynamic phosphorylation patterns of RNA polymerase II CTD during transcription. Biochim Biophys Acta. 2013;1829(1):55-62.
215. Tang X, Zhang Y, Tucker L, Ramratnam B. Phosphorylation of the RNase III enzyme Drosha at Serine300 or Serine302 is required for its nuclear localization. Nucleic Acids Res. 2010;38(19):6610-9.
216. Rambout X, Maquat LE. NCBP3: A Multifaceted Adaptive Regulator of Gene Expression. Trends Biochem Sci. 2021;46(2):87-96.
217. Yildirim O, Li R, Hung JH, Chen PB, Dong X, Ee LS, et al. Mbd3/NURD complex regulates expression of 5-hydroxymethylcytosine marked genes in embryonic stem cells. Cell. 2011;147(7):1498-510.
218. Zhang C, Chen L, Peng D, Jiang A, He Y, Zeng Y, et al. METTL3 and N6-Methyladenosine Promote Homologous Recombination-Mediated Repair of DSBs by Modulating DNA-RNA Hybrid Accumulation. Mol Cell. 2020;79(3):425-42 e7.
219. Feretzaki M, Pospisilova M, Valador Fernandes R, Lunardi T, Krejci L, Lingner J. RAD51-dependent recruitment of TERRA lncRNA to telomeres through R-loops. Nature. 2020;587(7833):303-8.
220. Arnould C, Rocher V, Finoux AL, Clouaire T, Li K, Zhou F, et al. Loop extrusion as a mechanism for formation of DNA damage repair foci. Nature. 2021;590(7847):660-5.
221. Wang H, Fan Z, Shliaha PV, Miele M, Hendrickson RC, Jiang X, et al. H3K4me3 regulates RNA polymerase II promoter-proximal pause-release. Nature. 2023;615(7951):339-48.